Advances in UWB-based Indoor Position Estimation and its Application in Fall Detection

Oladimeji Onalaja

Faculty of Engineering, Science and the Built Environment

London South Bank University

A thesis submitted to London South Bank University in partial fulfilment of the requirements for the degree of

Doctor of Philosophy

June 2015

I would like to dedicate this thesis to the loving memory of my dad who ensured that I remained focused in all my endeavors while he was still alive. In his own unique way, he made me understand that perseverance and hard work always pays off in the end as long as work is being done honestly. I would also like to dedicate this thesis to my mum who has continued to be my rock throughout my life so far; and most significantly these past four challenging years. I have done it mum, just as you've always said I would.

Abstract

In an indoor propagation environment, the position of an Object of Interest (OOI) is typically estimated by cleverly manipulating range or proximity measurements that are obtained from a series of reference node combinations. In a noise-free propagation scenario, these measured parameters are fed into conventional position estimation techniques and an accurate estimate of the OOI's position is obtained. In practice, the propagation scenario is never quite noise-free; hence the OOI's position estimate is obtained in error. Ultra-Wideband (UWB) is a wireless communication technology that is able to resolve individual multipath components and this ensures that it is capable of estimating the arrival time of the first signal path. The implication of this lies in the fact that the accuracy of the range or proximity measurements obtained from the reference node combinations is guaranteed; hence leading to a reliable estimate of the OOI's position.

In the research work presented in this thesis, the body of knowledge that relates to indoor position estimation is advanced upon. With a primary focus of enhancing the estimation accuracy of indoor position estimation systems, UWB is utilised as the underlying wireless communications technology. The challenges faced by current UWB-based position estimation systems are identified and tackled directly. Specifically, the position estimation error that is due to multipath propagation is addressed and a pre-localisation algorithm that serves the purpose of resolving individual multipath UWB signals in the immediate environment is proposed.

Additionally, a novel position estimation technique coined as Time Reflection of Arrival (TROA) is presented in this thesis. Through a series of Mean Squared Error (MSE) and Cramér-Rao Lower Bound (CRLB) analyses, TROA is shown to be very effective when compared to TOA and the typically unvoiced TSOA technique. In the last section of this thesis, an application of UWB in the area of Biomedical Engineering is demonstrated. Specifically, UWB-based position estimation is used to define a novel fall detection algorithm tailored for Dementia patients.

Acknowledgements

These past four years have been an exhilarating and extraordinary journey; it has presented me with a fairly well balanced vicissitude of experiences which have been both life-changing and character-building. All through this journey, I have been constantly supported, motivated and encouraged by several people who in their own way, have ensured that the intensity that my PhD has entailed did not hinder me from completing it successfully. At this junction, I would like to take this opportunity to express my gratitude to each one of them.

Firstly, I would like to thank God for enabling me to start and see my PhD through to its successful completion. I would also like to express my sincere gratitude to Prof. Mohammad Ghavami for recognising my potential earlier on when he supervised my final year undergraduate project at King's College London. I am forever indebted to him for ensuring that I got funded properly for the first three years of my PhD. Most importantly, I would like to express my sincere gratitude to him for his invaluable advice, motivational talks, timely feedback; and continuous encouragement. Without him, I really and truly would not be the researcher I am today. Thank you Sir!

I would like to express my sincere gratitude to Dr. Mounir Adjrad for being an inspiration to me and my fellow researchers ever since his arrival at LSBU. I met Dr. Adjrad at a point where I felt a little bit lost and confused with regards to the direction of my research work; and I am extremely fortunate that he took a keen interest in my research work. Through his kind words, timely feedback, hands-on troubleshooting sessions and numerous chain emails, he was able to help me focus my research work and devise a well thought out plan to complete my PhD successfully, in a timely manner; and without any unnecessary complications. Thank you Mounir!

Special thanks go to my supervisory team which consists of Dr. Perry Xiao and Dr. Sandra Dudley-McEvoy. Thank you both for your constructive feedback and the words of encouragement you uttered when

they were needed the most. Special thanks go to Markus Cremer and Keli Yao Kumordjie for taking time out of their busy schedules to proofread this thesis. I am very grateful, and forever indebted to you both. Special thanks also go to my Biomedical Engineering and Communications (BiMEC) research group family for creating a healthy and vibrant working atmosphere during my time at LSBU; I will most certainly miss our lunchtime shenanigans. Specifically, I would like to thank Dr. Steve Alty, Dr. Vincent Siyau, Dr. Zhining Liao, Dr. Thanachai Thumthawatworn, Dr. Bo Ye, Dr. Haruki Nishimura, Stephan Hoerster, Christian Koch, Mehran Ghafari, Muyiwa Oladimeji, Adewale Emmanuel Awodeyi and Hafeez Siddiqui. I will cherish the fun, intense and often stressful times we have spent together for as long as I live.

Finally, I would like to express my sincere gratitude to my family and friends, my mum: Khadijah Arinola Onalaja, my siblings: Simisola Olanrewaju Onalaja, Olamide Olasupo Onalaja and Oluwafunmilola Omoyeni Adunni Onalaja, my girlfriend: Oluwatosin Bimbola Akinfosile, my friends: Oladisun Abass and Hamnah Butt. I thank you all for your prayers, unconditional love and endless support all through my journey. We've done it; and now its on to the next exciting challenge.

Ola

Contents

List of Figures

List of Tables

Nomenclature

Acronyms	
2-D	Two-Dimensional
3-D	Three-Dimensional
AD	Alzheimer's Disease
AOA	Angle of Arrival
BPH	Benign Prostatic Hyperplasia
BPM	Bi-Phase Modulation
BPSK	Binary Phase-Shift Keying
cm	Centimetres
CPU	Central Processing Unit
CRLB	Cramér-Rao Lower Bound
dB	decibels
DSS	Desired Solution Space
DS-UWB	Direct Sequence Impulse Radio Ultra-Wideband
E-911	Enhanced 911
EHSC	Emergency Health Support Contact
EIRP	Effective Isotropic Radiated Power
EL	Elliptical Localisation
ESPRIT	Estimation of Signal Parameters via Rotational Invariance techniques
FCC	Federal Communications Commission
FM	Frequency Modulation
g	Grams
GHz	Giga-Hertz
GM	Geometric Multilatertion
GO	Geometric Optics
GPS	Global Positioning System
HDR	Habits and Daily Routine
Hz	Hertz
i.e.	That is
IFFT	Inverse Fast Fourier Transform

IFFT	Inverse Fourier Transform
IR-UWB	Impulse Radio Ultra-Wideband
LBS	Location-Based Services
LOS	Line-of-Sight
m	Metres
MAI	Multiple-Access Interference
MC-UWB	Multi-Carrier Ultra-Wideband
MHz	Mega-Hertz
ML	Maximum Likelihood
MPC	Multipath Component
MRC	Maximal Ratio Combining
MSE	Mean Squared Error
MUSIC	Multiple Signal Classification
MVDR	Minimum Variance Distortionless Response
NBI	Narrow-band Interference
NLOS	Non-Line-of-Sight
NOI	Node of Interest
ns	Nanoseconds
O2SS	Optimum 2-D Solution Space
OE	Observing End
OFDM	Orthogonal Frequency Division Multiplexing
OOI	Object of Interest
OOK	On-Off Keying
PA	Path Attenuation
PAL	Precision Asset Location
PAM	Pulse Amplitude Modulation
PC	Computer
PCS	Personal Communication Systems
PIC	Patient In Care
PL	Path Loss
PM	Phase Modulation
PPM	Pulse Position Modulation
PSD	Power Spectral Density
PSWF	Prolate Spheroidal Wave Functions
RF	Radio Frequency
RFID	Radio Frequency Identification
RMS	Root Mean Square
RSS	Received Signal Strength
SDP	Synchronisation Distribution Panel
SER	Symbol Error Rate
SM	Statistical Multilateration

S-V	Saleh-Valenzuela
TBWP	Time-Bandwidth Product
TDOA	Time Difference of Arrival
TH-UWB	Time Hopping Impulse Radio Ultra-Wideband
TOA	Time of Arrival
TOA-MV	TOA Measurement Variance
TROA	Time Reflection of Arrival
TSOA	Time Sum of Arrival
TV	Television
ULA	Uniform Linear Array
USA	United States of America
UWB	Ultra-Wideband
WLAN	Wireless Local Area Network
LTI	Linear Time-Invariant

Chapter 1

Introduction

1.1 Indoor Position Estimation

The continuous need for the ability to determine the absolute position(s) of an Object of Interest (OOI) at any given time is and always will be a multidisciplinary necessity. In medicine, the OOI is usually the patient; and with the recent advances in the 'Telecare' vision, the patient monitoring and catering process seem to be on the verge of switching from their wholly human dependence to technology driven alternatives [1–6]. The telecare vision postulates that an essential component of any technologically driven alternative solution should be a means to closely and remotely monitor and cater for the patient; and this is where the full effect of having an accurate position estimation system is felt [1, 2, 5]. Regardless of the underlying task any remote monitoring system is designed to complete, the need to ascertain and estimate the position of the patient being monitored will always be paramount. A system equipped with a non-accurate position estimation component ensures that the monitoring process is compro-

mised from the very start for a patient whose care is reliant on the accurate estimation of their real time location. In engineering, the OOI is generally either a mobile or a fixed device; and is often referred to as the Node of Interest (NOI) [7]. As an example, if engineering driven Location-Based Services (LBS) such as real time resource tracking and specific business or service locators within a fixed geographical area are considered, the NOI would be the resource being tracked and the business or service being located respectively [8]. The primary drivers of such services are the real time positions of the respective NOI's; hence in an event whereby the position estimation technique incorporated in the LBS is not accurate, the expectation is that the desired result from the resource tracking or service locating process is never achieved. Due to the apparent practical significance a successful realisation of an accurate position estimation technique or system would mean to a wide range of disciplines, both academic and industrial interest in position estimation research has seen an increase that is not short of the exponential [7, 9–15].

Regardless of it being carried out in either an indoor or outdoor environment, position estimation or localisation can be fundamentally defined as the estimation of the location of a NOI within a two-dimensional (2-D) or three-dimensional (3-D) solution space by means of an explicit cartesian coordinate system translation [7, 16–19]. This translation comes in the form of matching fixed or unfixed real-time positions of the localisation task-specific reference nodes in the defined environment with their cartesian coordinate equivalents; and thereafter placing them explicitly into either the 2-D or 3-D solution space. Conventionally, these task-specific reference nodes which are also referred to in literature as anchor nodes, beacons, landmarks, land references or simply references; are typically

receivers (i.e. they can only receive signals propagated in the specified environment) but could also take the form of transceivers (i.e. they can transmit and also receive signals propagated in the specified environment) depending on the technique being employed to complete the specified localisation task [7]. Prior to the translation of their real-time positions onto the coordinate system, the reference nodes ($RN_{i=1,2,3,...n}$) are typically placed in a very deliberate manner in the relevant indoor or outdoor environment; a manner which is trivial in concept and consequently unvoiced in literature. The integer value of the subscript 'n' is wholly dependent on both the solution space (i.e. 2-D or 3-D) and the specified solution to the localisation task. However, as a rule of thumb, if 'n' is equal to x_{number}[1] in the 2-D space of a specified solution, the inadvertent value of 'n' in the 3-D space of the same specified solution should be ideally 'x_{number} + 1'. Essentially, to determine the 3-D location of a NOI using an algorithmic extension of a technique used to determine its 2-D location, the ideal additional hardware requirement is a single reference node. In an initial attempt to cater for the environmentally driven constraints and also enhance the Line-of-Sight (LOS) provisioning for a specified solution to the localisation task, the aforementioned deliberate placement of the reference nodes usually involves the arrangement of each of them in such a way that there is a somewhat optimal LOS provisioning to complete the task when intrinsic position estimation or localisation limitations are considered [7, 18–20].

As depicted in Figure 1.1, the underlying idea behind the localisation of a NOI using these carefully placed reference nodes is to make distance, range, angle, Received Signal Strength (RSS) and other relevant range or proximity measurements

[1] x_{number} = Total number of reference nodes required to solve the position estimation task

based on a properly structured pairing methodology between subsets of the carefully placed $RN_{i=1,2,3,...n}$, and the NOI itself [7, 18, 19]. Based on the pairing methodology and the nature of the invoked position estimation technique, each pairing between the NOI and the corresponding subset usually leads to the definition of two or more ambiguous coordinates with the possibility of one of them being the location (absolute, relative or semantic) of the NOI.

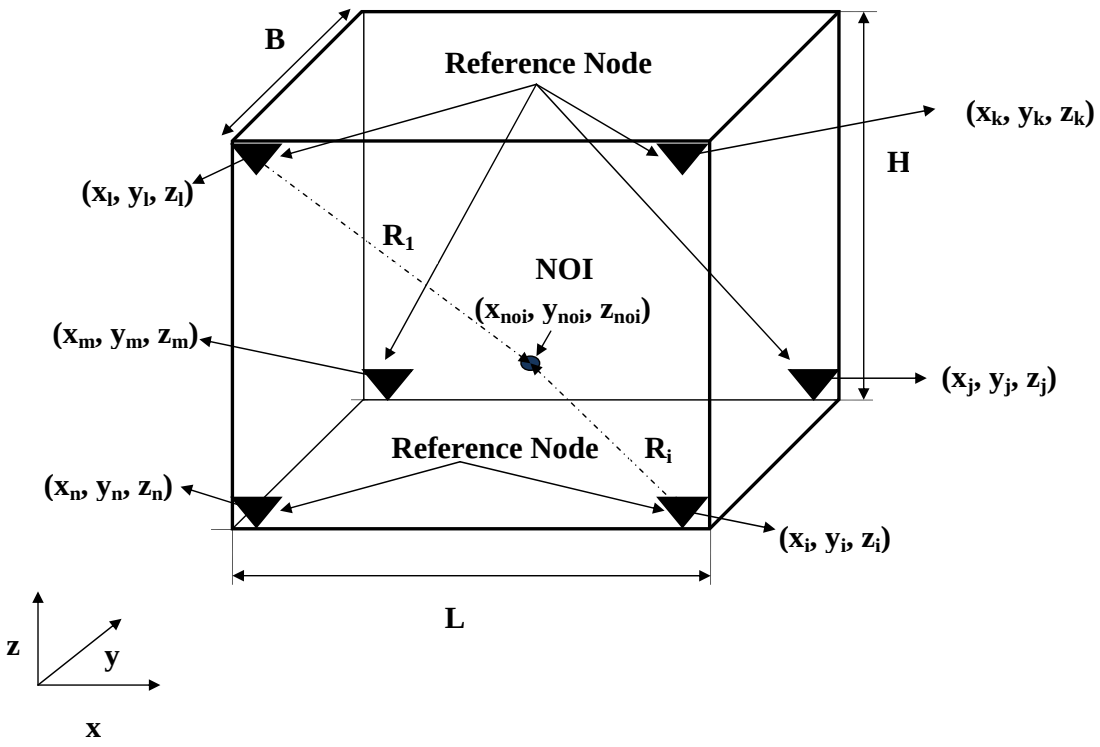

Figure 1.1: Spatially placed reference nodes in a defined environment

This coordinate ambiguity problem is eliminated once the pairing between the NOI and all the individual subsets in the structure have been completed; and a parameter driven cross-correlation is done to determine the true location of the NOI [7]. Ideally, on completion of all these localisation steps (i.e. the deliberate

arrangement of reference nodes, the coordinate system translation, the structured pairing between NOI and reference node subsets; and the cross-correlation), the location of the NOI is determined [7, 18]. However, in practice this idealistic solution to the localisation task is never realised due to a number of factors which range from incorrect reference node placements and location defining parameter measurement errors, to environmentally driven interferences. In subsequent chapters of this thesis, these factors as well as their direct impact on position estimation accuracy are detailed extensively.

1.2 Ultra-Wideband (UWB)

Ultra-Wideband (UWB) is a radio communication technology that is characterised by a large instantaneous bandwidth which typically exceeds the bandwidth required to effectively perform a wide range of communication tasks [21]. This large instantaneous bandwidth is one of the major differences between UWB and other narrowband communication technologies such as Global Positioning Systems (GPS), Personal Communication Systems (PCS), IEEE 802.11 and IEEE 802.11x[2] Wireless Local Area Network (WLAN) family, and ZigBee. The unique properties it presents have seen both industrial and academic interest in the UWB technology increase exponentially in recent years [21, 23, 24]. Despite its relatively recent commercial introduction, the UWB technology as a whole has been in existence for a life span that is in order of decades. The usage of the UWB radar spans for over 40 years to date; and its application area has evolved from its

[2] x = a (Frequency: 3.7/5 GHz, Bandwidth: 20 MHz), b (Frequency: 2.4 GHz, Bandwidth: 22 MHz), g (Frequency: 2.4 GHz, Bandwidth: 20 MHz), n (Frequency: 2.4/5 GHz, Bandwidth: 20/40 MHz), ac (Frequency: 5 GHz, Bandwidth: 20/40/80/160 MHz) [22]

earlier exclusive usage in military applications to its current use in state-of-the-art positioning, radar and medical applications [19, 21, 23, 24].

1.2.1 Commercialisation and Regulation of UWB

The commercial introduction and subsequent emergence of the UWB technology began in February 2002 in the Unites States of America (USA) when the Federal Communications Commission (FCC) issued a ruling that permitted the unlicensed usage of UWB for the purpose of data communication subject to emission constraints [23, 24]. The FCC's ruling which is also referred to as its 'First Report and Order' ensured that UWB-based systems were permitted to operate unlicensed within the 3.1 - 10.6 GHz frequency band of the electromagnetic spectrum; and this inadvertently meant that the UWB technology was allocated a bandwidth of 7.5 GHz which to date is still the largest bandwidth allocation for any commercial system. The mere fact that the allocated bandwidth was license-free ensured that research and development into potentially ground breaking UWB systems and applications, gathered a huge amount of momentum. However, as is the case with any new and emerging technology, UWB's commercial introduction was met with a great deal of resistance. Majority of the resistance came from mainstream technologies and work groups such as IEEE 802.11 WLAN, ZigBee and GPS; and their main concern has been tailored around the fact that they believe the large instantaneous bandwidth of the UWB technology would interfere with their technologies in a very destructive way [21, 23]. This potential interference issue was subsequently looked into by the FCC, and another ruling was made. The revised ruling ensured that the UWB technology remained oper-

ational in the previously allocated spectrum but was only able to transmit UWB signals with very low power because theoretically that would hinder any interference that could potentially result in the degradation of the existing systems. Notably, this revised ruling by the FCC has resulted in the severely restricted operation of UWB in both indoor and outdoor applications. For indoor applications, UWB's operations are restricted to short-range wireless communication in the order of tens of metres for high data rates which are typically greater than 100 Mbps [24]. Conversely, for outdoor applications, UWB's operations are restricted to extremely low data rates that are typically less than a few Mbps for distances that are in the order of a few hundreds of metres [23]. However, this operational duality ensures that individual UWB based systems can be designed to operate in various modes as either communication devices, radars or tracking devices. Essentially, the operational duality of UWB is a testament to its ability to continuously shift between high data rate-short link distance applications to low data rate-short link distances. The exceptionally low transmit power allocated to the UWB technology by the FCC, results in the generation of low energy, relatively short information-bearing and multiple UWB pulses or signals that are used for data communication in the allocated spectrum [23, 24]. To alternate between the high data rate-short link distance mode and the low data rate-long link distance mode, the number of UWB pulses that is used to transmit 1 bit of data, is varied [23, 24]. As [21, 23, 24] explain it, increasing the number of UWB pulses used for the transmission of 1 bit of data, reduces the data rate and inadvertently increases the transmission distance.

1.2.2 Fundamentals of UWB

As it was briefly mentioned in the previous section, UWB had been exclusively used in military applications for a number of decades prior to the FCC ruling in 2002 which led to its commercialisation [21, 23, 24]. In accordance with this FCC ruling, a signal or pulse is deemed as one of a UWB nature if it either has a fractional bandwidth (B_f) which is greater than 20% or if its instantaneous spectral occupancy is in the excess of 500 MHz. Also in accordance with the FCC ruling and with reference to [25], B_f is mathematically defined as:

$$B_f = \frac{B}{f_c} \tag{1.1}$$

where B denotes the -10 decibels (dB) bandwidth and is calculated as the difference between the upper frequency of the -10 dB emission limit (f_H) and the lower frequency of the -10 dB emission limit (f_L). f_c denotes the centre frequency of the signal or pulse and is calculated as half of the sum the lower and upper frequency (i.e. $(f_H + f_L)/2$). The FCC ruling stipulates that UWB systems with f_c values that are greater than 2.5 GHz, are required to have a B value that is not less than 500 MHz [25, 26]. Additionally, it stipulates that UWB systems with f_c values that are less than 2.5 GHz are required to have B_f values of nothing less than 0.20. As depicted in Figure 1.2, the 7.5 GHz bandwidth allocated to the UWB technology which spans from 3.1 GHz to 10.6 GHz, leads to the technology being overlaid on most of the existing narrowband radio communication technologies. According to literature, the emergence of the UWB technology as well as this inadvertent overlay resulted in the FCC receiving about 1000 oppositions to their ruling [24]. Consequently, the FCC proceeded to regulate the power levels they

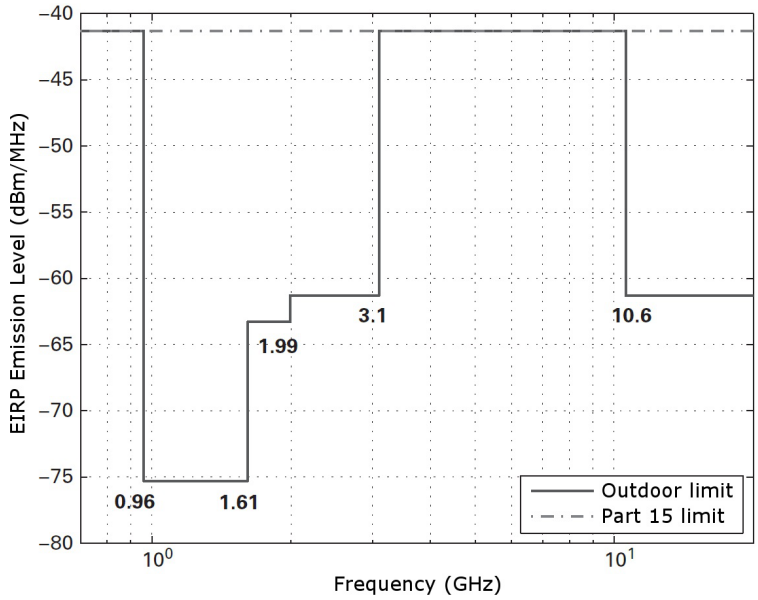

Figure 1.2: FCC spectral mask for indoor UWB systems [19]

they made available to UWB for transmission. Specifically and as it can be deduced from Figure 1.2, the FCC limited the Effective Isotropic Radiated Power (EIRP) emission limit for UWB transmission in the allocated spectrum that spans from 3.1 GHz - 10.6 GHz to approximately -41.25 dBm/MHz (i.e. the Part 15 limit [25]). Essentially, this means that if the whole allocated spectrum is used optimally, the maximum power available for signal transmission using a UWB transmitter, is approximately 0.562 mW[3]. Due to this FCC limitation on the EIRP, UWB signals are known to minimally interfere with existing narrowband radio communication. This is because the Part 15 limit is usually reserved for unintentional radiations from appliances such as PC monitors and TV's [25]. With reference to Figure 1.2, the 0.96 GHz - 3.1 GHz spectrum consists of a number of allocations for other wireless systems. The 1.56 GHz - 1.61 GHz

[3]Power $= 0.001 \times 10^{(-41.25/10)} \times 7500 = 0.562$ mW

spectrum is allocated to GPS, the 1.85 GHz - 1.99 GHz spectrum is allocated to PCS, and the 2.4 GHz - 2.48 GHz is allocated to bluetooth, cordless phones, microwave ovens and IEEE 802.11b [19].

Typically, to facilitate any form of data transmission, UWB systems rely on pulse waveforms that have ultra-short durations. These pulse waveforms are carrier free and have the ability to operate at baseband [23, 24]. The significant lack of carriers which is one of the many characteristics of the UWB technology highlights another major difference between radio communication based on narrowband technologies and communication based on UWB. The ultra-short pulse duration corresponds to the large spectral occupancy of UWB; and this theoretically paves a way for potentially ground breaking radar and communication applications [23]. The large spectral occupancy or bandwidth of UWB enhances the capability of UWB signal penetration through walls and general obstacles due to the fact that the UWB signal consists of various frequency components. Specifically, for radar applications, the large bandwidth results in very high precision ranging whose accuracy lies in the sub-centimetre region. [21, 23, 24]. For communication applications, the large bandwidth allows for scenarios whereby high data rates and high user capacity are simultaneously achieved while the amount of processing power required remains extremely low [23, 24].

1.2.3 Advantages of UWB

In addition to the advantageous effects of the large bandwidth of UWB on data communication, there are also a number of other significant advantages the UWB technology presents which makes it relevant for a host of diverse applications.

These diverse applications are typically either *communications*, *ranging* or *radar* based, and they include health-care, medical imaging, emergency support, intelligent sensing, indoor tracking of target objects, biomedical instrumentation and robotics [19]. Particularly, the key advantages of UWB which makes it suitable for these applications are as thus:

- **Low Probability of Unwanted Detection**: With the combination of its very low Power Spectral Density (PSD) and its pseudo-random characteristics which is utilised for spreading, UWB systems benefits from the generation of noise-like signals that have very low probabilities of interception or detection. This feature significantly reduces the probability of unwanted detection, and makes UWB well sought-after for a host of surveillance, tracking and remote monitoring applications [24].

- **Reusability of the UWB Radio**: Due to its relatively low PSD, UWB based systems make provision for the spatial re-use of its radio source [23]. This essentially means that UWB radio terminals that are located at dissimilar locations are able to use the UWB channel simultaneously as long as the separation distances between them is enough to ensure that mutual interference does not affect any transmission.

- **Robustness to Multipath and Jamming**: The discontinuous transmission of UWB signals when combined with the extremely large frequency diversity its huge bandwidth offers, enables UWB to perform robustly in severely dense multipath environments. The combination of these inherent properties enables UWB exploit more resolvable paths, and this consequently leads to a constant achievement of high levels of multipath resolu-

tion [24]. Additionally, this combination ensures that the transmitted UWB signal is resistant to jamming or interference by surrounding narrowband systems; and also resistant to multipath fading [24].

- **Very Low Complexity and Implementation Cost**: The low complexity and implementation cost of UWB based systems is attributed to the baseband nature of the signal transmission. With the transmitted UWB signals or pulses being carrier-less and characteristically having ultra short durations, they can be directly propagated without the extra transmission-driven requirement of conventional narrowband systems. Typically, conventional narrowband systems would require Radio Frequency (RF) mixers at the transmitting end to translate the baseband signal into a frequency that has the relevant propagation characteristics [24]. This translation usually consists of mixing the baseband signal with a carrier frequency; and in most cases, on completion of the translation, the resultant signal goes through linear power amplification before it is ready for propagation [24]. At the receiving end, the propagated signal is down-converted on arrival by the use of local oscillators and phase tracking loops. In UWB based systems, the wideband nature of the signal used for propagation ensures that the UWB signal spans across frequencies that are typically used as carrier frequencies; hence up-converting it becomes irrelevant [24]. Consequently, the RF mixer, local oscillator and phase tracking loops become redundant; and UWB based systems can be implemented with little complexity and at a very low cost.

- **High Range Resolution**: Due to the narrow nature of the UWB time-

domain pulses, UWB has the potential to offer a fine temporal resolution which allows for *precise location estimation* [23, 24]. According to literature, the level of precision offered by UWB is theoretically a lot better than GPS and other narrowband radio systems [24, 27]. Additionally, in as much as the usage of GPS has its general merits, it is widely known that they are incapable of working in an indoor environment, incapable of working amidst any obstruction to their propagation path, costly, energy prohibitive and are not adequately robust to jamming in some applications [26].

1.2.4 UWB vs. Narrow-band Technology

Albeit very fundamental, the specific advantages of UWB that emphasises its superiority when compared to the narrow-band technologies, are as follows:

- In harsh propagation environments, narrow-band systems suffer severely from fading which is due to the scattering or reflection of the transmitted signal(s) in the expected multipath propagation scenario [21, 28]. The transmitted signals are typically periodic waveforms; hence the superposition of the inversely phased signals result in overlapping and subsequent cancelations (i.e. destructive interference). Practically, this means that over space, frequency or time, the signal quality will continue to fluctuate intermittently. To combat fading, *diversity* is collected over space, time or frequency with multiple antennas. Diversity is defined as the number of independent or uncorrelated copies of the information-bearing signal that is available at the receiver [21, 24]. It is often attributed to operations such as channel coding, frequency hopping and interleaving which is carried out

at the transmitting end. In a communication system, diversity is inherently provided by the channel while the transmission scheme and the receiver enables and collects it respectively [29]. The comparatively large bandwidth of UWB ensures that in harsh propagation environments, the effect of fading is minimal. With the transmit pulse of UWB based systems being so small that their periodic parts are almost negligible, single multipath reflections can be resolved at the receiver. Additionally, the signal components from the environment driven multipath propagation do not overlap; hence there is no destructive interference and UWB systems are a lot less vulnerable to fading.

- With the scarcest and most valuable resource in narrow-band systems being the bandwidth, the major design goal is typically to transfer the maximum number of bits per second per hertz (bps/Hz) within a specified transmit power constraint [24, 29]. In order to achieve good system performances and high data rates, both complex signal processing and extremely expensive computations are required at both the transmitting and receiving ends. With system design using UWB, the comparatively large bandwidth available to the technology ensures that the emphasis shifts from bandwidth efficiency to the optimisation of the employed transmitters and receivers for low complexity and low power operation by the application which the system is designed for [29].

1.3 Motivations

As a direct consequence of both UWB's fine temporal resolution and its low implementation cost, it is widely regarded as a unique technology choice for the implementation of a wide range of short-range and low-data rate communication applications [19, 21, 23, 24]. Particularly, these properties sets it apart from other communication technologies when applications such as *time-based* indoor position estimation is considered [19]. As discussed earlier, despite GPS's numerous merits, it is not able to operate in indoor environments; and environments that present it with obstructions; hence it is not suitable for indoor position estimation [26]. Conversely, time-based indoor position estimation using UWB is feasible in indoor environments as well as environments that present it with an obstruction to its propagation path [21]. Additionally and a bit more significantly, time-based positioning using UWB allows for a position estimation accuracy that is in the order of tens of centimetres (cm) [19, 21, 23, 24, 26]. The unequivocal reason for this level of position estimation accuracy using UWB is best explained by equation 1.2 as it is done in [21, 23, 24, 30, 31].

$$\sqrt{\mathrm{Var}(\hat{d})} \geq \frac{c}{2\sqrt{2\pi}\sqrt{\mathrm{SNR}\beta}} \tag{1.2}$$

Equation 1.2 is the widely known expression for the lower bound on the best achievable accuracy of a distance estimate which is obtained from a specified Time of Arrival (TOA) estimator [30]. TOA based position estimation is explained explicitly in the next chapter, however this expression of its lower bound is introduced early on to explain UWB's significance. Where 'c' represents the speed of propagation (i.e. speed of light), 'SNR' represents the signal to noise

ratio, '$\hat{d}$' represents the distance estimate and 'β' represents the effective signal bandwidth, it can be deduced that the accuracy of the TOA based positioning technique is significantly enhanced by an increase in either the effective signal bandwidth or the SNR [30].

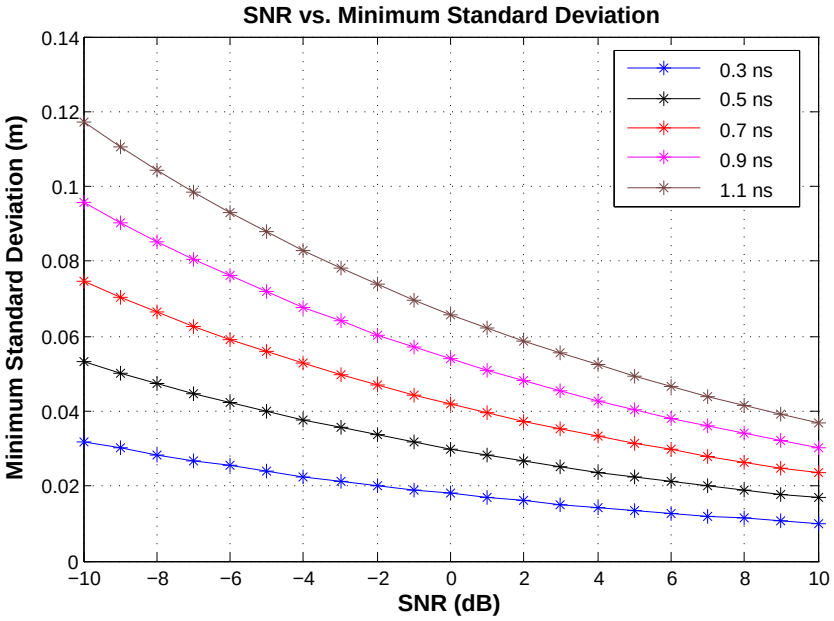

Figure 1.3: SNR vs. Minimum Standard Deviation for TOA

As mentioned, the accuracy of time-based position estimation approaches can also be improved by increasing the SNR. Just as Figure 1.3 depicts, the standard deviation[4] of the TOA position estimate increases at low values of SNR; hence the accuracy of the TOA approach decreases at low SNR values. With reference to Figure 1.3 once again, despite the fact that low SNR values result in a loss of accuracy, an increase in signal bandwidth (i.e. a reduction in pulse width of the UWB signal) leads to an overall reduction in the standard deviation which consequently increases the accuracy of the TOA position estimation approach

[4] Standard deviation $= \sqrt{\mathrm{Var}(\hat{d})}$

[19]. Recalling that UWB characteristically has a huge bandwidth, it suffices to conclude that UWB inherently enhances the accuracy of TOA based positioning. With most time-based positioning techniques being an intuitive derivative of TOA (i.e. Time Difference of Arrival (TDOA) is the difference between two TOA measurements and Time Sum of Arrival (TSOA) is involves the summation of two or more TOA measurements), it also suffices to conclude that their overall accuracies will also be influenced by an enhanced value of β.

1.3.1 Application in Telecare

The act of using technologically-driven methods to directly or indirectly care for the elderly and/or physically challenged people, is referred to as 'Telecare' [1–6, 32]. In telecare, the caring ranges from the remote monitoring of the biophysical conditions of the Patient in Care (PIC) to the remote monitoring and subsequent adjusting of the environmental conditions to suit the needs of the PIC where applicable [1, 2, 32–36]. At either ends of this range, telecare envisions a scenario whereby the designed monitoring system has built-in functionalities which facilitate its real-time response to conditions of the PIC that have been deemed as potentially fatal [2, 32]. Typically, the monitoring system responds to these conditions by notifying a pre-defined nearby hospital or primary care-giver about the PIC's condition; and on reception of this notification by either recipient, the necessary countermeasure is taken [2]. A standardised architecture that governs the design of a telecare system is yet to be defined, however, intuitively the architecture of a fully functional telecare system should comprise of a *central hub* and a *monitoring unit* [32]. The central hub could be further divided into three

building blocks namely the '*localisation block*', '*sensor network block*' and the '*communications block*' [32].

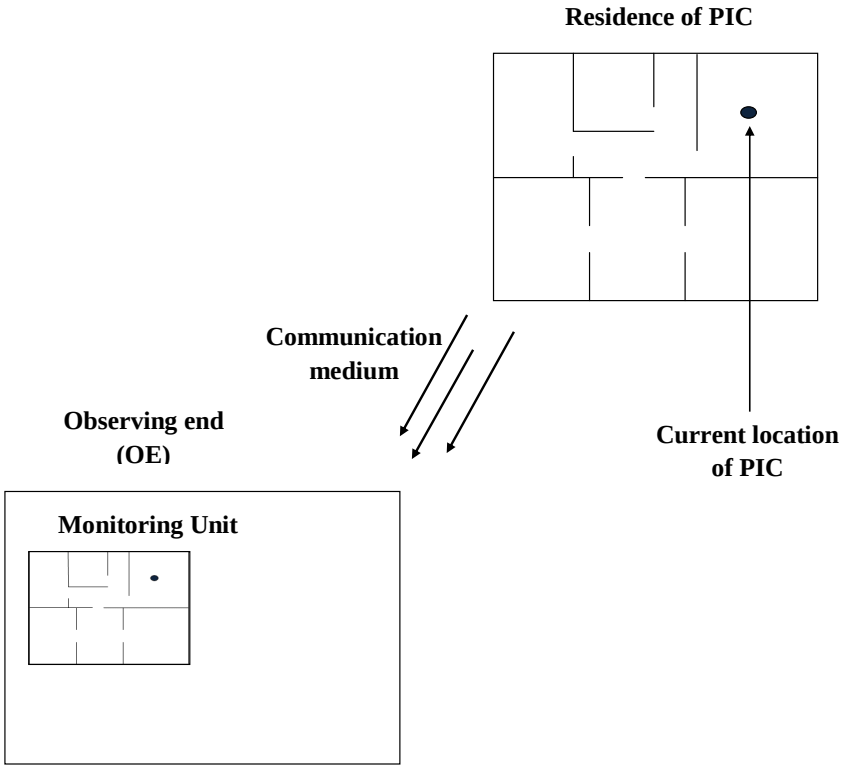

Figure 1.4: Monitoring unit snapshot of the ideal Telecare System

Collectively, the central hub would be responsible for continuously determining the real-time location of the PIC within the defined environment; continuously monitoring the real-time physiological conditions of the PIC; and communicating collated monitoring data to the designated monitoring unit [32]. As depicted in Figure 1.4, the monitoring unit will ideally be placed at the Observing End (OE) which could either be a pre-defined nearby hospital or the residence of the primary care-giver. The monitoring unit should ideally be able to give the current location of the PIC as well as the status of all the physiological sensors attached to them, to anyone at the OE at any time during the day. Other secondary information an

OE viewer would typically be able to receive via the monitoring unit include the current state of the room the PIC is in, the real-time status of all sensor nodes in the immediate environment of the PIC and the battery life information of all sensor nodes. Of the three building blocks of the central hub, the primary focus of the research work presented in this thesis lies within the '*localisation block*'; and the influence UWB has on ensuring that its accuracy is assured.

In recent years, the emergence of the UWB technology; and its promise of ensuring that indoor position estimation is achieved efficiently with high accuracy, has drawn keen interest in both academic and industrial based research activities [21, 23, 24, 37–39]. The research work presented in this thesis focuses primarily on the aforementioned efficiency and accuracy promise of the UWB technology with an aim of positively influencing the fundamental role of a typical localisation block (i.e efficiently and effectively determine the position of a NOI).

1.4 Thesis Outline

The primary aim of the research work presented in this thesis is to advance the current state of knowledge in the area of UWB-based indoor position estimation. This advancement is tailored strategically towards potential indoor biomedical and medical applications; with particular emphasis on Telecare. This research work explicitly tackles relevant hardware requirements and accuracy issues that current position estimation techniques face; and subsequently demonstrates how UWB is capable of both reducing the hardware requirements and enhancing the position estimation accuracy. With a view of applying it in a wide range of Telecare applications, a *novel* and wholly UWB-based position estimation technique

coined as Time Reflection of Arrival (TROA) is also presented in this thesis. TROA is defined using the fundamental principles of Geometric Multilateration (GM); the inherent properties of the UWB technology; and the response(s) of the employed UWB pulse/signal to both the defined indoor propagation environment and the NOI. By means of a series of comparative analyses, it is shown that TROA is capable of achieving an accuracy that is better than conventional position estimation techniques. In the latter phases of this work, a *novel* fall detection algorithm that demonstrates the direct application of UWB in Telecare, is presented. The structure of this thesis is as thus:

Chapter 2 details the basics of the UWB communications system and introduces a few fundamental concepts that are relevant to the research work presented in this thesis. It also classifies position estimation systems, gives an overview of existing position estimation techniques; and concludes by detailing the state-of-the-art techniques in UWB based position estimation.

Chapter 3 consists of two parts. In the first part, a complete 2-D position estimation solution is presented. The presented solution comprises of a *pre-localisation* algorithm that addresses the multipath issues; and the subsequent geometric solution to the estimation problem. The pre-localisation algorithm makes use of the reflection properties of UWB signals to extract position defining information from the reflected signals in the multipath environment; and ultimately reduces the multipath propagation scenario into a two-path propagation scenario based on these extracted information. The extraction process involves the regular sampling of the received signals, correlating the sampled signals with a predefined database of template reflected signals; and finally using a decision engine to determine the signals that would be required to complete the desired

localisation task. As a direct consequence to this pre-localisation, the latter parts of this chapter shows that by carefully considering the inherent properties of the UWB technology, UWB based 2-D position estimation can be efficiently achieved by using just two (**2**) receivers and one transmitter which contrasts current geometric approaches which require at least three (**3**) receivers and one transmitter to complete the same task. In the second part, a 3-D extension to a previously proposed 2-D UWB-based elliptical localisation (EL) technique is presented. It is shown that by homing in on UWB's inherent properties, the 3-D position of the NOI can be determined by splitting the 3-D solution space into two independent 2-D solution spaces. Thereafter, range measurements are made based on the combination of a single transmitter and three receivers that are placed in the environment of interest. Quite significantly, it is once again illustrated that the hardware requirement which for 3-D position estimation is currently set to at least four receivers and one transmitter can be reduced using UWB.

Chapter 4 presents the novel, UWB-based geometric multilateration technique which is coined as Time Reflection Of Arrival (TROA). TROA is defined to improve position estimation errors by carefully considering the inherent properties of the UWB technology; and specifically the reflection properties of transmitted UWB signals. By a direct comparison between TROA and two widely used multilateration techniques, it is shown that indoor position estimation can be done much more effectively using the proposed solution. A new Cramér-Rao lower bound for TROA multilateration is also derived and used to show its level of efficiency.

Chapter 5 presents a novel UWB driven algorithm that performs the task of detecting unrecovered falls by an Alzheimer's Disease (AD) patient by cleverly

using their location information to determine their real-time postural orientation in a specified indoor environment. To achieve this, the real-time vertical distance between the ground (i.e. coordinate 0,0,0) and a defined point on the patient's body, is continuously correlated with a pre-defined distance range which is analogous to the specific fall defining postural orientations to determine the patients current orientation.

Chapter 6 summarises the main conclusions drawn in this research work and highlights its contributions to the overall body of knowledge. This chapter also details the directions for future work based on this research.

1.5 List of publications

Conference Papers

Paper 1: O. Onalaja and M. Ghavami, "UWB based pre-localisation algorithm for aiding target location in a multipath environment", *Proc. IEEE ICUWB*, Bologna, Italy, Sept. 2011.

Paper 2: O. Onalaja and M. Ghavami, "Telecare: A Sensor Network approach", *Proc. SWICOM/APSR* , Manchester, UK, May 2012.

Paper 3: O. Onalaja, M. Ghavami and M. Adjrad, "UWB-based Elliptical Target Localisation in an Indoor Environment", *Proc. IEEE WoSSPA*, Algiers, Algeria, May 2013.

Paper 4: O. Onalaja, M. F. Siyau, S. L. Ling and M. Ghavami, "UWB-based Indoor 3-D Position Estimation for Future Generation Communication Applications", *Proc. IEEE FGCT*, London UK, December 2013.

Journal Papers

Paper 1: O. Onalaja, M. Ghavami and M. Adjrad, "A Novel UWB-based Multilateration Technique for Indoor Localisation", *IET Communications Journal*, Volume 8, Issue 10, July 2014.

Letters

Paper 1: O. Onalaja, M. Ghavami and M. Adjrad, "A Novel UWB-driven Fall Detection algorithm for determining unrecovered falls by Alzheimer's Disease (AD) Patients", *IET Healthcare Letters*, (to be submitted).

Co-authored Papers

Paper 1: M. F. Siyau, S. L. Ling, **O. Onalaja** and M. Ghavami, "MIMO Channel Estimation and Tracking using a novel Pilot Expansion technique with Paley-Hadamard codes for future generation fast speed communications.", *Proc. IEEE FGCT*, London UK, December 2013.

Paper 2: C. Koch, N. Islam, **O. Onalaja**, M. Adjrad and S. Dudley, "Cloud-based M2M Platforms to Promote Individualised Home Energy Management Systems", *Proc. IEEE SaCoNeT*, Paris France, June 2013.

Chapter 2

Related Work

In this chapter, an introduction to the UWB communications system is detailed. This introduction covers the representation and attributes of the UWB signal; the conventionally and universally adopted UWB propagation channel models; the available data modulation schemes; and the UWB receiver design process. In the latter sections of this chapter, a characterisation/taxonomy of indoor position estimation systems; a basic introduction to time-based position estimation; and the state-of-the-art with regards to UWB-based position estimation applications, are all detailed.

2.1 UWB Communications System

Recalling and summarising the introductory remarks on UWB which were given in chapter 1, intrinsic properties such as low complexity with regards to circuit design, relatively low implementation cost, ability to resolve multipath signals in the immediate environment, and a remarkable time-domain resolution which

facilitates task based precision that lies in the 'cm' region, has seen the UWB technology propel from its prior exclusive usage in military applications to becoming the principal candidate in the search for potential technology enablers for future applications and systems [17, 24, 40]. Of all its potential future applications, its role in ensuring that indoor position estimation and target detection is achieved efficiently and with high accuracy seems to be one that has drawn a keen interest in both academic and industrial based research activities; and is well documented in literature [7, 17–19, 21, 23, 24]. Prior to detailing UWB's effectiveness in ensuring accurate position estimation, a basic introduction to the UWB communications system is given.

There are two types of UWB communications systems, they are Impulse Radio UWB (IR-UWB) and Multi-Carrier UWB (MC-UWB). IR-UWB benefits from a carrier-less transmission which ensures that the implementation cost of an IR-UWB based system is significantly reduced. The design of IR-UWB based signals which was predominantly developed and coined by [41], is based on conveying the necessary information by the transmission of ultra- short pulses which are in the order of nanoseconds or picoseconds. In contrast to conventional radio communication technologies, in IR-UWB a train of baseband pulses with short durations (i.e. very high bandwidth) represents a transmit signal; and hence it does not rely on a modulated sinusoidal carrier to communicate information. IR-UWB can be further divided into two sub-categories namely Time Hopping Impulse Radio UWB (TH-UWB) and Direct Sequence Impulse Radio UWB (DS-UWB) [23, 24]. Typically, UWB signal design using TH-UWB involves the division of time into multiple frames which comprises of chips of ultra-short durations. For UWB signal design using DS-UWB, a pseudo-random sequence is used to spread

the data bit into multiple chips; with the UWB pulse taking up the role of the chip [21, 23, 24]. The main merits of signal design using IR-UWB include its robustness to multipath environments, direct applicability in position estimation; and the simple transmitter required for the propagation of the designed UWB signal [42]. MC-UWB systems which are based on Orthogonal Frequency Division Multiplexing (OFDM) utilise multiple simultaneous sub-carriers, and as a direct consequence have the ability to efficiently capture multipath energy with a single RF chain [21, 23, 24, 42]. The drawback of MC-UWB lies in the complexity increase which is due to Inverse Fast Fourier Transform (IFFT) requirement of the UWB transmitter. UWB signal design using MC-UWB makes use of multiple simultaneous carriers and is based on OFDM. OFDM itself is a multi-carrier modulation technique that uses densely spaced sub-carriers and overlapping spectra. Multiple access is supported by assigning each user a set of sub-carriers.

2.1.1 UWB Signal Model and Waveforms

Signal propagation using either IR-UWB or MC-UWB is fundamentally similar to most conventional communication systems. The modulated UWB signal is typically emitted by the UWB transmitter and once it is propagated through the specified UWB communications channel, it is detected (i.e. received) by the UWB receiver. In order to capture all the signal energy from the multipath components in the propagation environment, a rake receiver structure is typically adopted for the UWB receiver [21, 23, 24].

2.1.1.1 IR-UWB Transmit Signal

For a UWB system which is based on IR-UWB in a noiseless and distortion-less channel, the basic mathematical model for the unmodulated transmit pulse train signal $x_{ir-uwb}(t)$ just as the receiver observes it, is given in [23] as:

$$x_{ir-uwb}(t) = \sum_{i=-\infty}^{\infty} A_i(t)p(t - iT_f) \tag{2.1}$$

where $A_i(t)$ which refers to the amplitude of the pulse, is equivalent to $\sqrt{E}$; and E in turn refers to the energy per pulse. t refers to time, $p(t)$ refers to the received pulse which has normalised energy[1] and T_f refers to the frame duration or frame repetition time [23]. Denoting T_p as the duration of $p(t)$, the bandwidth occupied by $p(t)$ is defined as the inverse of T_p (i.e. $1/\ T_p$). Additionally, the UWB pulse repetition rate which can be denoted as R_f, is defined as the inverse of T_f (i.e. $1/\ T_f$) [23].

2.1.1.2 MC-UWB Transmit Signal

For a UWB system which is based on MC-UWB, the basic mathematical model for the UWB transmit signal has a complex baseband form and is also given in [23] as:

$$x_{mc-uwb}(t) = A \sum_{r} \sum_{n=1}^{N} {b_n}^r p(t - rTp) e^{(j2\pi n f_0 (t - rTp))} \tag{2.2}$$

where A refers to an arbitrary constant that typically controls the PSD of $x_{mc-uwb}(t)$ and also determines the energy per 1 bit. N refers to the number of subcarriers,

[1] $\int_{-\infty}^{\infty} |p(t)|^2 dt = 1$

${b_n}^r$ refers to the symbol transmitted in the r^{th} interval over the n^{th} subcarrier [23].

2.1.1.3 UWB Signal Waveforms

There are a wide range of waveforms which conform to the FCC UWB transmit signal specifications; and hence are typically adopted as UWB waveforms. These waveforms include hermite pulses, cubic monocycle waveforms, laplacian monocycle waveforms, prolate spheroidal wave functions (PSWF), rayleigh distributed waveforms, rectangular waveforms and *derivatives* of the gaussian pulse [21, 23, 24, 43]. Of all these pulses/signals/waveforms, the gaussian pulse derivatives are the most popular and are most widely used in the design of UWB systems [43]. The gaussian pulse in its original form is not suitable for wireless UWB systems because its inherent DC component reduces the radiating efficiency of the employed antenna. The derivatives of the gaussian pulse on the other hand, do not have a DC component and are hence practically suited for wireless UWB systems [43].

Gaussian pulse derivatives are adopted in most literature as the de facto UWB waveform because of the relative ease at which they can be described and directly implemented [23]. Additionally, they are readily employed for UWB systems because when compared to other pulses, they have the smallest time-bandwidth product (TBWP) of approximately 0.44 [26]. The TBWP of a given pulse is calculated as the scalar product of the pulse's duration and its bandwidth. It is an indicator of the closeness of the pulse's duration to the lower limit which is pre-set by the pulse's spectral width. As detailed in [44], equation 2.3 gives the

mathematical representation of the gaussian pulse $g(t)$:

$$g(t) = \exp\left[-2\pi \left(\frac{t}{\tau_g}\right)^2\right] \tag{2.3}$$

where t refers to time and τ_g refers to a constant that is used to determine the width of $g(t)$ [43]. Figures 2.1, 2.2 and 2.3 respectively depict $g(t)$, the gaussian monocycle $g'(t)$ and the gaussian doublet $g''(t)$. $g'(t)$ is the first derivative of the $g(t)$ while $g''(t)$

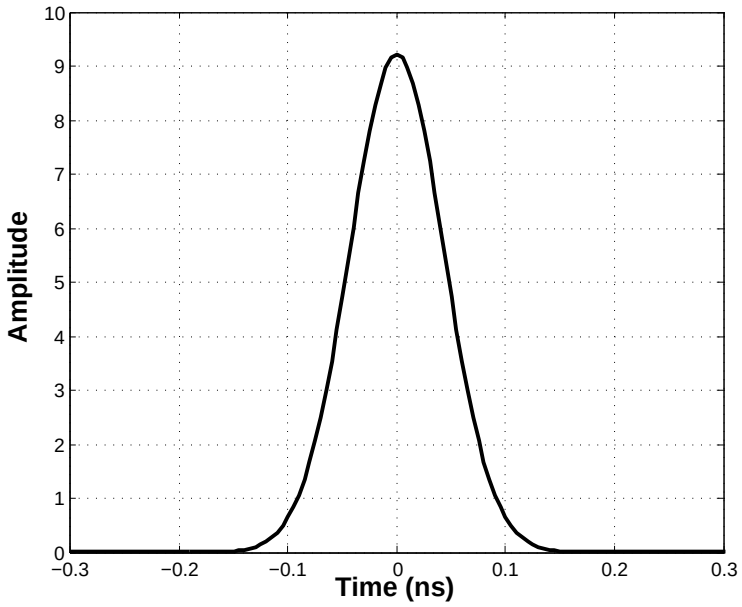

Figure 2.1: The gaussian pulse $g(t)$

is its second derivative. The bandwidths of all three signals are determined by inverting their pulse durations (i.e. $B = 1/T_p$). In contrast to $g(t)$, both $g'(t)$ and $g''(t)$ do not have an inherent DC component, and their zero crossing makes them relevant for wireless UWB systems and applications [43]. Having mentioned that, $g''(t)$ is a lot more useful than $g'(t)$ in position estimation and geo-location applications because of its comparatively lengthier bi-pulse width [24]. As detailed in

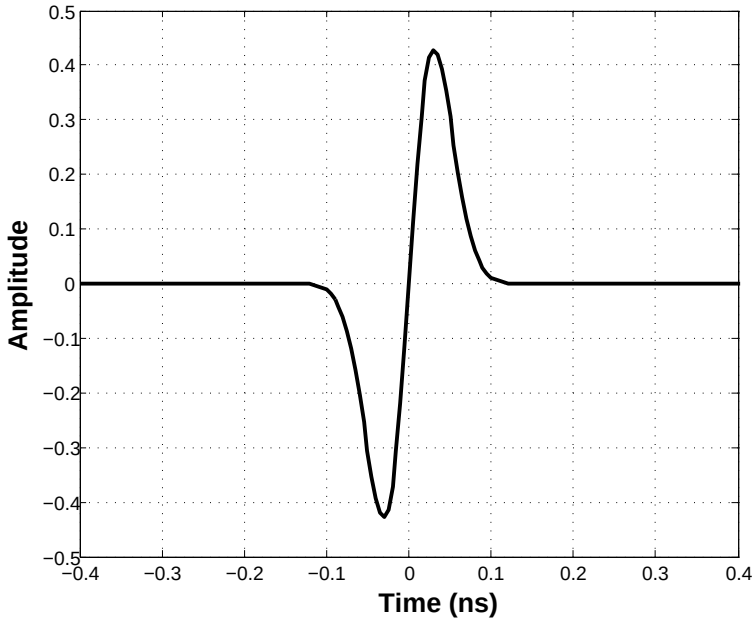

Figure 2.2: The gaussian monocycle $g'(t)$ with a pulse duration T_p of 0.24 ns

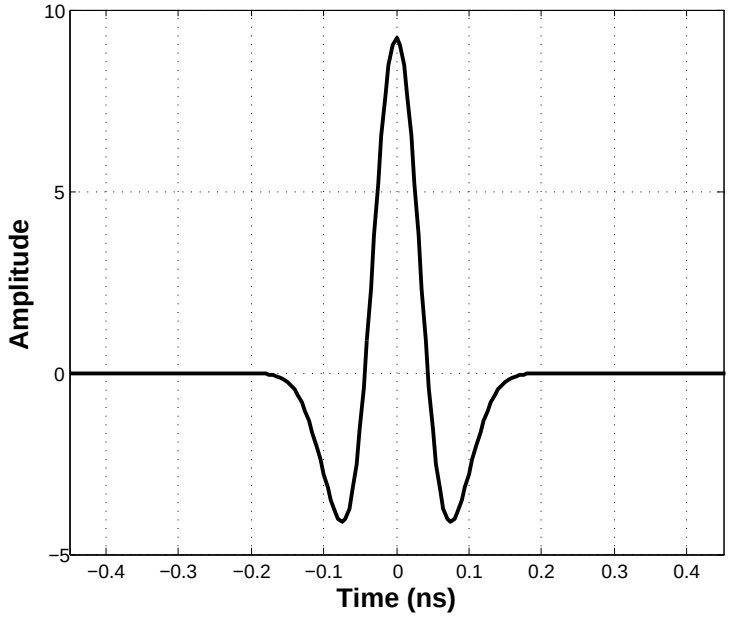

Figure 2.3: The gaussian doublet $g''(t)$ with a pulse duration T_p of 0.38 ns

[44], $g''(t)$ is mathematically expressed as:

$$g''(t) = \left[1 - 4\pi \left(\frac{t}{\tau_g}\right)^2\right] \exp\left[-2\pi \left(\frac{t}{\tau_g}\right)^2\right] \tag{2.4}$$

2.1.2 Data Modulation

Due to the fact that each UWB pulse comprises of a large number of frequency elements, Frequency Modulation (FM) or Phase Modulation (PM) is inapplicable for baseband signal propagation in UWB systems [21]. In UWB systems, it is possible to transmit bits on a baseband level[2] by modulating the amplitude; position; or both the amplitude and position of the UWB signal/pulse. Typically, the baseband modulation schemes employed for UWB systems can be divided into two categories namely *time-based* schemes and *shape-based* schemes. Time-based schemes consist solely of Pulse Position Modulation (PPM) while shape-based schemes consist of Bi-Phase Modulation (BPM), On-Off keying (OOK) and Pulse Amplitude Modulation (PAM) [21, 23, 24].

2.1.2.1 Pulse Position Modulation (PPM)

Time-based PPM is the most commonly used modulation scheme. In PPM, every UWB pulse is transmitted in advance of a regularly spaced time frame; and the nature of the data bit that is due for transmission, directly effects the position of the UWB pulse [21, 24]. Essentially, this implies that if data bit '0' is denoted by a UWB pulse that originates at time 0, data bit '1' is denoted by a time shifted version of the same UWB pulse from 0 [24]. The value of the time shift is typically determined in conjunction with the autocorrelation characteristics of the UWB pulse [24]. Equation 2.5 is the mathematical representation of a PPM

$$s(t) = \sum_{m=1}^{M} P(t - mT + b_m\delta) \tag{2.5}$$

[2]The baseband level refers to the original frequency range of a signal before it is up/down converted or modulated to a frequency range that is suitable for propagation

modulated signal where M represents the maximum number of transmitted bits, $P(t)$ represents the UWB pulse, $b_m \in$ [-1,1] represents the m^{th} data bit, T represents the pulse repetition period and δ represents the modulation index which to all intents and purposes is the 'time shift' value of the UWB pulse [24]. The detection of PPM modulated signals are typically done using template matching techniques [21, 23, 24]. Template matching techniques achieve this by correlating the received signal (i.e. a combination of the transmitted signal and the channel noise) with a pre-defined template which is usually identical to the transmitted signal. This correlation is done to maximise the SNR or the received signal and also to detect the desired signal from unwanted background noise [24].

2.1.2.2 Bi-Phase Modulation (BPM)

BPM is one of the other commonly used modulation schemes in UWB. It is shape-based, antipodal (i.e. opposite); and involves the inversion of the specified transmit UWB pulse in order to create a binary system [21]. In BPM, the UWB pulses represent digital bits by changing their polarity (i.e. a negatively polarised UWB pulse represents bit '0' while a positively polarised UWB pulse represents bit '1'). In total contrast to other modulation schemes, this antipodal nature of BPM ensures that there is a power efficiency gain of 3 dB [21, 45]. Equation 2.6

$$s(t) = \sum_{m=1}^{M} b_m P(t - mT) \tag{2.6}$$

which is detailed in in [21] gives the mathematical representation of a BPM modulated signal where all the equation parameters mimic those defined in equation 2.5. Due to the constant change in the polarities of the pulse, BPM modulated

pulses generate a smooth pulse train spectrum which ensures that they minimally interfere with both themselves and other narrow-band technologies [45]. BPM modulated signals are typically detected by using either template matching techniques or energy detectors [23, 24].

2.1.2.3 On-Off Keying (OOK)

OOK is shape-based and the simplest modulation scheme. It modulates the UWB pulse by switching the pulse generator *on* and *off*. This *on* and *off* switching represents the absence and presence of the pulse (i.e. '0' = pulse absent and '1' = pulse present); and despite its simplicity, with the transmitter being off for majority of the time, the OOK scheme is at a severe power disadvantage [21, 23]. Additionally, in the presence of multipath which is caused by reflections and echoes of either the transmitted UWB pulse or neighbouring pulses, it is very challenging to determine the absence of the desired pulse [21].

2.1.2.4 Pulse Amplitude Modulation (PAM)

In shape-based PAM, the amplitude of the UWB pulse is varied in an attempt to convey the data [21]. Typically, the use of PAM is very rare because a lot more power is needed when UWB pulses with higher amplitude are required to be transmitted. Additionally, in comparison to PAM modulated pulses with larger amplitudes, PAM modulated pulses with smaller amplitudes are a lot more prone to noise-driven interference [21]. However, in some applications, its low implementation complexity makes it the preferred modulation scheme [26].

All the aforementioned data modulation schemes have been used in UWB communications with relative success depending on the targeted application [46, 47].

In fact, their performance can significantly vary according to which system parameters are considered such as narrowband interference (NBI) robustness, symbol error rate (SER), system complexity, data rate, or maximum transmit power with respect to transceiver distance and channel capacity. For instance, if minimum complexity is important, then OOK modulation would be the best choice. However, it is very sensitive to noise. On the other hand, if interference robustness and power efficiency are the parameters to consider, binary PSK (BPSK) can be the best candidates [48, 49]. From a position estimation perspective and for the entirety of this thesis, a specific subset of these modulation schemes has not been explicitly considered. Wherefore position estimation purposes, the parameter of importance is the time of arrival of the transmitted pulse which can be determined by analysing the direct interaction between the pulse, the channel model and the OOI. Assuming that PPM is chosen for this application, it would not have a direct impact on the determination of the required performance criterions (i.e. Root Mean Squared Error) because as PPM postulates, the generated UWB signal or pulse will simply be advanced or delayed in time without any up-conversion and subsequently transmitted for ranging purposes [19].

2.1.3 UWB Channel Model

A properly defined channel model is an important part of any communication system. A channel can simply be defined as the propagation pathway a transmitted signal passes through enroute to the receiver in either an indoor or outdoor environment [21, 23, 24]. With reference to Figure 2.4, the basic model of the UWB communication system as well as any other system, can be likened to the

standard model of a linear time-invariant (LTI) system. Quite similar to an LTI system, the UWB communications system can be characterised by its impulse response $h(t)$. In an ideal situation, the main communications channel model consists of sub-models for both the environmentally-driven multipath as well as the path loss; and consequently, $h(t)$ encompasses these two vital submodels.

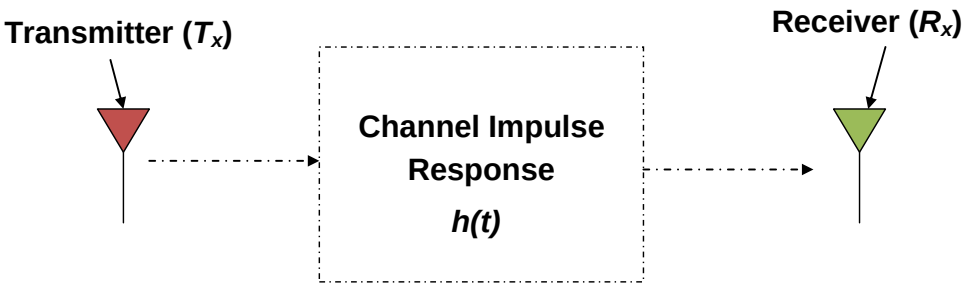

Figure 2.4: The basic communications system model

The path loss model typically defines the amount of power that R_x receives when T_x is placed at a specified separation distance from it; and in-turn, the multipath model typically illustrates the energy dispersion of the UWB pulse over the numerous resolvable multipath components [21, 23, 24].

2.1.3.1 Path Loss Model

The path loss (PL) or path attenuation (PA) experienced by a UWB signal which is typically expressed in dB, is usually due to either free space, reflection, diffraction, refraction, absorption, or a combination of either one of them [21]. The PL model describes the relationship between the transmit power (P_t) and received power (P_r) when the separation distance; and the effects of the environment on the signal propagation are considered [24]. As detailed in [24], the PL can be

represented mathematically in terms of P_t and P_r by equation 2.7, where d refers

$$\frac{P_r}{P_t} = \left(\frac{d}{d_0}\right)^{-n} \tag{2.7}$$

to the separation distance between the transmitter and receiver, d_0 refers to the reference distance[3]; and n refers to the environment-driven path loss exponent. The value of n is highest at '2' when free space is considered; and thereafter, it decreases considerably when other effects such as reflection, refraction, diffraction, etc., are considered [24].

2.1.3.2 Multipath Model

A concise multipath model typically consists of parameters that characterises the channel in terms of the multipath delay spread, *multipath intensity profile*, the number of resolvable multipath components, multipath amplitude-fading distribution and multipath arrival times [21, 50, 51]. Table 2.1 lists all the aforementioned parameters and gives a basic description of their roles in the overall modelling process. In most modern literature, the discrete impulse response of the UWB multipath channel is often referred to as the *multipath intensity profile* of the channel; and it can be represented mathematically by equation 2.8 [21].

$$h(t) = \sum_{l=0}^{L-1} \alpha_l \delta(t - lT_m) \tag{2.8}$$

l refers to the propagation path and α_l which is a function of both the separation

[3]The reference distance is usually set to 1 m [24].

distance between T_x and R_x; and time, refers to the amplitude attenuation factor on l [21]. L refers to the number of resolvable multipath components while T_m refers to the minimum resolution time of the UWB pulse [21].

Table 2.1: Multipath model parameters and description

Parameter	**Description**
Multipath delay spread	The multipath delay spread of a UWB channel is portrayed by its root mean square (rms) value; and this value typically increases when the separation distance between T_x and R_x increases [21, 26]. For indoor channels, the rms delay spread values lie between 19 ns to 47 ns [52].
Multipath arrival times	Due to the fact that objects which are randomly placed in an environment inadvertently cause multipath propagation, the arrival times of the multipath are typically modelled as a Poisson process [21]. In the Saleh-Valenzuela (S-V) channel model proposed in [53], each of the different paths arrive at the R_x in clusters and at arrival rates that are poisson distributed [26, 54].
Multipath amplitude fading distribution	The amplitude-fading of the multipath is typically modelled by a log-normal distribution [51]. As a result of its inherent ultra-short duration,

Continued on next page

Table 2.1 – *Continued from previous page*

Parameter	**Description**
	UWB pulses tend to experience less fading than other pulses. The fading experienced by UWB pulses are usually a lot less than 5 dB [55].
Number of resolvable multipath components	The average value for the number of resolvable multipath components is reliant on the separation distance between antennas (i.e. T_x - R_x separation distance) [21, 51]. Based on investigative work conducted in [51], it has been deduced that the standard deviation of the number of resolvable multipath components increases with an increase in separation distance between antennas.

2.1.4 UWB Receiver Design

Just as the name implies, a *receiver* is designed primarily to detect, capture and pass relevant or meaningful data on to the back-end application or system that the transmitted data is originally destined for [21, 23, 24]. Conventionally, the typical wireless propagation channel is prone to multipath which could either be mild or severe based on the nature of the defined indoor/outdoor environment. Consequently, being able to detect and capture signal energy from all the numerous paths, becomes a prerequisite for the receiver design process [21, 23, 24]. As it is widely known, signal propagation using UWB entails using pulses or

signals of ultra-short durations which are capable of resolving multipath; and hence the UWB technology as a whole is deemed to be rich in multipath diversity [23, 24, 26]. Consequently, correlation-based *rake receivers* are predominantly used by most UWB systems in order to enhance system performance in environments that are characterised by severe multipath [24]. By ensuring that its number of sub-receivers or fingers[4] is equivalent to the number of multipath components, a correlation-based rake receiver is able to predominantly capture a majority of the conveyed signal energy [24, 43]. Typically, in an attempt to ensure that the maximum amount of signal energy is captured, additional fingers are added to the rake receiver. Having mentioned that, there are a few negative implications of this addition. They lie in the intuitive increase in the complexity of the rake receiver design and an unwanted increase in the consumed energy [56]. On completion of the signal capturing process by all the fingers and in an attempt to guarantee its optimal performance, the rake receiver employs the Maximal Ratio Combining (MRC) technique to coherently combine the signal components of the different paths [24, 26]. The MRC output is typically a weighted sum of the individual SNR value of each rake receiver finger [24].

2.2 Classification of Position Estimation Systems

Position estimation systems are typically classified by either the signalling scheme they employ, the parameter(s) they require to determine the position of the NOI, the underlying position estimation technique, the position estimation unit, the

[4]The sub-receivers or fingers of a rake receiver is usually likened to the *tines* of a garden rake. In the same way that each tine picks up the required leaves, each finger captures signal energy from the multipath component that has been assigned to it [24, 43].

propagation environment, the nature of the determined position of the NOI, the nature of the position estimation system; or the dependence of the system on the distances or angles between the NOI and surrounding reference nodes [7, 17, 19, 57–60]. In no particular order, Table 2.2 lists a number of these classification criterion and describes the ways in which position estimation systems could be classified based on them.

Table 2.2: Classification of position estimation systems

Criterion	**Description**
Signalling Scheme	This refers to the type of signals used for position estimation, as well as their underlying propagation characteristics [24]. The conventional signalling schemes employed by position estimation systems are Radio Frequency (RF), Infrared (IR), Optical and Ultrasound. In most cases, the selected scheme is reliant on the nature of the environment and its influence on the proposed scheme; or the position estimation distance [7, 19, 21, 60].

Continued on next page

Table 2.2 – *Continued from previous page*

Criteria	**Description**
Parameter of Relevance	Position estimation systems are designed in such a way that the position determining parameter is a function of either the Time of Arrival (TOA), Time Difference of Arrival (TDOA), Angle of Arrival (AOA) or Received Signal Strength (RSS) measurements; or a combination of two or more of them [18, 19, 23, 24].
Position Estimation Technique	This refers to the process in which the position of the NOI is obtained. Typically, position estimation systems could be designed to perform this task by either cell ID localisation, *multilateration* or pattern recognition [7, 16, 18, 19, 24].
Position Estimation Unit	Position estimation systems could perform NOI position identification either on-site by using a mobile handset; or remotely by means of a Central Processing Unit (CPU). The former method is referred to as self-positioning, and systems that employ it are known as *location-aware* systems, while the latter which is referred to as remote-positioning, is employed by *location-support* systems [7, 16–19, 24].

Continued on next page

Table 2.2 – *Continued from previous page*

Criteria	**Description**
Propagation Environment	With signal propagation characteristics varying significantly in different environments, it becomes a necessity to classify position estimation systems according to the environment [19, 24]. Consequently, position estimation systems are classified as either *indoor* or *outdoor* systems. Outdoor systems such as GPS and Enhanced 911 (E-911) [61] are not used in indoor environments because they are not equipped to overcome the accuracy challenges indoor position estimation present [7, 17–19].
Range Dependency	Position estimation systems could be classified by their range dependencies. Those that require some form of range (i.e. distance) measurement to estimate the position of the NOI are referred to as *range-based* systems. Conversely, those that do not require any range measurements are referred to as *range-free* systems [57, 62].
Nature of determined NOI position	Position estimation systems can also be classified according to their ability to determine the *absolute*, *semantic* or *relative* location of the NOI.

Continued on next page

Table 2.2 – *Continued from previous page*

Criteria	Description
	An absolute location such as 51 0' 26.0"N 0 7' 39.0"W, refers to the physical coordinate of the NOI with respect to a global reference. A semantic location such as 'London South Bank University, London, UK' refers to the symbolic location of the NOI. A relative location refers to the location of the NOI with respect to a local reference node [19, 24].

2.3 Time-based Position Estimation

Indoor position estimation can be explicitly referred to as the estimation of either the absolute, relative or semantic position(s) of a NOI in either the 2-D or 3-D solution space within an explicitly defined indoor environment [7, 16–19]. Typically, the utilised solution space is wholly dependent on the given position estimation task; and its definition in the indoor environment is tailored to match the coverage distance limitations as well as other stringencies of the employed communications technology [7, 17–19]. The defined indoor environment is characterised by its confinement to the perimeter (for a 2-D solution space) or volume (for a 3-D solution space) of the surrounding building. It could be any space within the confined space (i.e. a hospital ward in a hospital; a room within a hall of residence; the

entire volume of the hall of residence or the hospital) [7, 19].

As it has been explicitly detailed in Section 1.3, UWB's performance is comparatively very good when time-based position estimation is considered. This is because the duration of a transmitted time-domain signal is inversely proportional to its bandwidth (i.e. equation 1.2) [19, 24]. With its fine time-domain resolution facilitating its ability to properly determine the time of arrival of received signals with a high level of accuracy, UWB is capable of ensuring that the position of a NOI is estimated with a very high accuracy [19]. A single time of arrival value is never enough to estimate the position of a NOI; and hence it becomes a necessity to have time-based techniques that estimate the position of the NOI by cleverly manipulating several time of arrival measurements [7, 17, 18, 24].

Time-based position estimation techniques can be categorised into one of two primary variants; they are either based on a completely defined 'geometric' or a 'statistics' driven approach. Geometric driven approaches which are commonly referred to in literature as GM, estimate the position of a NOI by establishing a geometric link between deployed reference nodes or anchors (i.e. a base station, receiver) and the NOI itself using time of arrival measurements [7, 18]. Relevant distance information are thereafter extracted from the link; and the estimation of the NOI's position is attempted. The word 'multilateration' refers to position estimation that occurs when multiple established geometric links are considered during the process of determining the NOI's position. The widely known GM variants include TOA, TDOA, TSOA, the received signal strength (RSS) and AOA [7, 9–12, 18]. In contrast, statistically driven techniques such as those described in [13–15] shift the position estimation focus from the goal of achieving numerical values (albeit relative in most GM variants) for location of the NOI,

to statistical approximations and estimation error alleviation measures. In this thesis, we focus wholly on GM variants due to their dependence on time of arrival estimates.

2.3.1 Time of Arrival (TOA)

Classical TOA tackles the underlying position estimation problem by exploiting or utilising the a priori knowledge of the wave propagation speed[5] [19, 24]. In the scenario depicted in Figure 2.5, the position of the NOI is required to be determined in a square-shaped 2-D solution space. Representing the length and width of the square-shaped environment as 'D', three land reference nodes R_{x1}, R_{x2} and R_{x3} are placed in the defined environment. R_{x1} is placed at coordinate (D, $\frac{D}{2}$), R_{x2} is placed at coordinate (0,D) of the 2-D grid, and R_{x3} is placed at the origin (0,0) of the 2-D grid. With an assumed knowledge of the clock synchronisation between all reference nodes and the active transmitting medium (i.e. T_x) which the NOI is equipped with, T_x transmits a signal to all three land reference nodes [19]. The TOA of the transmitted signal at all three reference nodes are determined and subsequently multiplied with 'c' to determine their respective distances from the NOI (i.e. d_1, d_2 and d_3). Using the placement coordinate of each reference node as the *origin* and their determined distances from the NOI as the *radius*, three circles similar to those in Figure 2.5 can be constructed. Assuming that the propagation scenario is noise-free, the intersection of all three circles results in a *single* intersection point or coordinate; this intersection point defines the 2-D position of the NOI [7, 19, 24].

In practice, the propagation scenario is hardly ever noise-free and as a direct

[5]Speed of light = $c = 3 \times 10^8$ m/s

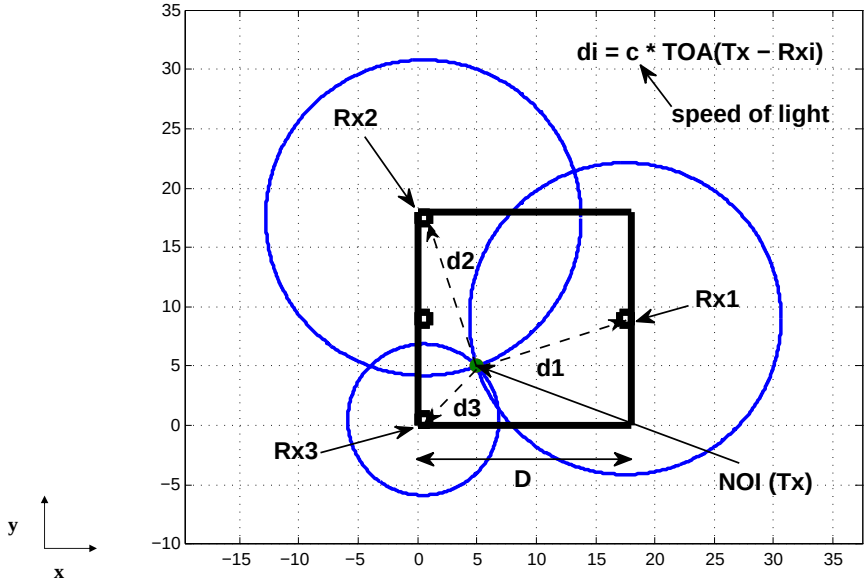

Figure 2.5: Illustration of Time of Arrival (TOA) based Geometric Multilateration

result, the constructed circles will be displaced in the solution space [19]. This displacement leads to the intersection of the three circles yielding a polygon which is typically averaged to determine singular values for the coordinates of the NOI's position [7, 19, 24].

2.3.2 Time Difference of Arrival (TDOA)

TDOA is a variant of TOA, it uses the differences between two or more TOA measurements to estimate the position of the NOI [7, 19]. Albeit a variant of TOA, unlike TOA, TDOA does not require any knowledge of clock synchronisation between the NOI and the relevant reference nodes for it to estimate the NOI's position. This is the major advantage TDOA has over TOA [7, 17, 24, 63]. However, this is only valid when there is clock synchronisation among the relevant

reference nodes [19, 63]. Once again, with reference to a scenario similar to that which is depicted in Figure 2.5, if the reference nodes combinations R_{x1} - R_{x2}, R_{x1} - R_{x3} and R_{x2} - R_{x3} are considered individually, their TDOA measurements can be determined by one of the following methods:

- The TDOA measurements for individual combinations can be determined by initially estimating the TOA of the transmitted signal at each constituent reference node. Once these estimates are obtained, they are subtracted from each other to get the TDOA measurement[6]

- The TDOA measurements for individual combinations can also be determined by performing a cross-correlation between the signals received by the reference nodes in each combination. Once completed, the time delay that corresponds to the highest cross-correlation value (i.e. highest peak when cross-correlation product is plotted), is defined as the TDOA measurement [24].

Each TDOA measurement defines a hyperbola with a constant distance[7] and a focus located at the reference nodes associated with the measurement. In a noise-free scenario, with three (3) hyperbolas defined based on three (3) different reference node combinations, the singular intersection point of the hyperbolas, defines the position of the NOI [7, 64].

[6]For combination R_{x1} - R_{x2}, TDOA measurement = $TOA_{R_{x2}}$ - $TOA_{R_{x1}}$; for combination R_{x1} - R_{x3}, TDOA measurement = $TOA_{R_{x3}}$ - $TOA_{R_{x1}}$; and for combination R_{x2} - R_{x3}, TDOA measurement = $TOA_{R_{x3}}$ - $TOA_{R_{x2}}$.

[7]constant distance = $c \times$ (TDOA measurement) [7, 64].

2.3.3 Angle of Arrival (AOA)

The estimation of a NOI's position using AOA is typically achieved by making a series of angular *direction* observations that are measured using either a set of directional antennas or antenna arrays [7, 24]. AOA measurements provide information about the direction of an incoming transmitted signal by means of the phase differences between either the relevant directional antennas or elements of the antenna arrays [24]. Typically, to determine the position of a NOI in a 2-D scenario, at least two AOA measurements from two dissimilar reference nodes, are required. However, in an attempt to increase the position estimation accuracy, more than two reference nodes (i.e. more than two AOA measurements) are often used in practice [7]. Conventionally, the AOA measurement for each reference node is determined using either the uniform linear array (ULA) model [7], minimum variance distortionless response (MVDR) AOA estimator [7], maximum likelihood (ML) AOA estimator [65–68], multiple signal classification (MUSIC) algorithm [7, 69, 70]; or the estimation of signal parameters via rotational invariance techniques (ESPRIT) algorithm [7, 71]. Each AOA measurement estimates the position of the NOI as one of the several points that lies along the estimated line of bearing [7]. With two or more AOA measurements estimated and their lines of bearing translated onto a 2-D grid, the intersection point of the lines gives the definitive estimate of the NOI's position. In addition to the advantageous fact that AOA can be performed using one less reference node than both TOA and TDOA, in a similar manner to TDOA, AOA geometric multilateration technique also benefits from the lack of clock synchronisation [7].

2.4 Error Sources of Time-based Position Estimation

In a noise-free propagation environment, TDOA, TOA, AOA; or a combination of two or more of them (i.e. TOA and AOA [7, 72–75]) are all capable of estimating the position of NOI with a comparatively good level of accuracy. As it has been explicitly discussed, the level of position estimation accuracy is significantly increased when the UWB technology is employed. Even with UWB employed, the propagation environment is never noise-free in practice, and the estimated position of the NOI is always prone to error [7, 19, 24]. The main sources of the position estimation error are 'multipath propagation', 'Non-Line-of-Sight (NLOS) propagation' and 'multiple-access interference'.

2.4.1 Multipath Propagation

As it is detailed in Section 2.3.1, estimating the TOA of a transmitted signal in a multipath-free environment is fairly straightforward once the solution space has been defined and the relevant reference nodes properly placed in the environment. In practice, this is not the case because the reflection and refraction of the transmitted signal in the propagation environment leads to multiple received signals (i.e. multipath) with dissimilar attenuation and delays, at the receiver end [19, 24]. The TOA estimate used for position estimation is typically obtained from the strongest Multipath Component (MPC). In narrowband systems, due to the longer durations of the utilised pulses, there is an insufficient amount of time delay between two MPCs. This leads to interference and superposition of

the multipath signals; and ultimately inaccurate estimates of the TOA [19, 76]. In UWB-based systems, this is not an issue because of the extremely short durations of UWB pulses/signals. The short pulse duration allows for a sufficient amount of time delay between received MPCs, and this facilitates the resolution of all the MPC's in an attempt to determine the strongest MPC [19, 21, 24]. The strongest MPC is then used to determine the TOA estimate. In some scenarios, the strongest MPC arrives at the receiver at a much later time than the first MPC, and hence the TOA estimate is obtained using the first MPC [19, 21].

2.4.2 Multiple-access Interference (MAI)

Time-based position estimation suffers from a reduced level of accuracy when it is performed in the presence of multiple-access interference (MAI). MAI predominantly occurs in communication systems that employ non-orthogonal multiplexing (i.e. multiple-access systems), however, it also occurs in communication systems that employ orthogonal multiplexing (i.e. UWB-based systems). Its occurrence in UWB-based systems is in the form of a significant amount of interference from users in networks that operate simultaneously [19, 24]. Conventionally, the effects of MAI are mitigated by a number of techniques which are collectively referred to as multiuser detection (MUD) [19, 77].

2.4.3 Non-Line-of-Sight (NLOS) Propagation

As the name implies, a NLOS propagation scenario refers to one that is characterised by the blockage of the direct LOS propagation path between transmitters and receivers [7, 19, 24]. Depending on the nature of the blockage in the LOS

path, a transmitted signal suffers from an attenuation that ranges from mild to severe; and in some cases, the severity level of the attenuation is so much that the transmitted signal is never observed at the receiver [19]. Consequently, in a NLOS propagation scenario, the estimated TOA measurement always includes a *positive bias* that represents the influence of the NLOS error. In modern literature, the modelling of the NLOS error is dependent on the propagation channel; and the NLOS error itself is typically modelled as either a 'constant' along a time interval or as random variables that are either of uniform, exponential or Gaussian distribution [78–82]. For the entirety of this research work, only LOS propagation scenarios are considered.

2.5 UWB Position Estimation Systems

Among other inherent properties of the UWB technology, its fine time-domain resolution, inexpensive circuitry and its ability to resolve multipath makes it the ideal technology candidate for ensuring that position estimation of a NOI in short to medium distances, is done accurately, efficiently and quickly [18, 19, 21, 23, 24]. Typically, for localisation distances that are less than 300 m, UWB is capable of estimating the position of a NOI with an accuracy that lies in the sub-metre range [19, 21]. Typical applications that benefit from the sub-metre ranging of UWB include environmental sensing, aerial surveillance, structural monitoring, home security, personal safety devices; and medical sensing [7, 18, 19, 24, 60]. As expected, individual applications will have their accuracy requirements. However, with a guarantee of achieving an accuracy that lies in the sub-metre range, UWB has been shown to be capable of ensuring that the implementation of these

applications are possible [19, 83]. Table 2.3 which is based on [19, 24, 83] lists the range and accuracy requirements for a number of key position estimation applications that UWB is capable of facilitating.

Table 2.3: Range and Accuracy Requirements of key position estimation applications

Application	**Range [m]**	**Accuracy [cm]**
Personnel tracking at offices (Commercial)	100 - 300	0.15
Cargo tracking at large depots (Commercial)	300	3
Inventory tracking at warehouses and manufacturing plants (Commercial)	100 - 300	0.3 - 3
Cargo Tracking at depots (Commercial)	300	3
Search and rescue operations (Military)	300	3
Rural and urban situational awareness (Military)	300	0.3
Training facilities (Military)	300	0.3
Landing systems (Aviation)	300	0.3
Anti-collision systems (Aviation)	300	0.3
Tracking of Prisoners (Security)	300	0.3
Tracking of Miners (Safety)	300	0.3
Tracking of Emergency Responders (Safety)	300	0.3
Detection and rescue of Avalanche victims (Safety)	300	0.3

Continued on next page

Table 2.3 – *Continued from previous page*

Application	**Range [m]**	**Accuracy [cm]**
Tracking of firefighters (Safety)	300	0.3
Tracking and monitoring of patients (Medical) [84]	300	0.3

2.5.1 State-of-the-art UWB Position Estimation Systems

The existing brands of UWB-based position estimation systems are manufactured using TOA, TDOA, AOA, or a combination of two or more of them, as the underlying GM technique [19]. In addition to the state-of-the-art UWB-based position estimation systems detailed below in the next sections, unvoiced UWB-based position estimation systems manufactured by IMEC Microelectronics centre [85] and Thales Research [86] have also had comparatively good accuracy values that lie in the sub 10 cm region.

2.5.1.1 Time Domain PulsON350 RFID tracking system

The PulsON350 tracking system depicted in Figure 2.6 is a TDOA-driven, UWB-based position estimation and tracking system manufactured by Time Domain Corporation [27]. Depending on the propagation environment, PulsON350 is capable of estimating the position of a NOI in all solution spaces (i.e. 2-D and 3-D) with remarkable accuracies [19]. It achieves a position estimation accuracy of less than a foot in idealistic environments and an accuracy that is approximately

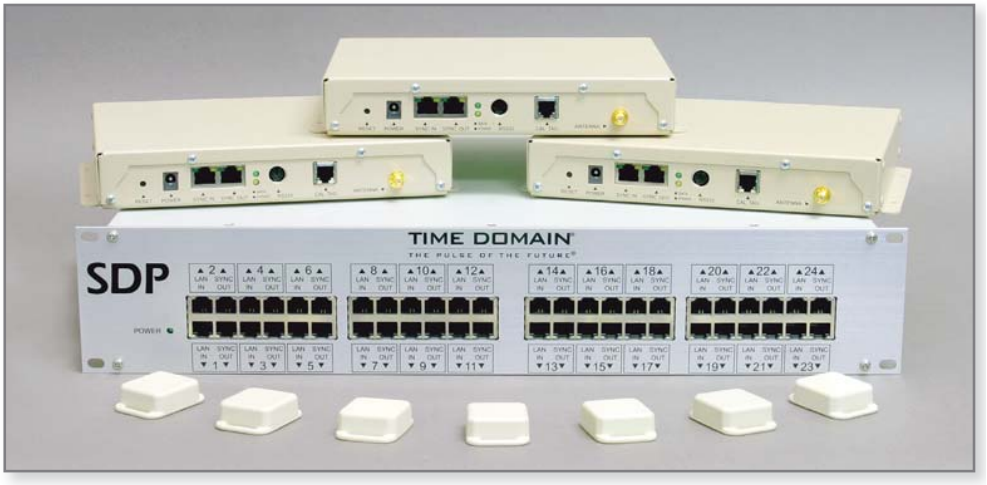

Figure 2.6: The PulsON350 RFID tracking system [87]

less than 3 feet in practical environments [19, 27]. PulsON350 comprises of an RF tag, a reader and a synchronisation distribution panel (SDP). The RF tag is compliant with the FCC emission limit, weighs 11.8 grams (g), has a battery life of 4 years; and transmits RF packets at a frequency of about 1 Hz [27]. The reader which weighs 816 g and has an antenna gain of 2 dBi, receives transmission made by the RF tag, determines the time of arrival and decodes data [27]. The SDP is responsible for the powering-up and time synchronisation of the reader.

2.5.1.2 PAL650 Precision Asset Location System

The PAL650 precision asset location system depicted in Figure 2.7 was manufactured by Multispectral Solutions, Inc (now Zebra Enterprise Solutions [89]) and is regarded as the world's first FCC certified UWB-based tracking system [21, 90]. It comprises of a set of active tags, UWB receivers and a central processing hub [21]. The design and manufacturing of PAL650 is as a direct consequence of the commercialisation of the precision asset location (PAL) system which was exclu-

Figure 2.7: The PAL650 precision asset location system [88]

sively used for military applications prior to the FCC rulings [19, 21, 91]. The active tags which typically have a life-span of 4 years, have a centre frequency of 6.5 GHz, operate at 3.0 V and have a current consumption of 30 μA. PAL650 is driven by TDOA and can estimate the location of a NOI with an accuracy of up to 30.48 cm.

2.5.1.3 Ubisense Real-Time Localisation System

Figure 2.8: Ubisense sensor(left) and tag (right) [92]

Ubisense is a UWB-based position estimation technology that is driven by both TDOA and AOA [92]. It comprises of active tags, sensors and a software package for interpreting received data [92]. Each tag is assigned a unique ID and attached to the NOI so that when it transmits its location to surrounding sensors, the received signals are used to estimate the position of the specific tag; and the NOI consequently [19, 92]. As a direct consequence of the inherent properties of UWB such as its large bandwidth and the small duration of the transmitted UWB pulse, there are theoretically little or no limitations to the scalability of real-time position estimation using Ubisense [92]. Ubisense is capable of locating and tracking multiple NOIs simultaneously without overlapping and compromising the accuracy of every estimated position. Figure 2.8 depicts the Series 7000 industrial standard Ubisense sensor and tag. The sensor contains UWB receivers and an antenna array which facilitates the determination of the tag's location to within a 15 cm accuracy [92].

2.5.1.4 Zebra DART UWB (prev. Sapphire DART UWB)

The Zebra DART UWB real-time position estimation system which is depicted in Figure 2.9 was also manufactured by Multispectral Solutions, Inc. [89]. It is an active RFID system that comprises of UWB driven active tags that have a very impressive tag battery life-span of 10 years; sensors; and a control hub. The active tags typically weigh about 10 g; and are certified for estimating the position of a NOI in hazardous and multipath-rich locations with an average expected accuracy of 10 cm [19, 89]. Zebra DART UWB systems are designed to be flexible enough to support position estimation in the harshest or toughest indoor and outdoor applications [89].

Figure 2.9: The Zebra DART UWB system [89]

2.6 Summary

The accurate estimation of the position of an NOI or OOI is vital to the operational success of a host of multidisciplinary systems and applications. In noise-free scenarios, TOA, AOA, TDOA and other hybrid position estimation techniques are capable of estimating the position of the NOI or OOI with an acceptable accuracy. However, in practice the propagation scenario is never noise-free; and hence the level of position estimation accuracy by conventional techniques, drastically diminishes. With the inherent properties of the UWB technology such as its extremely large bandwidth and ultra-short pulse durations considered, high level position estimation accuracy is typically achieved when it is employed as the underlying technology behind any time-based position estimation technique. Even though the utilisation of UWB for position estimation enhances the accu-

racy, a practical propagation environment that is characterised with noise, will also diminish the level of accuracy. The research work presented in this thesis aims to increase the level of accuracy of UWB-based position estimation when a noisy practical propagation environment is considered.

Chapter 3

UWB-based Elliptical Localisation of Objects of Interest

3.1 Introduction & Problem Statement

Conventionally, geometric UWB-based approaches to indoor position estimation are either defined on the assumption that multipath signals in the immediate environment have been resolved in a pre-position estimation or pre-localisation step; or defined without an explicit consideration of the impact multipath signals will have on the specified approach [18, 37, 93–95]. Intuitively, this assumption is justified due to the fact that one of the inherent properties of the UWB technology is its ability to resolve multipath signals [21, 41]. However, barring several assumptions, this multipath resolving property has not been coherently elaborated upon in practice [21, 23, 24, 41]. Assuming that the multipath signals have

been resolved in a pre-localisation step ensures that the multipath propagation scenario which is expected in practice, is easily simplified and downgraded to a two-path propagation scenario which simultaneously simplifies the underlying position estimation task. In this chapter, a full position estimation solution which comprises of a pre-localisation step that precedes the actual task of estimating the position of the NOI, is proposed. The proposed pre-localisation step makes use of the electrically-driven reflection properties of the employed UWB signals to extract relevant position-defining information from them when they interact with specific objects in the immediate environment. In turn, the extracted information is used to reduce the multipath propagation scenario into a two-path propagation scenario. As depicted in Figure 3.1, in the two-path propagation scenario, the two paths are the LOS path between the transmitter and receiver, and the path travelled from the transmitter to the receiver via the NOI (i.e. T_x - NOI - R_x).

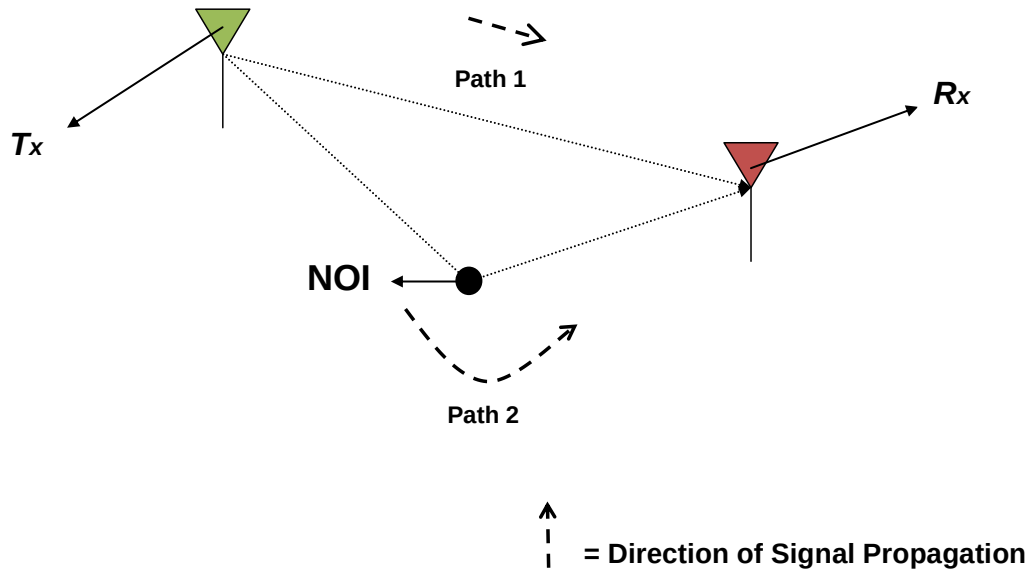

Figure 3.1: The two-path propagation scenario

As a direct consequence of this change in propagation scenario, a way is paved for the direct implementation of typical position estimation techniques to solve the simpler two-path position estimation problem. Having mentioned that, for the entirety of this chapter, the UWB-driven geometric multilateration technique referred to as 'Elliptical Localisation' (EL) by Zhou *et al.* [37], is utilised to solve the simpler two-path position estimation problem once the pre-localisation step has been completed.

The EL position estimation technique determines the position of a NOI by converting information extracted from the geometric links between paired transmitters and receivers into a series of ellipse defining parameters [37]. These parameters are then used to define n ellipses which are cleverly manipulated in an attempt to determine the position of the target. Conventionally, n which refers to the number of defined ellipses, is required to be at least three and four for 2-D and 3-D position estimation respectively [7, 19, 24]. With n restricted to three for 2-D position estimation using the EL approach, a minimum of three intersecting ellipses are required to estimate the position of the NOI.

In this chapter, it is shown that by carefully considering the inherent properties of the UWB technology, the 2-D estimate of a NOI's position in an indoor environment using the EL technique can be achieved efficiently when n is restricted to two. The restriction of n to three for 2-D position estimation using the conventional EL is equivalent to a hardware requirement of three receivers and one transmitter. Therefore, with n restricted to two, only two receivers and one transmitter are required to complete the position estimation task. As a direct consequence, it is shown that the current hardware requirement for 2-D position estimation using the EL technique, can be reduced.

3.2 Background

In a similar manner to that which Figure 3.2 depicts, Zhou *et al.* [37] attempt to determine the absolute coordinates of their NOI (i.e. a tag) by initially transmitting a UWB signal from a single transmitter which they place at the centre of their setup/experiment. The transmitted signal is received by the tag, amplified by a mini-circuit ZX60-14012L amplifier and then re-transmitted to m receivers. For the 2-D case which they consider, m is three; hence the re-transmitted signal is received by three receivers (R_{x1}, R_{x2} and R_{x3}) at different distances and times of arrival respectively. With each transmitter and receiver combination (i.e. T_x - R_{x1}; T_x - R_{x2}; T_x - R_{x3}) defining an ellipse that is relative to the position of the tag; the position of the tag then becomes the unique intersection point of all the defined ellipses [7, 37].

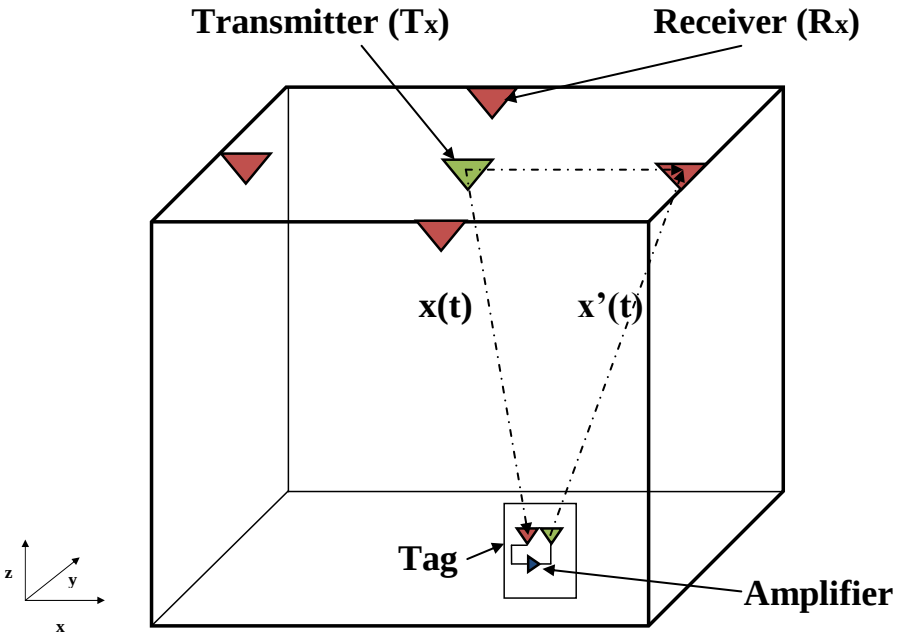

Figure 3.2: Setup for Elliptical Localisation in Indoor Environment

To ensure that the intersection points gave the absolute coordinate of the tag and not its relative one, the placement of R_{x1}, R_{x2}, R_{x3}, T_x as well as the tag in their setup had to also be an absolute one. As Zhou *et al.* were quick to point out, the amplification of the received UWB signal at the tag prior to its re-transmission introduced a time delay which from a time-based position estimation vantage point can be regarded as an error source [19, 24, 37]. The time delay is due to the additional signal propagation time required during re-transmission. Due to the dependence of time-based position estimation on the accurate measurement of the relevant times of arrival, this time delay ultimately ensures that the measured times of arrival of the transmitted signal at all the relevant receivers are never accurate. Consequently, the level of accuracy of the estimated position(s) of the NOI based on these measurements will always be relatively low.

Another important observation made from the research work presented in [37] is that they assumed a noise-free two-path propagation model all through their analysis as compared to a much more realistic multipath propagation model which is the most practical model especially when a UWB signal is used for transmission in an indoor environment. To this effect, for the entirety of the research work presented in this chapter, we tackle this by considering a practical multipath propagation scenario. With that considered, a pre-localisation algorithm which is capable of extracting position estimation relevant UWB signals from the available multipath signals in the environment. This algorithm caters for the problem of ensuring that the locations of all the variables involved in the position estimation process are absolute without having to make unnecessary and potentially erratic estimations, is proposed. Moreover, the proposed algorithm also ensures that no

additional delay is introduced as a direct result of either an additional amplification circuitry or any other process. Essentially, this pre-localisation step ensures that the EL position estimation technique achieves a high level of accuracy in a practical environment.

3.3 Problem Formulation

Succeeding the interaction of a UWB signal $x(t)$ with a lossy material of known electric properties such as its dielectric constant, permittivity, return loss; and its conductivity, $x(t)$ reflects back to the receiver; and its shape changes [21, 41]. Having a priori knowledge of some of these electrical properties ensures that it is possible to determine the shape of the UWB signal that results from this interaction. The dielectric constant (ϵ_r) of a lossy material is a dimensionless number that serves as a measure of the relative permittivity of the lossy material; and it is a parameter of relevance when defining the reflection coefficient $r(t)$ of the lossy material [21, 96, 97]. From [96] and [98], the time domain reflection coefficient of a lossy material can be expressed as:

$$r(t) \approx \pm \left[K\delta(t) + \frac{4k}{1-k^2}\, e^{-\alpha t} \sum_{i=0}^{4} f_i(t) \right] \tag{3.1}$$

$$\text{where } K = \frac{1-\beta}{1+\beta},$$

$$\beta = (\sqrt{\epsilon_r - \cos^2\theta_i}\,)/\epsilon_r \sin\theta_i \,, \alpha = \frac{120\pi\sigma c}{2\epsilon_r},$$

$$A = \frac{K\alpha t}{2} \,, X = e^{-K\alpha t/2},$$

$$\sigma = \text{electrical conductivity of lossy material,}$$

$$f_0(t) = \frac{\alpha K}{2} X,$$

$$f_1(t) = -\frac{\alpha}{2K} \left[(A+1)X - 1\right],$$

$$f_2(t) = \frac{\alpha^2 t}{8K^2} \left[(A+2)X - 2 + A\right],$$

$$f_3(t) = -\frac{\alpha^3 t^2}{48K^3} \left[(A+3)X - 3 + 2A - A^2/2\right],$$

$$f_4(t) = \frac{\alpha^4 t^3}{384K^4} \left[(A+4)X - 4 + 3A - A^2 + A^3/6\right].$$

With the values of ϵ_r and σ of the lossy material as well the incident angle of the transmitted signal (θ_i) known, the other sub-parameters (i.e. β, X, A, e.t.c.) that define $r(t)$, can also be determined accordingly. Theoretically, with a priori knowledge of ϵ_r, convolving $r(t)$ in equation 3.1 with the impulse response of a UWB channel $h(t)$; and the transmitted UWB signal $x(t)$ should yield the expected reflected signal $s(t)$ when a UWB signal is reflected off a lossy material with a reflection coefficient expressed as $r(t)$ [21, 23, 24].

In [96], an attempt was made to determine the ϵ_r of a lossy material by measuring it experimentally across a range of frequencies (2 GHz to 11 GHz). Following the measurement in this frequency range, the values were averaged and the mean value was determined. Consequently and contrary to what is expected from a UWB signal, $s(t)$ did not show a significant amount of distortion when the convolution described previously was performed. This is because averaging the relative dielectric constant values does not necessarily account for all frequencies in the UWB communications spectrum range [21, 24]. This issue is tackled later

on in this chapter by performing an IFFT on the measured relative dielectric constant waveform to get its time domain equivalent $\epsilon_r(t)$. Replacing all ϵ_r dependent terms in equation 3.1 with $\epsilon_r(t)$, ensures that all the frequencies in the UWB spectrum are considered; and consequently a better estimate is generated for the expected received signal $s(t)$ [21, 23, 24].

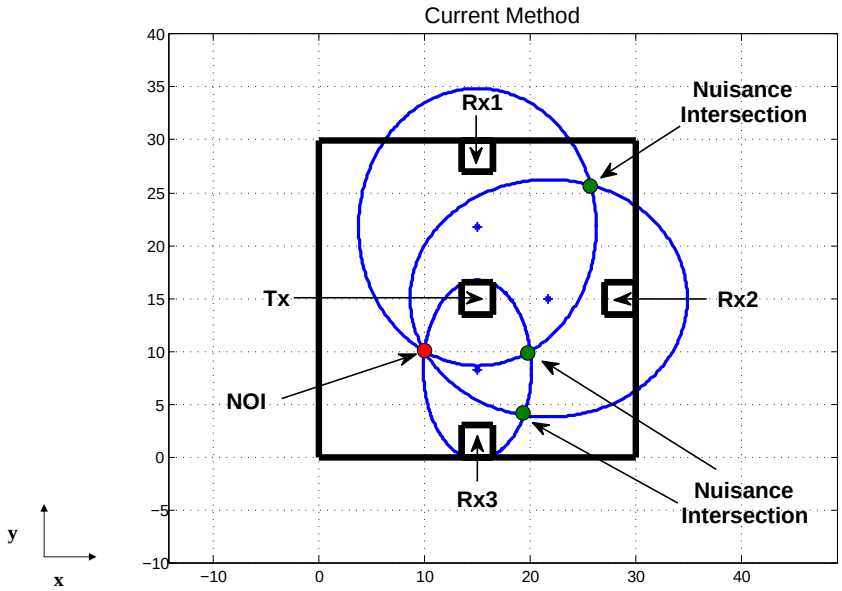

Figure 3.3: Depiction of UWB-based Elliptical Localisation

In a similar manner to that which Figure 3.3 depicts, UWB-based EL is predominantly achieved by initially placing a sole transmitter (T_x) at the center of the environment or room where the NOI is located. Thereafter, three receivers (R_{x1}, R_{x2} and R_{x3}) are placed in the environment or room in such a way that there is a direct LOS path between each transmitter-receiver combination (i.e. T_x - R_{x1}, T_x - R_{x2} and T_x - R_{x3}) [37]. For each of these combinations, an ellipse that comprehensively includes a unique coordinate that denotes the 2-D location

of the NOI can be constructed based on the 'range sum' which is a function of their Time Difference (TD). To all intents and purposes, the TD is defined as the scalar subtraction of the time it takes for the transmitted $x(t)$ to travel from T_x to $R_{xi(i=1,2,3)}$ respectively by virtue of the LOS provisioning; from the time it takes for the reflected UWB signal $s(t)$ to arrive at $R_{xi(i=1,2,3)}$ if the propagation path of the signal was from T_x to the passive tag and then to $R_{xi(i=1,2,3)}$ (i.e. the amplification and subsequent re-transmission).

With three ellipses collectively constructed for all the transmitter-receiver combinations, there will be one unique set of intersection coordinates of the three ellipses. This set of coordinates defines the position of the NOI. However, this process can only be executed in a straightforward manner if it occurs in a two-path propagation where the effect of multipath signal propagation is not considered. Generally, an UWB transmission inadvertently introduces a large number of indistinguishable reflected multipath signals which are usually a direct consequence of the fact that objects in a given environment or room are made from materials with dissimilar electrical properties.

This fact means that the downgrading of the multipath propagation scenario to a two-path propagation scenario to cater for EL approach proposed in [37] can only be plausible if there was a way of distinguishing between all the reflected multipath signals in an attempt to identify the signals that were reflected off the NOI. On identification of these signals, the TD could then be found, and in turn it could be used to determine the ellipse defining range sum for any of the transmitter-receiver combinations as discussed earlier by simply multiplying it with the speed of light [19, 24, 37].

3.4 Proposed Solutions

3.4.1 Frequency Dependency of Dielectric Constant

With the bulk of the research work presented in this chapter reliant on the proper estimation of the reflection coefficient of the NOI, it becomes a necessity to address the previously mentioned averaging of the ϵ_r performed in [96]. Essentially, the aim of the analysis presented in this section is to demonstrate that from a position estimation vantage point, it does not suffice to average the ϵ_r value when defining the $r(t)$ of a NOI whose position is to be determined using the UWB technology. Averaging the ϵ_r value effectively ensures that it is impossible to properly predict or define the expected reflected signal when a UWB signal interacts with a lossy material with known electrical properties.

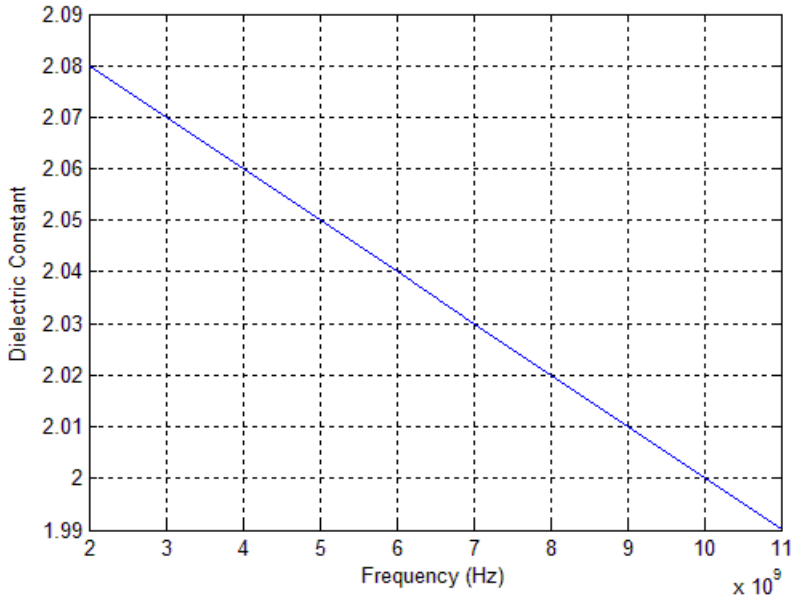

Figure 3.4: Dielectric constant of a wooden door

For this analysis, the same lossy material experimented upon in Nia-tong *et al.*

[96] is used. From [96] and Figure 3.4, it is clear that the dielectric constant of the lossy material in question assumes the shape of a straight line equation of the form:

$$\epsilon_r = -Uf + 2.1$$

$$\text{where } U = 1 \times 10^{-11}\ (Hz)^{-1}$$

$$\text{and } f \text{ ranges from 2 GHz to 11 GHz}$$

Taking the IFT of ϵ_r would yield its time-domain equivalent $\epsilon_r(t)$. From [96], the time domain reflection coefficient of a lossy material is expressed by equation 3.1 where the angle of incidence of the transmitted UWB signal is denoted by θ_i. From equation 3.1, it can be deduced that the ϵ_r dependent parameters of $r(t)$ are

$$K = \frac{1-\beta}{1+\beta},$$

$$\beta = (\sqrt{\epsilon_r - \cos^2\theta_i}\ )/\epsilon_r \sin\theta_i,$$

$$\alpha = \frac{120\pi\sigma c}{2\epsilon_r}$$

Replacing ϵ_r with its time domain equivalent $\epsilon_r(t)$ will change the above parameters respectively to

$$K = \frac{1-\beta}{1+\beta},$$

$$\beta = (\sqrt{\epsilon_r(t) - \cos^2\theta_i}\ )/\epsilon_r(t) \sin\theta_i,$$

$$\alpha = \frac{120\pi\sigma c}{2\epsilon_r(t)}$$

With $s(t)$ defined as the expected reflected signal when a UWB signal interacts with and reflects off the lossy material, Figures 3.5 and 3.6 depict $s(t)$ when ϵ_r and $\epsilon_r(t)$ are respectively used as the dielectric constant of the material. By comparing both figures, it is evident that the UWB signal suffers a lot more distortion in the case where $\epsilon_r(t)$ defines the dielectric constant of the lossy material. This is the expected result based on the fact that an UWB signal has a wide bandwidth (i.e. different frequency components). In contrast to what [96] concludes, a UWB signal that is reflected from a lossy material will not preserve its waveform during propagation, its resultant waveform will be a function of $\epsilon_r(t)$ and $r(t)$ (i.e. equation 3.1) consequently.

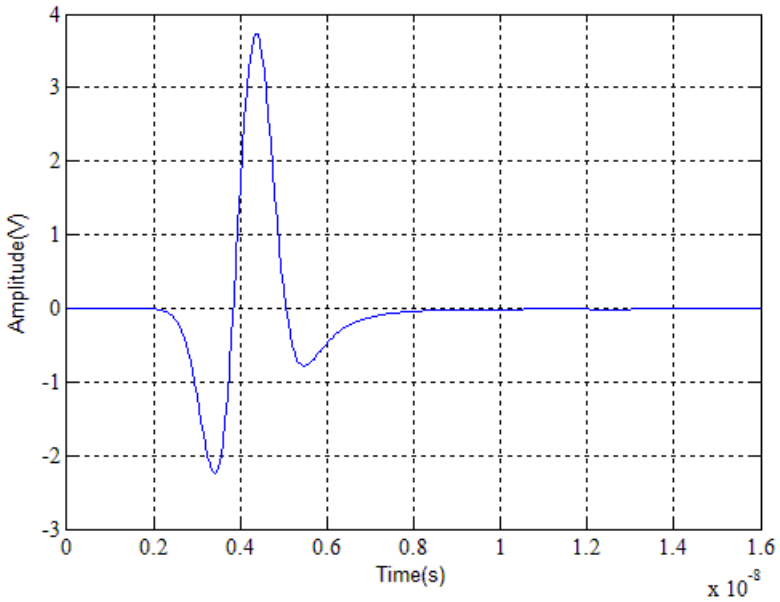

Figure 3.5: $s(t)$ when ϵ_r is considered

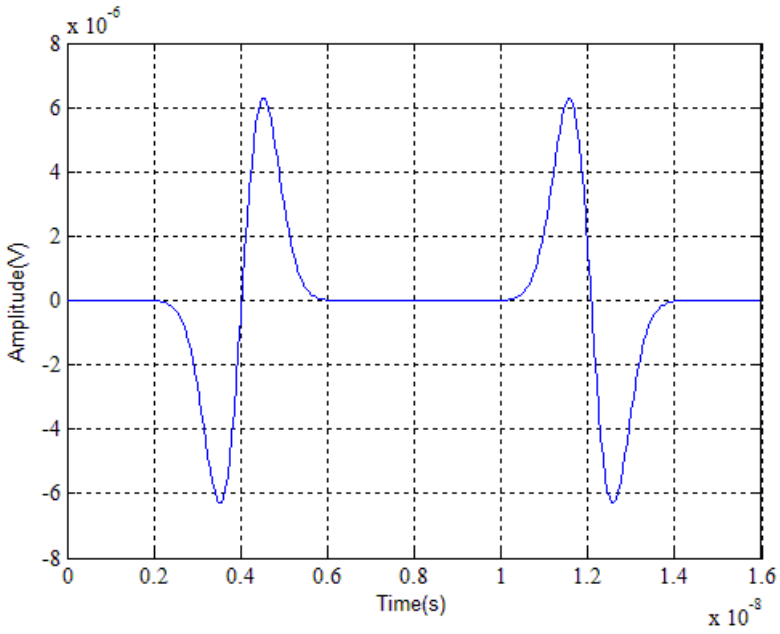

Figure 3.6: $s(t)$ when $\epsilon_r(t)$ is considered

3.4.2 Pre-Localisation in Multipath Environment

As it is subtly hinted in the previous section, it is possible to estimate $s(t)$ when a UWB signal reflects off a lossy material whose dielectric constant is known [21, 23, 24]. One of the keys to estimating this expected waveform lies within the angle of incidence θ_i of the UWB signal. When the signal strikes a lossy material at an angle of θ_i, $s(t)$ assumes a specific shape. The relationship between θ_i and $s(t)$ forms the basis for the proposed pre-localisation algorithm when a multipath environment is considered. In a typical multipath propagation environment, when a UWB signal is transmitted, there will be a number of received multipath signals due to the interaction of the transmitted UWB signal with different objects in the immediate environment. As a result of the predictably high number of received multipath signals, it is almost impossible to properly define the ellipses that are required for the exact estimation of the NOI's position using EL without knowing

the exact multipath signal that reflected off the NOI. To this effect, it becomes a necessity to put in place a mechanism that is able to extract the necessary signals that are required to define the ellipses and ultimately solve the underlying position estimation task.

3.4.3 Signal Extraction Process

Prior to the signal extraction process, it is assumed that in addition to knowing $\epsilon_r(t)$, all the electrical properties and parameters that are relevant to the proper definition of the reflection coefficient $r(t)$ of the NOI (i.e. passive tag) is known. With these parameters assumed to be known, it becomes possible to define $s(t)$[1]. Figure 3.7 depicts the proposed signal extraction process.

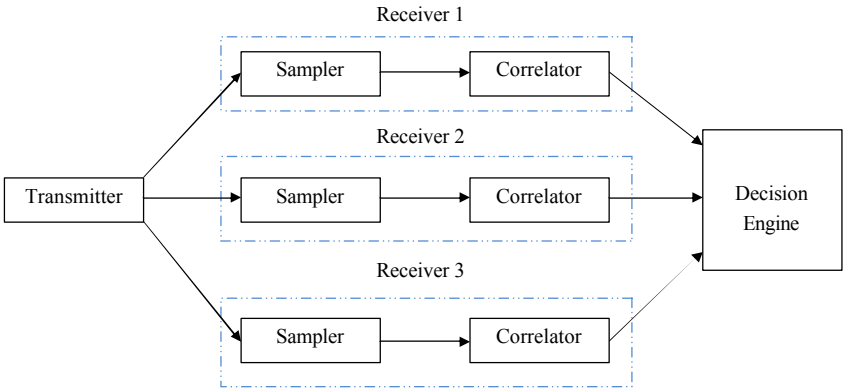

Figure 3.7: Diagrammatic representation of signal extraction process

The signal extraction process involves the sampling of the received signal at all three receivers (R_{x1}, R_{x2} and R_{x3}) at regular intervals, correlating the sampled signal with a database of template signals to find out if the signal is indeed one

[1] $s(t)$ is the received signal and it is defined as the convolution product of $x(t)$, $h(t)$ and $r(t)$

that was reflected off the NOI; and finally using a decision engine to determine the signals that would be either used for generating the ellipse in the EL approach or extrapolated for use with other geometric-based localisation approaches.

Step 1: The first step in this process is a so-called 'machine learning step'. In this step, the database of template signals for each transmitter-receiver combination (i.e. T_x - R_{x1}, T_x - R_{x2} and T_x - R_{x3}; where T_x = Transmitter, R_{x1} = Receiver 1, R_{x2} = Receiver 2 and R_{x3} = Receiver 3) is generated. Due to the fact that the generation of $s(t)$ is dependent on the reflection coefficient of the NOI and the angle at which the transmitter strikes it, it is possible to determine the exact form of $s(t)$ when the transmitted UWB signal strikes the NOI at any angle by varying the values of θ_i in equation 3.1 between 0 and 2π. It was observed during simulation that at various values of θ_i, there is a change in the shape of $s(t)$. To ascertain the level of dissimilarity, a cross-correlation[2] between two samples of $s(t)$ variants which were obtained at two different values of θ_i, was performed. As expected, the cross-correlation resulted in a correlation value which was less than one[3] (i.e. those two samples are uncorrelated). Consequently, it was hypothesised that if the process of correlating samples of $s(t)$ variants for θ_i values that ranged from 0 and 2π continuously resulted in correlation values that are less than one, all samples between 0 and 2π could be collated and used to populate the database of template signals. To verify this hypothesis, $s(t)$ for a constant $\epsilon_r(t)$ and values of θ_i being 0.25π, 0.26π, 0.28π, 0.29π, 0.30π and 1.30π, were generated.

The primary reason for using these arbitrary values was to facilitate the de-

[2]Cross-correlation is measure of the similarity between a pair of waveforms. A cross-correlation measure of '0' infers that the compared waveforms are not similar while a cross-correlation measure of '1' infers that the compared waveforms are similar.

[3]This is expected because theoretically, there will not be two completely identical samples of $s(t)$.

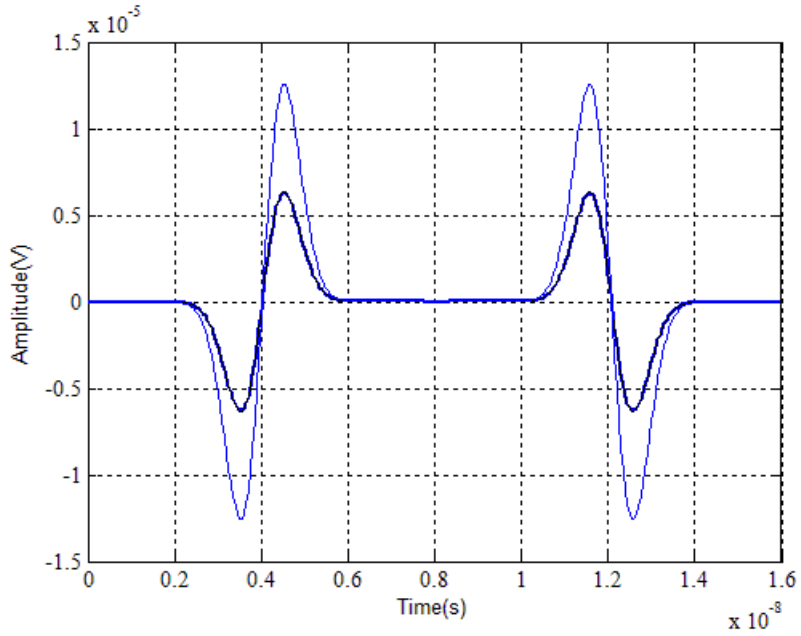

Figure 3.8: $s(t)$ for different values of θ_i when $\epsilon_r(t)$ is considered

piction of the various shapes of the resultant signal $s(t)$ when the values of θ_i is increased gradually and then a lot more significantly. Figure 3.8 shows $s(t)$ for these six values of θ_i. The plot with a higher amplitude in the figure is the reflected signal when θ_i is 1.30π while the other plot is a concatenation of the plots for the five other values of θ_i. Because 0.25π, 0.26π, 0.28π, 0.29π, 0.30π all differ from each other very slightly, the change in waveform seems less apparent as compared to the change in waveform when θ_i becomes 1.30π. However, a cross correlation between any two of the signals generated from these set of θ_i values yield a cross correlation value which is less than one;hence the reflected signals generated by all values will be uncorrelated with respect to each other. This verifies the hypothesis and validates the collation of $s(t)$ for θ_i ranging from 0 and 2π. Consequently, for each transmitter-receiver combination, the generated $s(t)$ in the 0 and 2π range is stored and the collection of all stored received signals

are referred to as the *database* of template signals.

Step 2: At this stage of the pre-localisation process, the EL position estimation technique is invoked and at time t_{sample}, the received signals at all three receivers are sampled. t_{sample} is typically equal to twice the time taken for a direct path propagation between any transmitter-receiver combination. The sampling of the received signal occurs at t_{sample} because it is expected that all three receivers would have received at least one reflected signal by then [21, 24]. For each combination, all sampled signals are respectively cross correlated with the database of template signals to determine if the sampled signal is indeed one reflected off the object; and also to determine the angle of incidence θ_i of the UWB signal that generated reflected multipath. A cross correlation value of '1' would mean that the signal is indeed one reflected from the target object and a non '1' value would mean otherwise. In practice, a cross correlation value of '1' is never achieved due to the nature of the propagation environment amongst other factors, hence the sampled signal that leads to the highest correlation value is deemed as the template signal. Once this template signal is identified, θ_i can be inferred. This inferred angle is equivalent to the θ_i of $s(t)$ because the θ_i of the signal that generated the template signal will intuitively be the same as that of the signal that generated $s(t)$.

Step 3: At this point of the signal extraction process, the decision engine process is invoked. Once θ_i is determined for all three receivers, they are paired in the following manner: angle of incidence of R_{x1} is paired with that of R_{x2} whilst that of R_{x2} is paired with R_{x3}. Figures 3.9 and 3.10 depicts the pairing process. Letting θ_1, θ_2 and θ_3 denote the θ_i of the (T_x - R_{x1}), (T_x - R_{x2}) and T_x - R_{x3}) combinations respectively, θ_4 is defined as the sum of θ_1 and θ_2; and θ_5 is

defined as the sum of θ_2 and θ_3. As depicted in Figures 3.9 and 3.10, when three ellipses intersect at any point on the x-y plane, either θ_4 or θ_5 has to be 0.5π (90°). In order to extract the signal, the pair of reflected signals that maximizes the values of either θ_4 or θ_5 to 0.5π with every aforementioned pairing, are singled out.

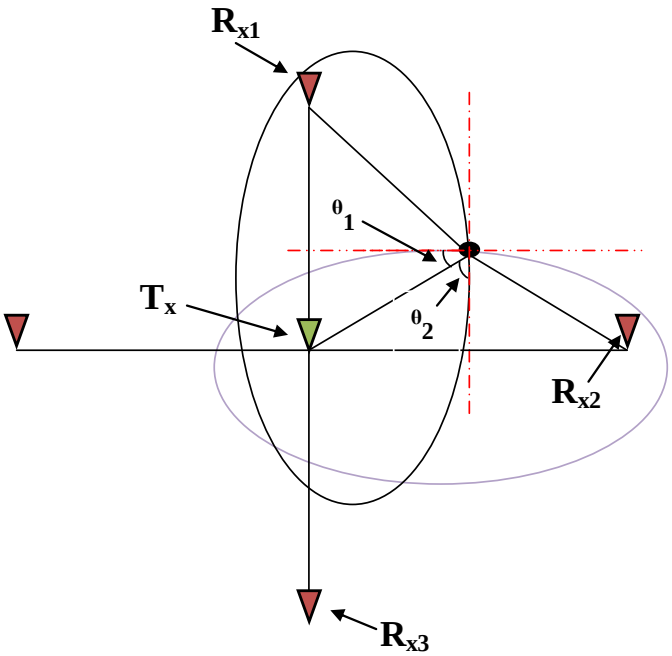

Figure 3.9: Intersection of ellipses generated by the R_{x1} and R_{x2} pairing

If it is impossible to single out a pair of reflected signal that maximises these values in both combinations for the current sampled signals, the sampled reflected signals are discarded and after t_{sample} has elapsed, another set of received signals are sampled. In the case of finding that a pair of reflected signals that maximizes the sum of the two values of θ_i lies in the R_{x1} and R_{x2} pairing at a fixed time t, this pair of signals is used as two of the three geometric parameters needed to fully define the ellipse. The last geometric parameter is taken from the R_{x2} and R_{x3}

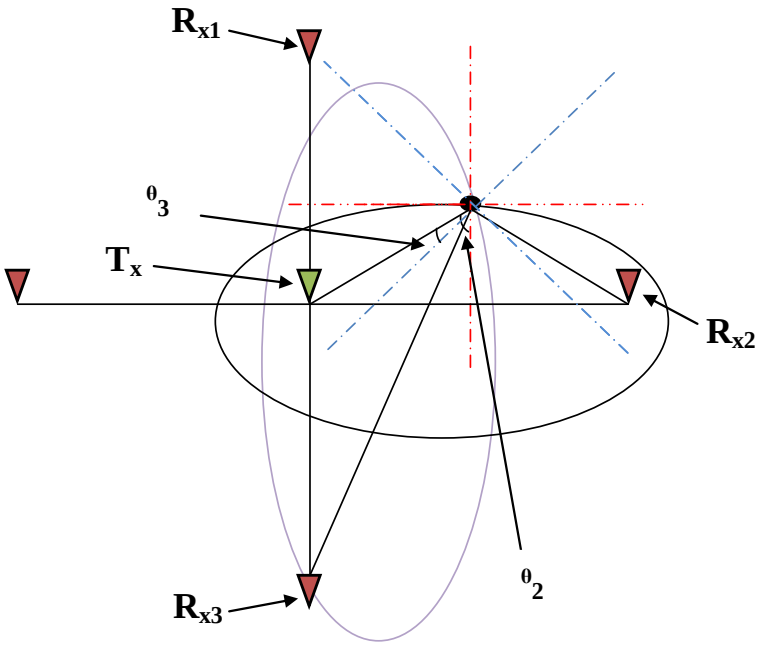

Figure 3.10: Intersection of ellipses generated by the R_{x2} and R_{x3} pairing

pairing. From Figure 3.10, it is clear that θ_5 (i.e. $\theta_5 = \theta_2 + \theta_3$) would not be 0.5π, however it can be inferred that $\theta_3 < \theta_2$. Based on this inference and by comparing θ_3 with θ_2, the third parameter can be defined as the signal with a property of $\theta_3 < \theta_2$. With all the three ellipse defining parameters determined, it becomes possible to downgrade the multipath propagation scenario into the simpler two-path propagation scenario described in [37]. At this junction, it is noteworthy to mention that range sum required for the execution of the EL position estimation technique could be alternatively determined as follows:

- Following the successful implementation of the pre-localisation algorithm, if the time of arrival (TOA) of the direct LOS propagated UWB signal for each combination is denoted as $t_{i=1,2,3}$, the TOA of the reflected received signal determined from the pre-localisation step can be denoted as $t_{i=1,2,3}$ + $\alpha_{i=1,2,3}$. t_1 refers to TOA for combination T_x - R_{x1}, t_2 refers to TOA for

combination T_x - R_{x2} and t_3 refers to TOA for combination T_x - R_{x3}. The difference in both signal arrival times gives $\alpha_{i=1,2,3}$ which is defined as the time delay between the two dissimilar received signals. Multiplying $\alpha_{i=1,2,3}$ by the speed of light and then adding it to the direct distance between the respective transmitter-receiver combination yields a distance D. This new distance D is the total distance travelled by the reflected UWB signal and is equivalent to the 'range sum' described in [37]. This range sum is then used to define the three ellipses and the position of the NOI at the same time.

3.4.4 UWB Driven Elliptical Localisation

The transmission range for indoor (residential or office) UWB systems is typically less than or equal to 30 m [21, 23, 24]. With this range considered during the deployment of relevant position defining transmitters and receivers in the defined solution space, the hardware requirement for the EL position estimation approach can be reduced by one receiver. Despite the reduction being a sole receiver, it is shown in the following sections that it leads to an increase in the position estimation accuracy when the Mean Squared Error (MSE) implications are considered. It is also shown that this hardware requirement reduction leads to the NOI's position estimate being dependent on the intersection of two ellipses in contrast to the three intersecting ellipses required for EL. This consequently implies that there is also a reduction in the computational cost required to determine the NOI's position estimate.

As depicted in Figure 3.11, the proposed full solution to the position estima-

tion task operates in two phases. The required hardware are two receivers (R_{x1} and R_{x2}) and one transmitter (T_x) which are placed at coordinates (q, $p-q$), ($p-q$, q) and (q, q) respectively[4]. In the first phase which is referred to as 'post pre-localisation', $s_1(t)$ and $s_2(t)$ are defined as the resultant reflected signals due to the T_x - R_{x1} and T_x - R_{x2} combinations respectively when the pre-localisation algorithm is invoked. Denoting the angle of incidence as $\theta_{ia(a=1,2)}$ (θ_{i1} for T_x - R_{x1} and θ_{i2} for T_x - R_{x2}), θ_{i3} is defined as the sum of θ_{i1} and θ_{i2}. with reference

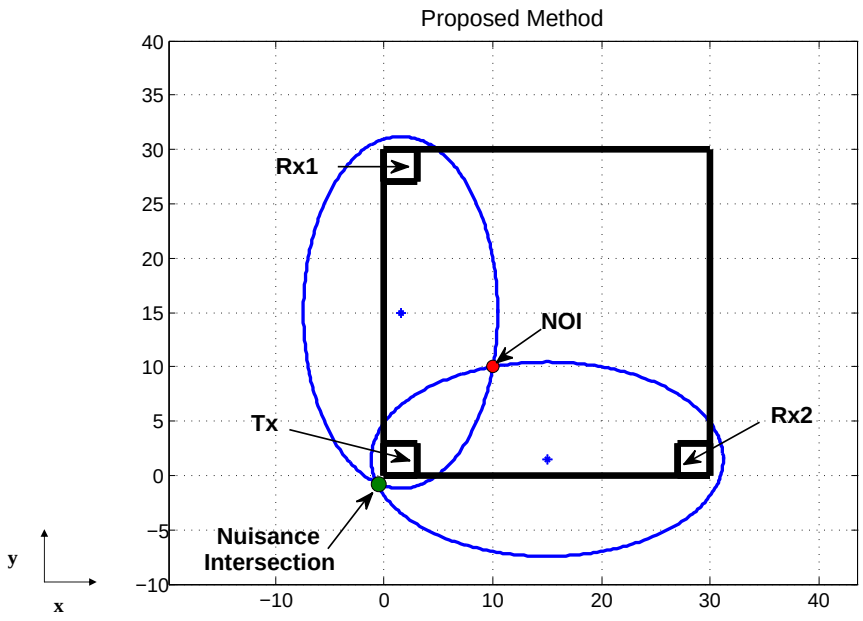

Figure 3.11: Proposed Full Position Estimation Solution

to the operational principles of the EL position estimation technique, the relevant ellipse defining parameters are extrapolated from $s_1(t)$ and $s_2(t)$ and two ellipses similar to those depicted in Figure 3.11 are defined. It was observed that by fixing

[4]With the maximum transmission range being 30 m, p assumes this value. q represents an arbitrary integer value that enforces a separation distance between the transmitter/receiver and the walls of the 2D solution space if required.

the centers of both ellipses to (0, 0.5p) for the T_x - R_{x1} combination and (0.5p, 0) for the T_x - R_{x2} combination, there will be two unique and trivially differentiable intersection points of both ellipses.

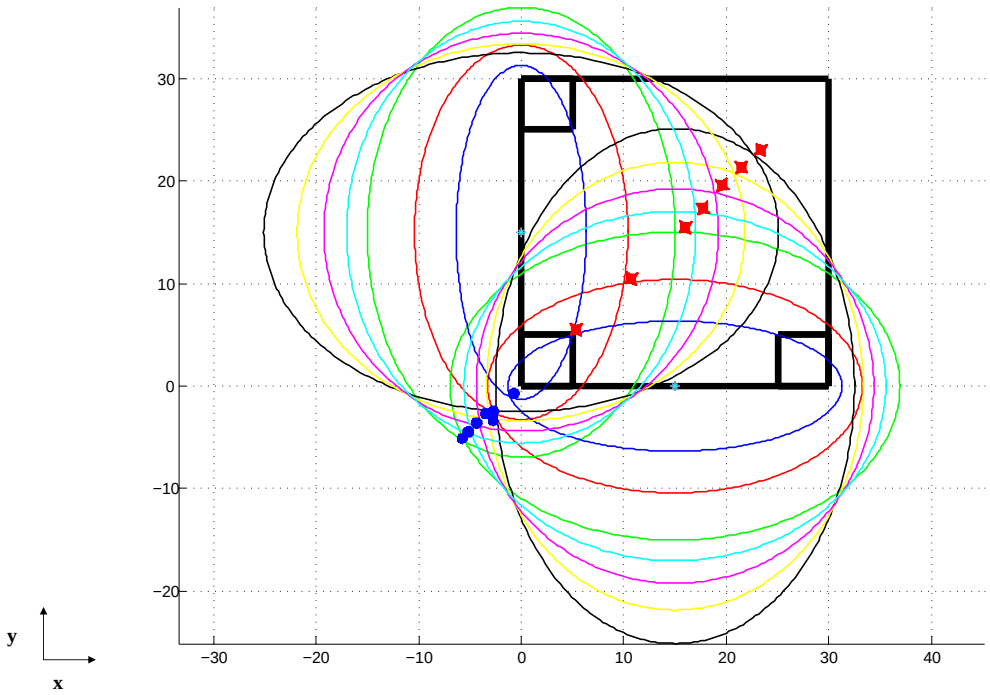

Figure 3.12: NOI Localisation for 7 different positions

The second phase which encompasses the main position estimation process identifies all the intersection points of the two ellipses generated in the first phase and categorises them with an aim to clearly distinguish between intersections that reveal the position of the NOI from intersections based on geometry. As Figure 3.11 illustrates, one of the intersection points will always be a coordinate inside the defined solution space while the other intersection point will always be outside the defined solution space. Additionally, it is clear from Figure 3.11 that the coordinate which lies in the defined solution space would have *positive*

values while the other coordinate would have *negative* values. The geometric dependence of EL ensures that the required coordinate (i.e. position of the NOI) coincides with the positive values which lie in the defined solution space. The robustness of this was then put to test by varying a priori positions of the NOI in the grid whilst keeping the center of the generated ellipses for both combinations fixed as (0, $0.5p$) and ($0.5p$, 0) respectively. As Figure 3.11 depicts, when the NOI is placed at seven different positions, there will be fourteen intersection points. With the stars symbolising intersections in the positive region of the grid and the circles symbolising negative intersections, it is clear that there are seven intersections within the grid and an equal amount of seven outside the grid. This shows that for any position of the NOI within the solution space defined by the UWB transmission range, there will *always* be two dissimilar and easily identifiable intersection points when the ellipse are defined using the fixed center coordinates.

3.4.5 The 3-D Solution Space

To successfully complete the required position estimation task in most applications, it is sufficient enough to determine the 2-D coordinates of the NOI's position; hence the vertical distance component (i.e. 'z' coordinate or height) of the NOI's position is usually omitted from the estimation process. However, in some position estimation applications which require an estimate of the NOI's height/'z' coordinate for its successful completion, this omission is inappropriate. For example, in healthcare applications such as the UWB-based fall detection presented in chapter 5 of this thesis, the 'z' coordinate plays a vital role in defin-

ing the postural orientations required to determine if a patient has fallen down. Having mentioned that, an explicit definition of a full 3-D position estimation technique or a 3-D extension to any 2-D position estimation technique is never quite detailed in modern literature[5]. It is usually ambiguously written that the 3-D estimate of the NOI's position could be obtained by including an extra receiver to the configuration employed for the 2-D solution, in a 3-D solution space [7, 19, 24]. Without any clear information about the placement (optimum or sub-optimum) of the additional receiver in the 3-D solution space based on the underlying 2-D positioning technique, the transition from 2-D to 3-D remains very probable but expectedly, it becomes very cumbersome. To this effect, a 3-D extension to the complete 2-D UWB-based EL technique presented in the previous section is presented in this section. The placement of the extra receiver based on EL is explicitly defined in the 3-D solution space and it is shown that the 3-D estimate of the NOI's position can be determined by splitting the 3-D solution space into two independent 2-D solution spaces (i.e. $x-y-z$ grid is split into $x-y$ grid and $y-z$ grid).

Following the solution space splitting and with reference to the principles of EL, range or proximity measurements are then obtained from the independent 2-D spaces by initially applying the pre-localisation algorithm and then making two transmitter-receiver combinations per 2-D space. More significantly, it is once again illustrated that by considering the properties of UWB in the design process, the hardware requirement which for 3-D position estimation is currently set to at least four receivers and one transmitter, can be reduced by one receiver. Figure 3.13 depicts the front view of the proposed 3-D solution. For ease of

[5]The 3-D solution contains the vertical distance component (i.e. (x, y, z))

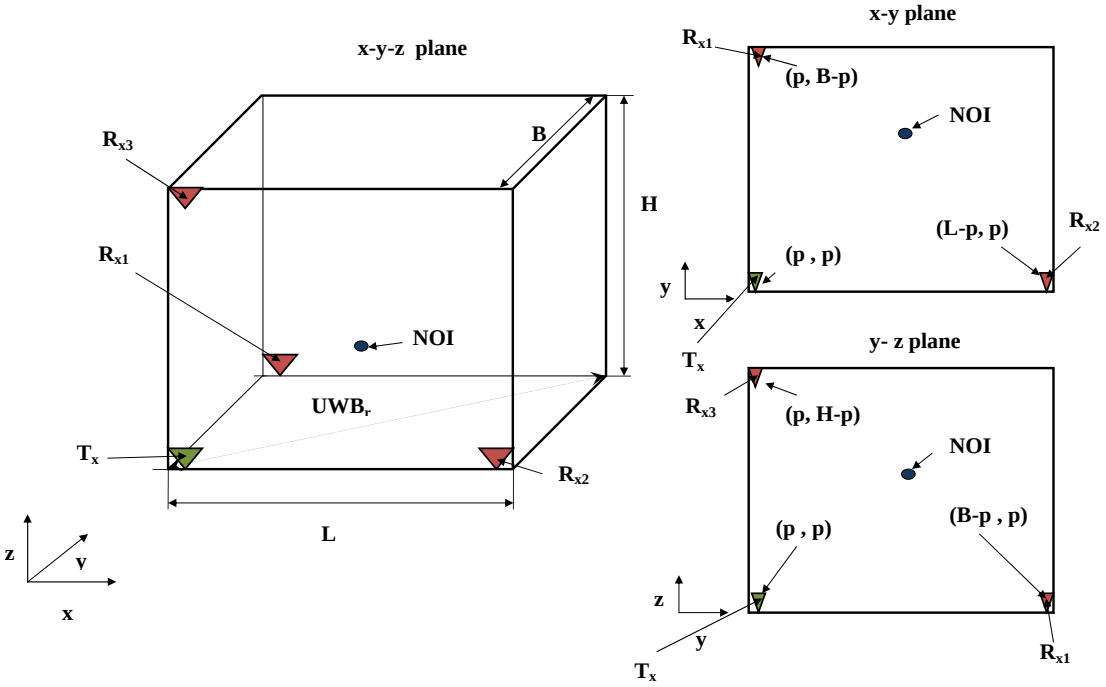

Figure 3.13: Front view of proposed 3D solution

demonstration, it is assumed that the indoor environment takes the form of a cube; hence the Length (L), Breadth (B) and Height (H) of the room are equal (i.e. L = B = H). Additionally, 'L' is set to any value that ensures that the UWB transmission range (UWB_r) is either at a maximum of 30m or does not exceed it [21]. 'p' is an arbitrary integer value that enforces a non-mandatory separation of all transmitters/receivers from the side of the walls. With reference to Figure 3.13, T_x, R_{x1}, R_{x2} and the height/z coordinate defining receiver R_{x3} are placed in the environment. The 3-D solution space is split into the $x-y$ and $y-z$ 2-D grid, and independently, they are used to determine coordinates (x, y) and (y, z) of the NOI's position respectively. Table 3.1 details the coordinate allocation for the relevant transmitter and receivers in both 2-D grids.

Transmitter/Receiver	x-y grid allocation	y-z grid allocation
T_x	(p,p)	(p,p)
R_{x1}	(p, B-p)	(B-p, p)
R_{x2}	(L-p, p)	-
R_{x3}	-	(p, H-p)

Table 3.1: Coordinate allocation of transceivers in independent 2-D solution space

3.4.5.1 The 3-D position estimation

In both 2-D grids and with reference to the operational principles of EL, the employed UWB signal is transmitted asynchronously, range or proximity measurements are made, range sums are determined and corresponding ellipses are constructed for all the grid-relevant transmitter-receiver combinations[6]. The range sum for each combination is used to define the parameters for the individual ellipses as explained in the previous sections and Algorithm 1.

The construction of the ellipses for the $x-y$ grid has been detailed in the previous section; hence only the process of generating the ellipses for the $y-z$ grid is illustrated here. Considering the T_x - R_{x1} and T_x - R_{x3} combinations, when the UWB signal is transmitted, $sd(t)$ and $sr(t)$ are received; and based on their time difference, the range sum is defined. Consequently, ellipses $E_{(i=1,2)}$ in Figure 3.14 are defined in accordance with equation 3.1 (this process is summarised as Algorithm 2 in Appendix A)[7].

$$\frac{(x_i - h_i)^2}{{a_i}^2} + \frac{(y_i - k_i)^2}{{b_i}^2} = 1 \tag{3.2}$$

[6] T_x - R_{x1} and T_x - R_{x2} for the $x-y$ grid; T_x - R_{x1} and T_x - R_{x3} for the $y-z$ grid

[7] $sd(t)$ refers to the resultant signal when the signal travel path is from the transmitter to the receivers by means of the LOS propagation and $sr(t)$ refers to the resultant reflected signal when the UWB interacts with the NOI.

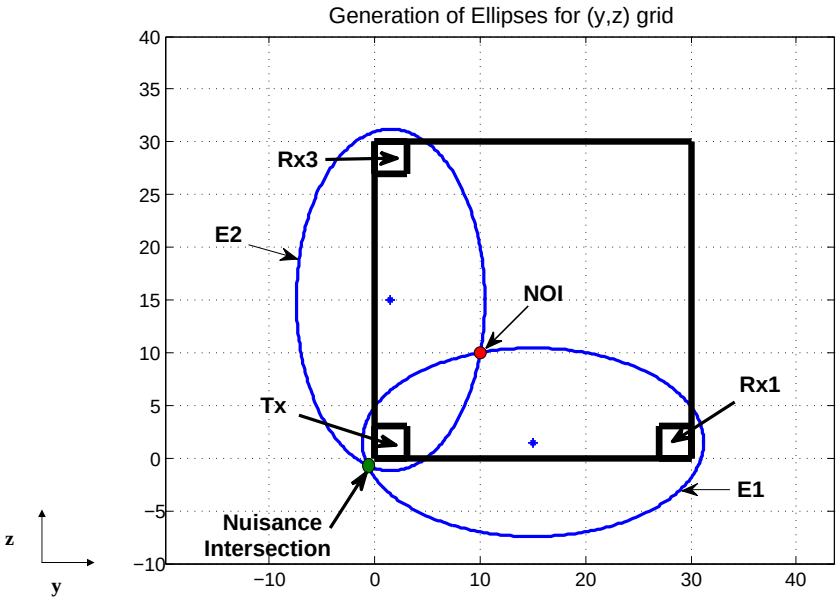

Figure 3.14: Generation of Ellipses for (y, z) grid

a_i is defined as half the range sum; and b_i is defined as $a_1\sqrt{1-e_i^2}$. In turn, e_i represents the eccentricity of the ellipse and is defined as the ratio of f_i to a_i where f_i is half the distance between the two foci of the ellipse. (h_i, k_i) is the center coordinate of the ellipse and it is defined as E_1 are fixed to (0.5B, p) and (p, 0.5H) for ellipses E_1 and E_2 respectively. The intersection of E_1 and E_2 leads to two intersection points which are differentiated accordingly to determine the position of the NOI. The intersection coordinate that defines the position of NOI, becomes the (y, z) coordinate; and upon completion of this same process for the x-y grid, the intersection coordinates that define the position of the NOI become the (x, y) coordinates.

3.5 Numerical Simulations

3.5.1 Proposed Method vs. EL Method (2-D)

Intuitively, the efficiency of both methods rely heavily on the accuracy of the initial TOA measurements obtained from the individual T_x - $R_{xi(i=1,2,3,...n)}$ pairings [7]. Consequently, the necessary comparison parameter between two or more TOA-driven position estimation techniques become the MSE value obtained while performing the position estimation task in the presence of a common TOA measurement variance (TOA-MV). The MSE of a specified estimator in either a 2-D or 3-D ranging solution space is a measure of its accuracy and it is defined fundamentally as the difference between the true value of a parameter and the value that is implicitly defined by the estimator [7, 99].

$$\mathrm{MSE}(\theta_{\mathrm{i=x,y,z}}) = \mathrm{E}[(\theta'_{\mathrm{i=x,y,z}} - \theta_{\mathrm{i=x,y,z}})^2] \tag{3.3}$$

$$\text{where } \theta_{i=x,y,z} = \text{true value and } \theta'_{i=x,y,z} = \text{implied value}$$

Equation 3.3 gives the mathematical representation of the MSE; and the subscript 'i' defines the specific element in the coordinate structure that is under test (i.e. i could either be x, y or z). Considering LOS propagation conditions, the TOA-MV is modelled as a normally distributed gaussian random variable $N(0,\ \sigma^2)$ and 1000 random samples each for a fixed range of standard deviation (σ) of the TOA measurements were generated. The range of σ was fixed to coincide with a localisation accuracy that spans from 3 cm to 30 cm (i.e. 0.1 ns to 1 ns). For the simulation based comparison an indoor environment with a perimeter that is within the UWB transmission range was considered. The NOI was subjected to

a number of fixed coordinates but for demonstration purposes, three randomly picked coordinates namely (28, 28), (10, 10) and (14, 17) are chosen. The initial TOA measurements that result in the determination of all three coordinates using both the current and proposed methods are each corrupted with the randomly generated Gaussian noise samples over the defined σ range; and then the NOI's location is redetermined using both methods. Figures 3.15, 3.16 and 3.17 show

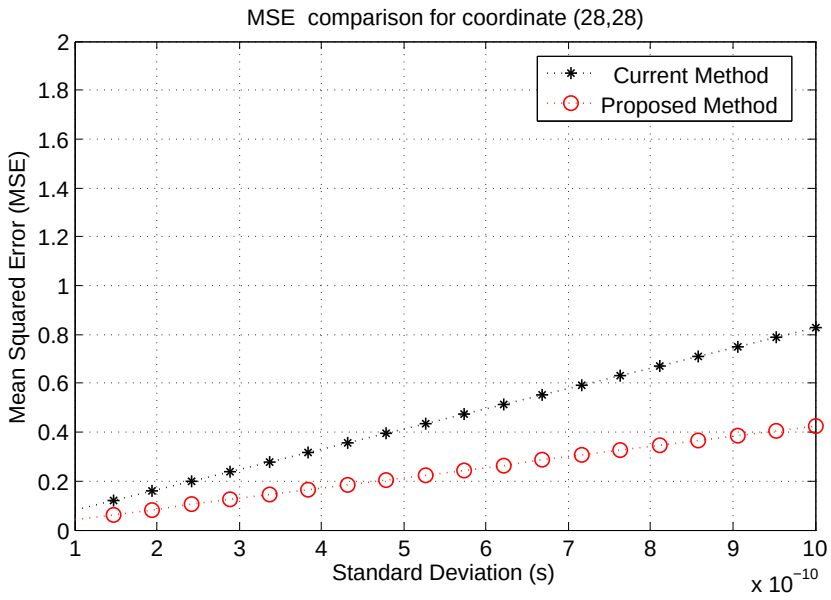

Figure 3.15: Mean Squared Error (MSE) comparison for coordinate (28, 28)

the resultant standard deviation σ vs. MSE plots for the specified σ range when the fixed coordinates are compared with the coordinates redetermined using the corrupted TOA measurements. These plots clearly show that a corruption in the TOA measurements just as it is bound to happen in practice by means of interference or unresolved multipath signals, has as expected a negative effect

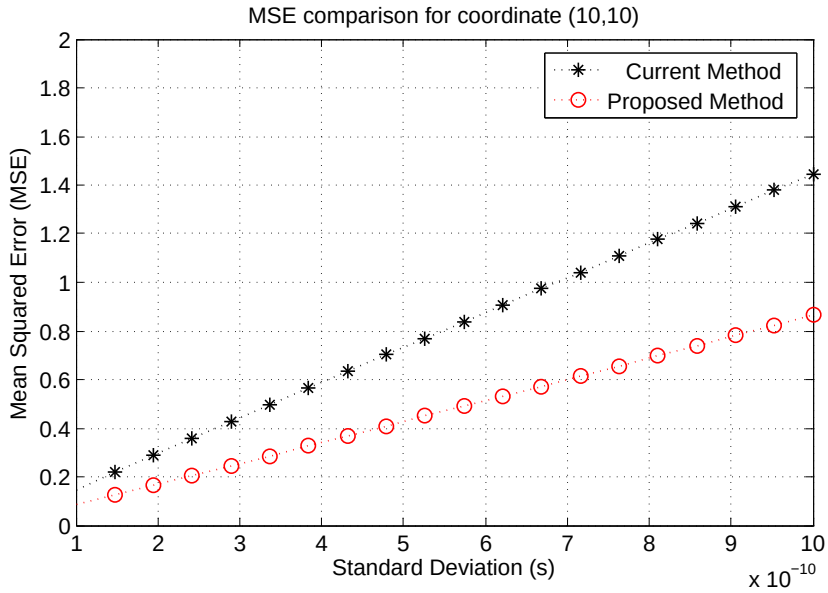

Figure 3.16: Mean Squared Error (MSE) comparison for coordinate (10, 10)

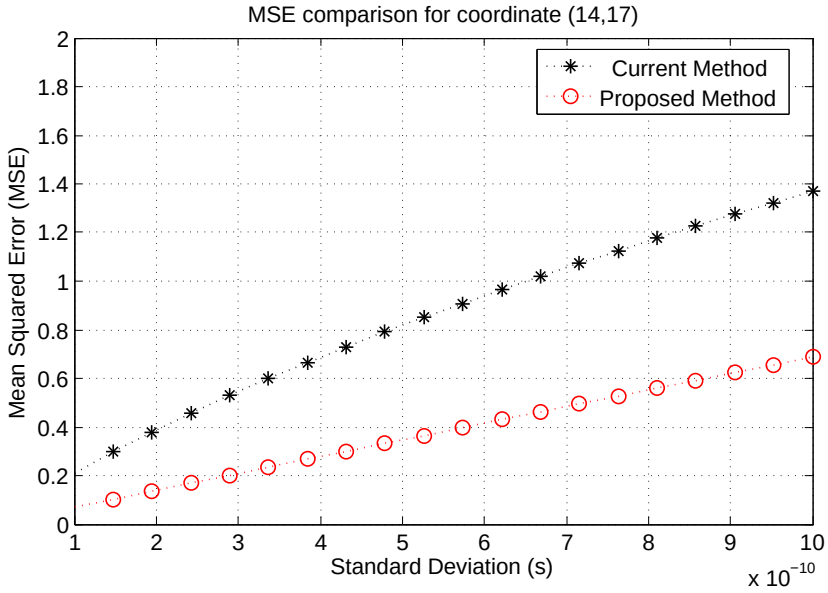

Figure 3.17: Mean Squared Error (MSE) comparison for coordinate (14, 17)

on the localisation effectiveness and efficiency of both the proposed and current EL methods. Additionally and most importantly, it is also clear to see that the proposed method will always have a better location estimation accuracy in terms

of MSE when compared to the current EL method in a 2-D solution space.

3.5.2 Proposed Method vs. EL Method (3-D)

Considering the EL approach and the proposed solution in both the x-y and y-z grids, the NOI was yet again subjected to a number of fixed coordinates. The simulation results for a fixed 3-D coordinates namely (10,9,8) is described below. For the EL approach and the proposed solution in the independent 2-D grids,

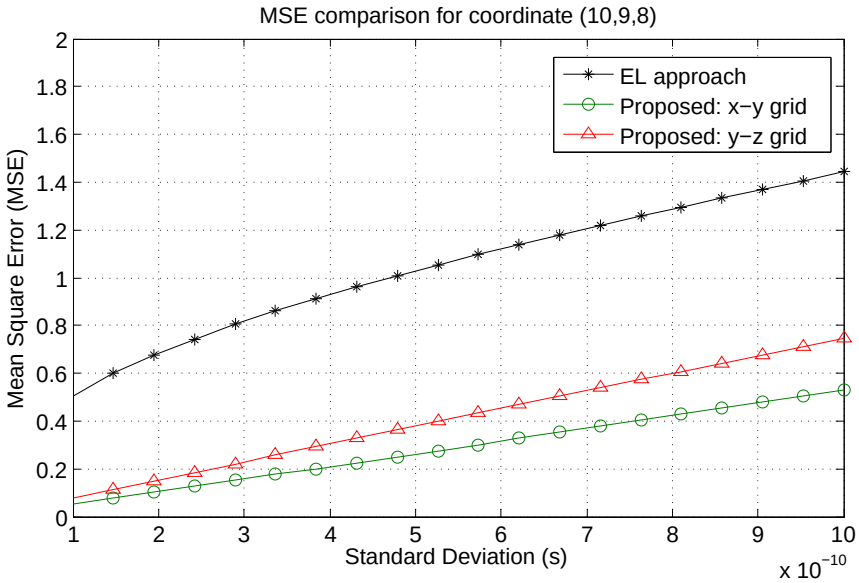

Figure 3.18: Mean Squared Error (MSE) comparison for coordinate (10, 9, 8)

the TOA measurement for the relevant combinations based on Figures 3.3, 3.11 and 3.14 were corrupted with TOA-MV and the position estimate was determined. With both 2-D solution spaces deemed to be independent from each other, it is assumed that the indirect effect of interference, mild NLOS propagation scenarios

and multipath signal propagation, and their collective impact on the defined TOA-MV used in the MSE analysis will be dissimilar in both spaces. To this effect, in order to define the TOA-MV for the two independent solution spaces accordingly, different sets of 1000 random variables were generated within the fixed σ range which was defined in the previous section (i.e. the 2-D case).

Additionally, for the purpose of a fair comparison between all three approaches, the TOA-MV used in the MSE analysis for the EL approach is the same as those defined for the x-y independent solution space due to the fact that EL approach also lies in the x-y grid. Figure 3.18 shows the MSE comparison results of the specified coordinate for the EL approach and the independent grids. As expected, position estimation using the proposed approach for either of the two 2-D grids performs much better than position estimation using the EL approach. It can also be observed from Figure 3.18 that the MSE values of x-y is lower than y-z in the simulated scenario. This MSE value dissimilarity is due to the dissimilar and random nature of the normally distributed Gaussian random variable N(0, 2) that was used to the generate the TOA-MV which was used for the MSE analysis.

3.6 Case Study: Benign Prostatic Hyperplasia (BPH)

In some telecare-driven position estimation application scenarios such as those described in [33–36, 100, 101], the need for an effective means of tracking the real-time positions and movements of a Patient In Care (PIC) could arise. For example, consider a PIC who by virtue of their gender, age and some hereditary

factors is being monitored for early signs of benign prostatic hyperplasia (BPH) or enlarged prostate [102, 103]. BPH is a non-malignant disease (i.e. not cancerous) and it is characterised by an increase in the size of the prostate gland. This increase usually results in the retention of urine in the bladder and ultimately an increase in the frequency at which the BPH patient urinates all through the day and night; hence monitoring the patient's urination patterns over a period of time for any anomaly is potentially a good way to identify early signs of BPH.

A telecare solution would eliminate the tedious and time consuming process a continuous interaction between a medical personnel and the patient would involve in an attempt to monitor the patient's urination patterns over a period of time; and replace it with an alternative system that is not only capable of monitoring the patient's urination patterns and give statistical feedbacks to a control centre, but potentially also intelligent enough to make health related decisions based on these patterns. The research work reported in [104, 105] demonstrates this potential. The telecare task here becomes one that requires the constant monitoring of a patient's urination habits by means of tracking them in an attempt to determine if the observed trends are similar to that which is expected for either an early or a developed BPH case.

One possible approach to solving this task is by remotely tracking the patient's daily visits to the lavatory. By tracking the daily visits to the lavatory, the frequency at which the patient uses the lavatory can be determined, stored and compared with a typical frequency chart for a typical early or developed BPH case to determine the patient's current status. The underlying principle behind any position estimation solution to this task is as thus:

- Each time the patient's location in the defined solution space is determined

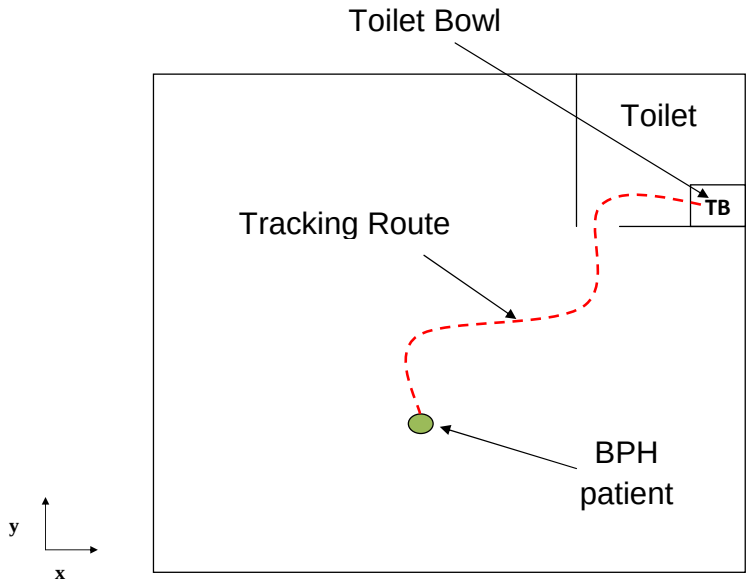

Figure 3.19: Aerial view of proposed tracking scheme

by the employed position estimation system, the location coordinates are translated to the control centre as a symbol (i.e. '+', '-', '*', etc.); and as the patient moves along in the solution space, so does the symbol in the solution space to mimic a progressive moving motion.

- The set of 2-D coordinates that encompasses the lavatory in the defined solution space is fixed, will always be known, and would always be visible to the control centre; and hence once the translated real time coordinate that depicts the location of the patient positively correlates with any of those coordinates that encompass the lavatory, the patient's location would be inferred to be the lavatory.

- Each time the patient is inferred to be in the lavatory, its occurrence is noted and the lavatory visit frequency count is increased by 1

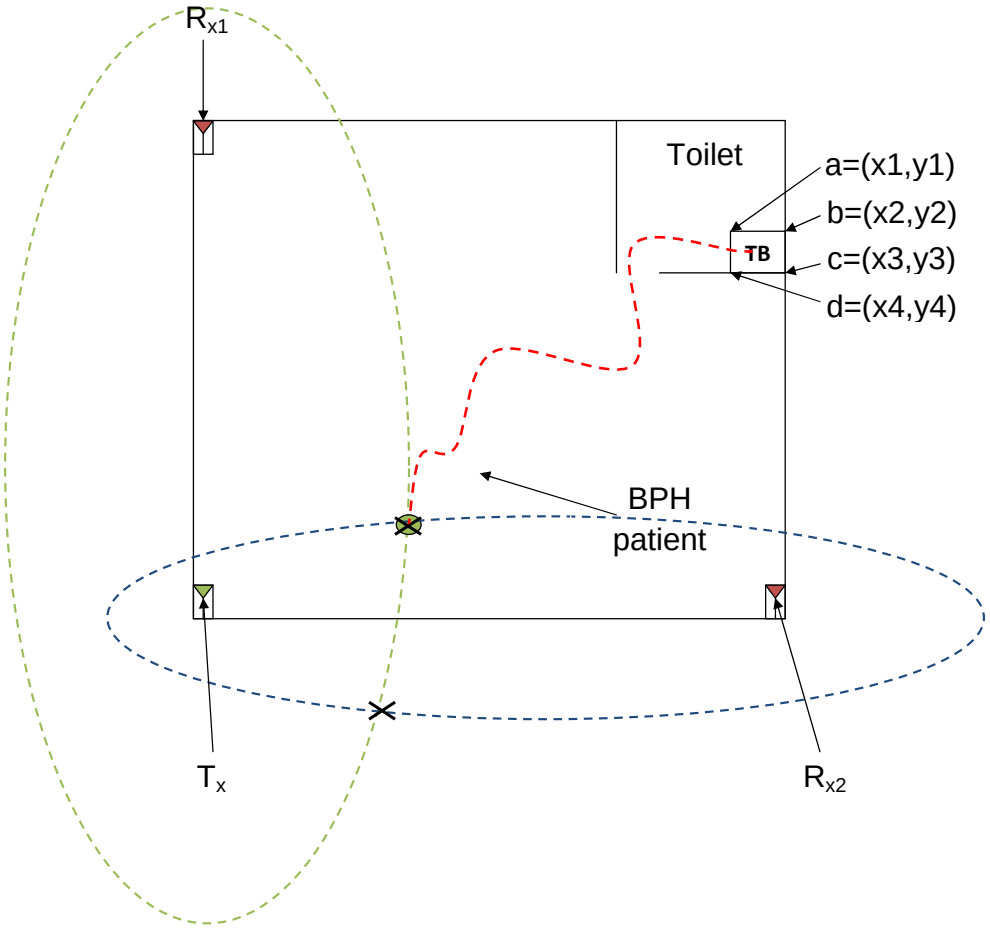

Figure 3.20: Aerial View of Proposed Tracking Scheme

3.7 Conclusion

3.7.1 Summary

In conclusion, a full solution to the position estimation task of estimating the location of NOI has been proposed. The proposed solution is capable of determining an estimate of the NOI's position in either a 2-D or 3-D solution space. It determines an estimate of the NOI's position by initially tackling the problem of multipath propagation using a pre-localisation step. Succeeding the pre-

localisation step, the required number of transmitter and receivers, are placed strategically in a defined environment and the estimate is obtained using EL. In this chapter, it has been shown that the hardware (i.e. transmitter/receiver) requirement for EL can be reduced by a single receiver. It has also been shown through a series of simulation that this hardware reduction leads to an increase in the position estimation accuracy. Additionally, just as Table 3.2 depicts it, the proposed solution has the least number of total hardware requirement when compared to conventional position estimation techniques. More significantly, with all the techniques listed in Table 3.2 being reliant on TOA for their implementation, it can be intuitively deduced that the proposed solution has the lowest computational cost.

Positioning Technique	Tx (2-D)	Rx (2-D)	Tx (3-D)	Rx (3-D)	Total
TOA	1	3	1	4	5
TDOA	1	3	1	4	5
TSOA	1	4	1	5	6
Current UWB-EL	2	4	2	5	7
Proposed UWB-EL	**1**	**2**	**1**	**3**	**4**

Table 3.2: Hardware requirement for different time-based position estimation techniques

3.7.2 Contributions

The main research contributions presented in this chapter can be summarised as follows:

- Definition of a pre-localisation algorithm that identifies position defining

UWB signals from a group of multipath signals in a defined indoor environment.

- Reduction of hardware requirements for EL position estimation by the explicit consideration of the UWB transmission range in the position estimation process.

- Explicit definition of the 3-D position estimation technique and the solution space. This 3-D solution space is characterised by the addition of a receiver to an already defined 2-D solution space. The presented technique determines the estimate of the NOI's position by initially splitting the defined 3-D space into two 2-D independent spaces, and thereafter solving for the required coordinates.

These research contributions have been documented and reported in three technical conference papers titled "UWB based Pre-localisation Algorithm for Aiding Target Location in a Multipath Environment", "UWB-based Elliptical Target Localisation in an Indoor Environment" and "UWB-based Indoor 3D Position Estimation for Future Generation Communication Applications". In September 2011, May 2013 and December 2013, all three papers were accepted for presentation and subsequent publication by the IEEE Conference on Ultra-Wideband (ICUWB) [106], IEEE Workshop on Systems, Signal Processing and their Applications (WoSSPA) [107] and the IEEE Conference on Future Generation Communication Technologies (FGCT) [108].

Chapter 4

A Novel UWB-based Multilateration Technique for Indoor Localisation

4.1 Introduction & Problem Statement

In this chapter, a *novel* multilateration technique which is based on UWB communications is presented. Albeit novel and dissimilar with regards to the approach taken to solve the underlying position estimation problem in comparison with other position estimation techniques, the proposed solution which is coined as Time Reflection of Arrival (TROA) is also geometrically driven. However, as it is shown and described during the course of this chapter, by carefully considering the inherent properties of the UWB technology as a whole; and the reflection properties of transmitted UWB signals specifically, the position estimation error is reduced. The fundamental working principles of the ostensibly overlooked vari-

ant of the TOA position estimation technique namely TSOA, is exploited; and subsequently used to derive the proposed TROA multilateration technique. By a direct comparison between TROA and two existing multilateration techniques, it is also shown that indoor position estimation can be achieved much more effectively using the proposed solution. In the latter sections of this chapter, a new theoretical lower bound on the covariance of the TROA estimator based on the Cramér-Rao lower bound (CRLB) is derived. The CRLB is subsequently used to show the level of efficiency of the proposed TROA multilateration technique when the MSE implications are considered. The rest of this chapter is organised as thus: Section 4.2 gives an in-depth introduction into the concept of TSOA based multilateration; Section 4.3 illustrates the proposed techniques functionality right from its initial conception; and also bridges any inadvertent gap between its conceptualisation, practical ramifications and theoretical accuracy. Section 4.4 discusses the UWB channel modelled for the proposed TROA multilateration scheme; Section 4.5 validates the technique by means of simulation and CRLB analysis; and Section 4.6 summarises and concludes this chapter.

4.2 Background

Essentially, TSOA multilateration involves the propagation of signals from a NOI to known and fixed reference nodes ($RN_{i=1,2,3....n}$) or anchors [7, 19]. The reference nodes are typically receivers; and conventionally, the NOI is required to be either active (i.e. a mobile station) or semi-passive (i.e. a semi-passive radio frequency identification (RFID) tag); or alternatively have an inherently active or semi-passive component that facilitates its signal propagation to the various reference

nodes required for multilateration [7, 18, 19]. As depicted in Figure 4.1, following the signal propagation from the NOI, two reference nodes are usually paired together to generate a range sum estimate which is used to define a conic section whose semi-major axis is always greater than its semi-minor axis (i.e. an ellipse) [19, 64].

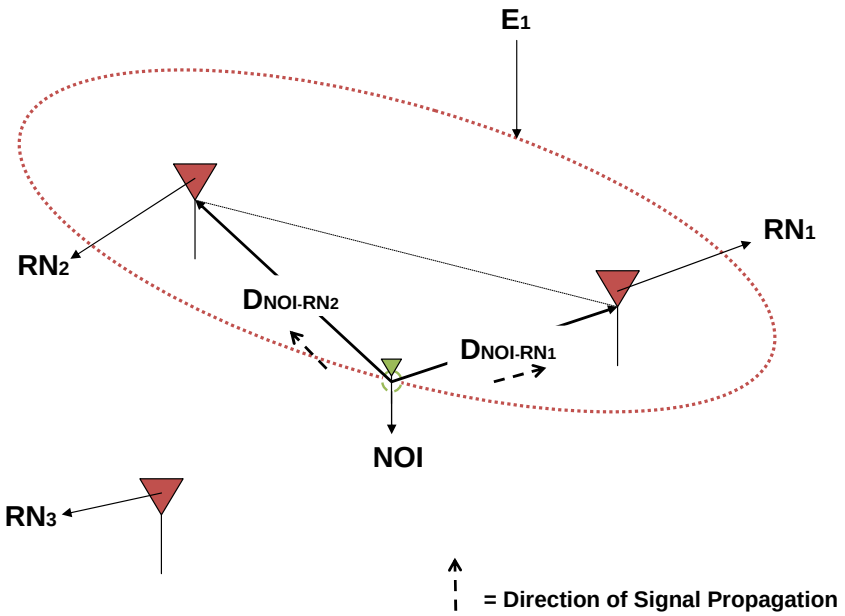

Figure 4.1: Generation of a single ellipse using two RN's

With reference to Figure 4.1 and considering the pairing between RN_1 and RN_2, the range sum is defined as the algebraic sum of D_{NOI-RN_1} (distance between NOI and RN_1) and D_{NOI-RN_2} (distance between NOI and RN_2). Assuming a LOS separation between the NOI and both reference nodes, D_{NOI-RN_1} and D_{NOI-RN_2} are determined by multiplying the arrival time of the propagated signal at the respective nodes by c. The general equation for the defined ellipse (E_i) based on the range sum is given by equation 4.1 where (h_i, k_i) is its centre coordinate, a_i

is its semi-major axis; and b_i is its semi-minor axis [64].

$$\frac{(x_i - h_i)^2}{{a_i}^2} + \frac{(y_i - k_i)^2}{{b_i}^2} = 1 \tag{4.1}$$

Denoting E_1 of centre coordinate $(h_1,\ k_1)$, semi-major axis a_1 and semi-minor axis b_1 as the ellipse defined by the pairing between RN_1 and RN_2, when a third reference node (RN_3) is introduced and paired with RN_2 just as Figure 4.2 depicts, another ellipse (E_2) with center coordinate $(h_2,\ k_2)$, semi-major axis a_2; and semi-minor axis b_2 is defined.

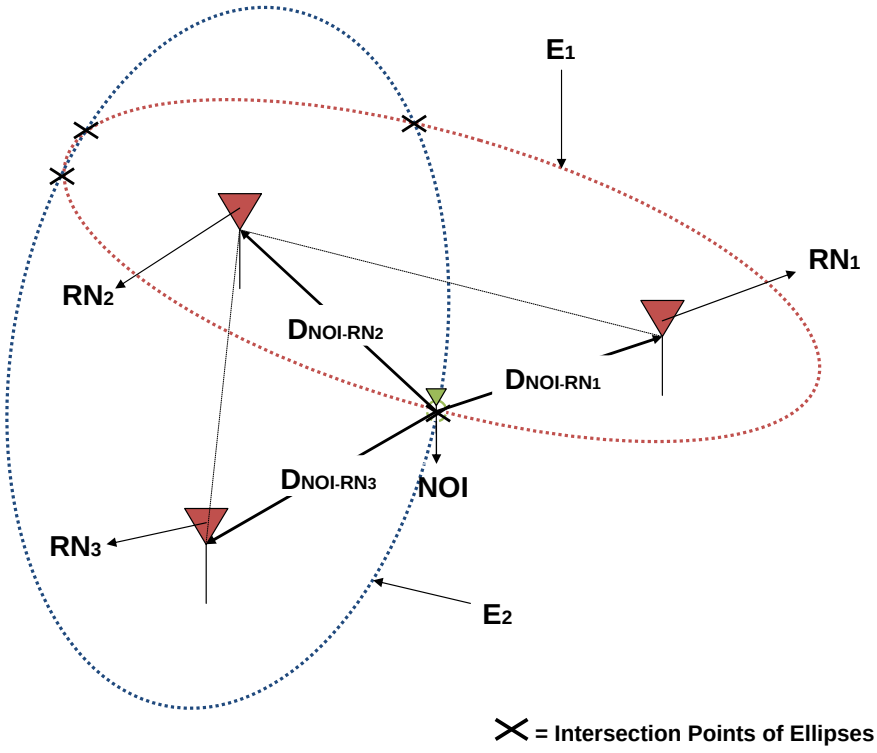

Figure 4.2: Generation of two ellipses using three RN's

Based on the fact that the definition of both E_1 and E_2 are dependent on the common NOI, their intersection will *always* result in a set of intersection points

(I_p) with one member of the set identifying the position of the NOI. However and with reference to Figure 4.2, identifying the intersection point that denotes the exact position of the NOI tends to become a cumbersome task when the intersection between E_1 and E_2 results in more than two I_p's. Ultimately, there is a need for a practical way to differentiate intersection coordinates between E_1 and E_2 that define the position of the NOI from those that come about as a direct consequence of the general geometry. To this effect, the classical trilateration process which is a feature of most hyperbolic driven positioning techniques is usually invoked [7, 19, 24]. In general, trilateration is a multilateration process that locates a NOI using exactly three vantage points ($VP_{i=1,2,3}$).

In the scenario depicted by both Figures 4.1 and 4.2, VP_1 would be the reference node pairing between RN_1 and RN_2 that defines E_1; and VP_2 would be the reference node pairing between RN_2 and RN_3 that defines E_2. Introducing a third vantage point just as the trilateration process postulates introduces a third ellipse which brings us a step closer to resolving the 'coordinate of the NOI' ambiguity problem. By introducing another reference node RN_4, and considering the vantage point that would bring about the pairing between itself and any of the previously defined three reference nodes, a third ellipse E_3 with center coordinate (h_3, k_3), semi-major axis a_3; and semi-minor axis b_3 is defined. As before, by virtue of all three ellipse definitions being dependent on the NOI, there will be one common coordinate between all three ellipses when they intersect. However, when they do intersect, there will be quite a number of intersection coordinates between the vantage point pairings but there will only be one unique intersection coordinate for the intersection of all three conic sections. That unique coordinate of intersection is (x_{noi}, y_{noi}) and as a consequence, the location of the NOI. At

this junction, it is noteworthy to mention that the success of the described trilateration process is partially dependent on the proper placement of the reference nodes in a defined indoor environment prior to its execution [7, 18]. Figure 4.3 depicts the aerial view of a typically effective placement configuration of all four reference nodes required for the trilateration process. The reference node pairings RN_1 - RN_2, RN_1 - RN_3 and RN_1 - RN_4 assume the form of VP_1 (E_1), VP_2 (E_2) and VP_3 (E_3) respectively; and the TSOA trilateration process is completed accordingly to determine the coordinates of the NOI [7, 18]. Algorithm 2 (in Appendix A) serves as a summary of the TSOA multilateration process.

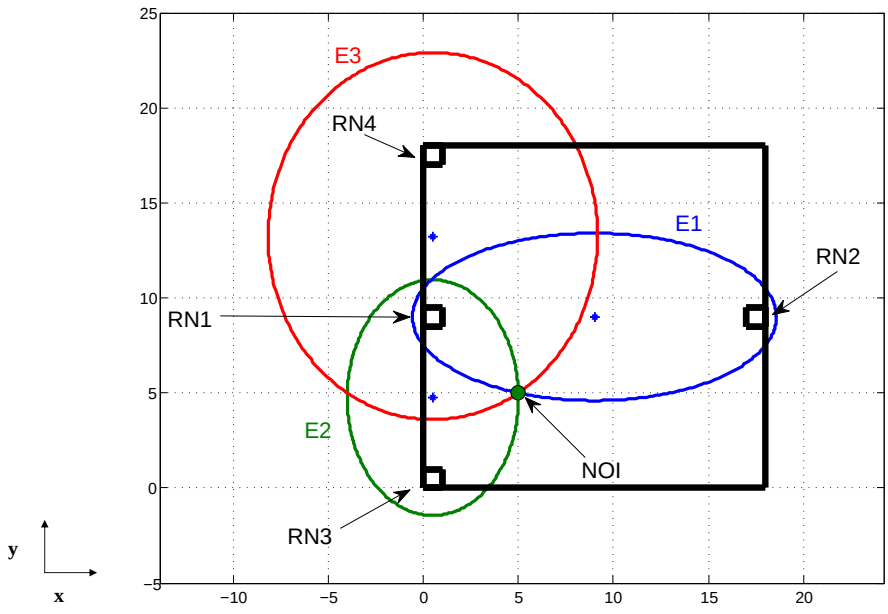

Figure 4.3: Generation of two ellipses using three RN's

4.3 Proposed TROA Multilateration Technique

As the demand for an increase in the accuracy and a substantial decrease in the complexity of position estimation techniques has seen an exponential increase in recent years, TSOA based multilateration techniques have seemingly not been considered as potential accuracy enablers. As [7, 18, 19, 24, 109] explain, the general consensus seems to be that they do not provide any additional performance advantage(s) over the widely used hyperbolic based multilateration techniques. In this chapter, this is proven to be right by means of a direct comparison with the TOA multilateration technique as well as the proposed TROA. Furthermore, and as previously mentioned, the fundamental operational principles of the TSOA driven multilateration process are used to define the novel and UWB-driven TROA multilateration technique.

4.3.1 The Optimum Solution Space

The proposed TROA system is optimised for position estimation in both a square and rectangular shaped indoor environment; and its setup in both quadrilaterals are depicted in Figure 4.4. Prior to its setup in the environment, the value of 'A' which would intuitively always be the largest distance in both quadrilaterals, is determined ($A = \sqrt{2L^2}$ for the square and $A = \sqrt{L^2 + B^2}$ for the rectangle). This is carried out to ensure that all signal propagation in both cases is within the indoor UWB transmission range (R_{UWB}) which is in the order of tens of metres; and typically less than or equal to 30 m [19, 21, 23, 24]. To this effect, any squared or rectangular shaped indoor environment that satisfies the condition of $A \leq R_{\text{UWB}}$ is defined as the 'Optimum 2D Solution Space (O2SS)'. In an event

of the TROA system being setup outside the O2SS, there will be regions with no signal propagation; and this would lead to a high reduction in the performance of the system and ultimately a failure in the localisation task.

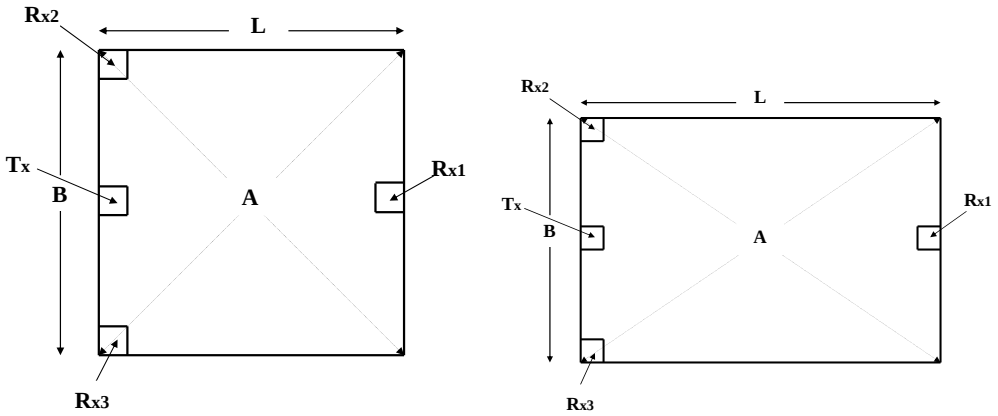

Figure 4.4: Aerial view of TROA system setup for a square and rectangular shaped indoor environment

4.3.2 TROA Multilateration

In contrast to both the conventional TOA and TSOA based multilateration techniques that require either an active or a semi-passive NOI to enable signal propagation from it (the NOI) to the relevant reference nodes, TROA is conceived to rely wholly on an inherently passive NOI. In most indoor residential applications, the NOI tends to range from secondary targets such as key electrical appliances and other non-electronic devices to much more primary and inherently animate targets such as the human body [19, 21, 24]. For position estimation using the proposed method, the NOI which could either be a primary or secondary target is equipped with a passive lightweight material of known electrical properties (i.e. conductivity, permittivity, loss tangent, dielectric constant). In [110], it was

shown that based on the reflection properties of UWB signals as well as having a priori knowledge of the electrical properties of the material that is used to make up an OOI (lightweight material attached to the NOI in this scenario), it is possible to determine and predict the expected reflected waveform at any UWB receiver (reference node in this scenario) when a UWB signal is incident on the object of interest. Taking this into consideration, TROA multilateration is initially defined in accordance with that which is depicted in Figure 4.5. With reference to Figure 4.5, TROA replaces TSOA's dependence on RN_1 and RN_2 with a UWB transmitter (T_x); and a UWB receiver (R_x) respectively. When T_x transmits a UWB signal, a version of it will be received at R_x by virtue of the LOS provisioning at a distance of D_{LOS}; and after a time delay which is brought about by the reflection of the UWB signal off the lightweight material attached to the NOI, a version of the signal is also received at R_x.

Considering a simplistic albeit realistic two-path propagation model and a square shaped indoor environment, it is initially assumed that there are no multipaths in the environment (i.e. noise-free propagation environment); and hence no destructive reflections in the environment during the propagation of the UWB signal. Additionally, it is also assumed that there is always a LOS separation distance between the transmitter (T_x) and the corresponding receivers (i.e. $R_{\mathrm{xi=1,2,3...n}}$). Once the environment gets tested for compliance with the O2SS requirement and passes it (i.e. $A \leq \mathrm{R_{UWB}}$) , a transmitter (T_x) and three receivers (R_{x1}, R_{x2} and R_{x3}) are deployed in the square as thus. Likening L and B which is defined in Figure 4.4 to the typical x and y axis on a 2-D x-y grid respectively, T_x is deployed at coordinate ($0.5p$, $0.5L$), R_{x1} is deployed at coordinate (L - $0.5p$, $0.5L$), $\mathrm{R_{x2}}$ is deployed at coordinate ($0.5p$, L - $0.5p$) ; and R_{x3} is deployed at co-

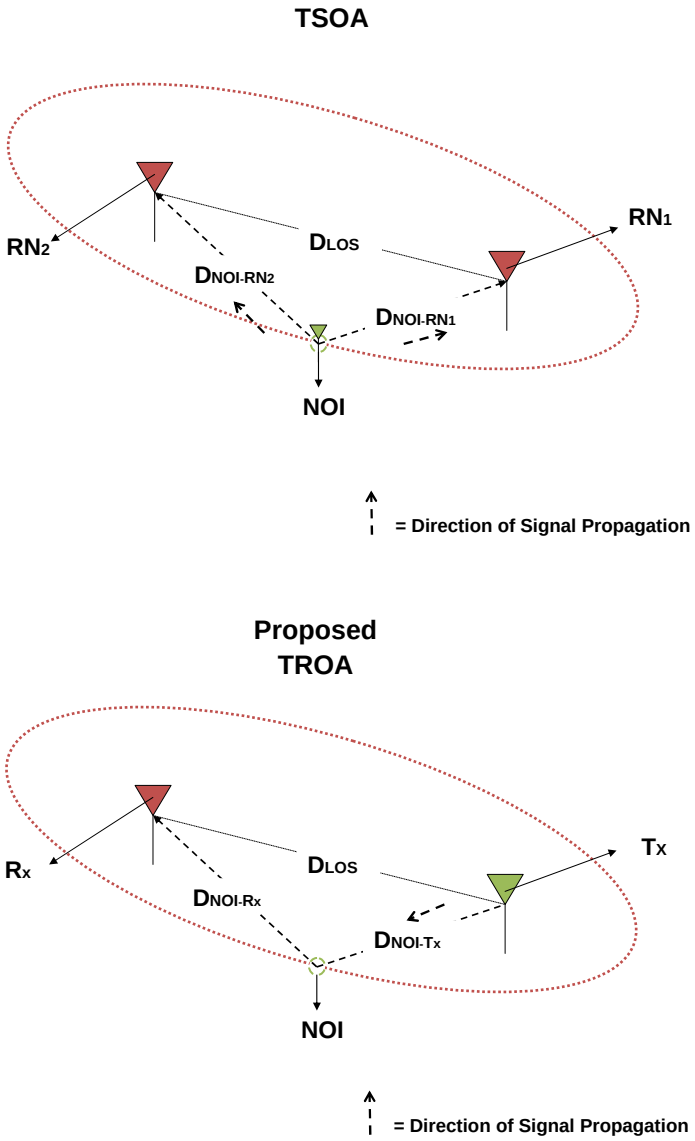

Figure 4.5: Generation of ellipses using TSOA and TROA Multilateration approaches

ordinate $(0.5p, 0.5p)$ where p is strictly an arbitrary positive integer that enforces a displacement of both the transmitter or receiver from the edges of the O2SS.

In liaison with Figure 4.6, VP_1 becomes the pairing between T_x and R_{x2} while

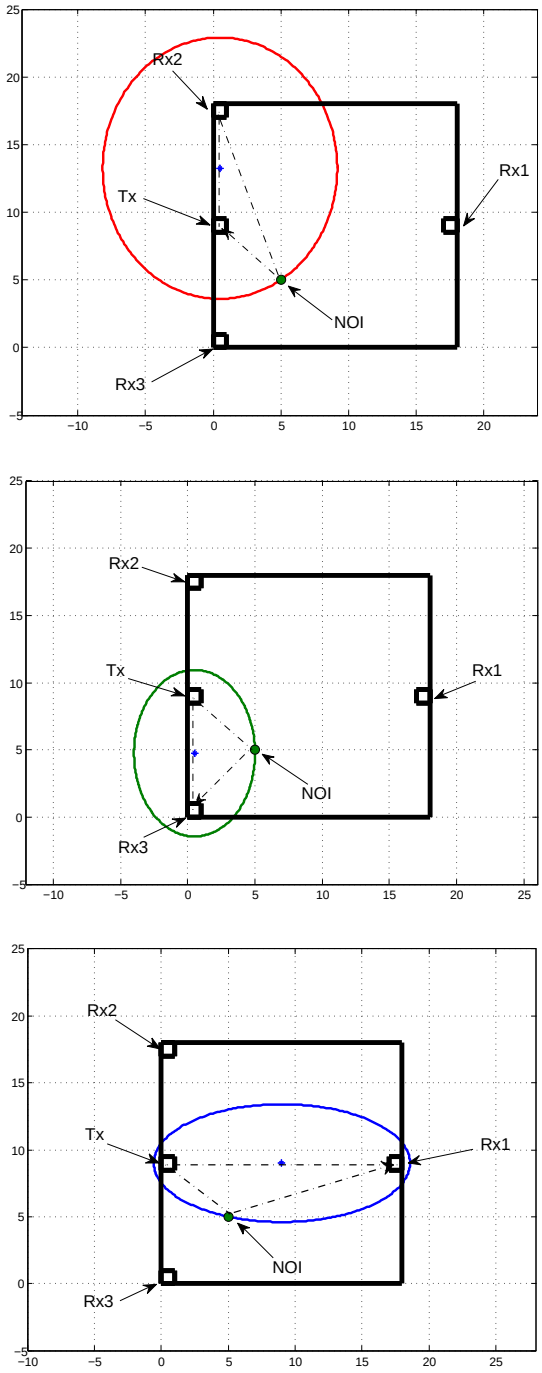

Figure 4.6: Generation of ellipses using proposed TROA approach

VP_2 and VP_3 become the pairings between T_x and R_{x3}; and T_x and R_{x1} respectively. D_{LOS1}, D_{LOS2} and D_{LOS3} are the respective LOS separation distances between the VP_1, VP_2 and VP_3 pairings. Considering VP_1, when an UWB signal $x(t)$ is transmitted by T_x, $x'(t)$ is received by R_{x2} at time t_1 by virtue of the LOS provisioning. At time t_2, $s(t)$ is also received by R_{x2} by virtue of $x(t)$ reflecting off the NOI. Since α is the time delay between the reception of $x'(t)$ and $s(t)$, considering the ideal nature of the assumed environment, α is determined by cross correlating $s(t)$ and $x(t)$ (i.e. $R_{sx}(\tau)$). A simple plot of $R_{sx}(\tau)$ will lead a single peak occurring at the point where $\tau = \alpha$; hence the value of α can be easily deduced from the plot. However this can only be done by an initial estimation of $s(t)$ which is achieved by a convolution between $x(t)$, the impulse response of the indoor UWB channel $h(t)$ and the reflection coefficient of the UWB signal $r(t)$ [21, 23, 24]. A multiplication of α with c and then adding it to D_{LOS1}, generates the 'range sum' associated with VP_1. Repeating the same process for both VP_2 and VP_3 generates the range sum associated with them.

4.3.3 Conic Section Definition and NOI Identification

With reference to the general equation of an ellipse given by equation 4.1; and taking all three vantage points into consideration, 'a_i' is defined as half the range sum (i.e. range sum/2); and 'b_i' is defined as $a_i\sqrt{1-e_i^2}$ where 'e_i' denotes the eccentricity of the ellipse. e_i in turn is defined as f_i / a_i where 'f_i' is half the distance between the two foci of the ellipse. Consequently, 'f_i' can be re-defined as half the distance between the LOS separation between T_x and the corresponding receivers (i.e. $f_1 = D_{LOS1}/2$ for VP_1, $f_2 = D_{LOS2}/2$ for VP_2 and $f_3 = D_{LOS3}/2$

for VP_3). Just as Figure 4.6 depicts, for all three vantage points, three ellipses E_1, E_2 and E_3 which are respectively centered at $(0.5p$, $((L$ - $0.5)+(L/2))/2)$, $(0.5p, 0.5f_2)$ and $(0.5f_3, 0.5L)$ are constructed accordingly. Usually, at this stage of the multilateration process, trilateration is invoked to determine the coordinate of the NOI just as we discussed earlier for the TSOA scenario. However, for our proposed TROA, we perform the trilateration process in a non-conventional manner by a series of ellipse grouping and comparisons. Essentially, the coordinate of the NOI's location is determined using Algorithm 1 (in Appendix A) by an initial grouping of the defined ellipses; and thereafter a direct comparison of intersection points for similarities. For a given execution cycle, ellipses E_1 and E_2 are grouped; and their intersection coordinates $\{(x(1), y(1))$ and $(x(2), y(2))\}$ are determined. In a similar manner, ellipses E_1 and E_3 are also grouped; and their intersection coordinates $\{(x(3), y(3))$ and $(x(4), y(4))\}$ are also determined. With a combination of four intersection coordinates determined for both groupings, Algorithm 1 completes its current execution cycle by identifying a pair of coordinates in both groups that have similar values. This identified similar values denotes the coordinate of the NOI; and ultimately its location in the given indoor environment.

4.3.4 Determination of Intersection points of ellipse

Ellipses E_1 and E_2 are said to have common roots based on them intersecting on a x-y grid if their Bezout determinant is zero [111].

$$\frac{(x_1 - h_1)^2}{{a_1}^2} + \frac{(y_1 - k_1)^2}{{b_1}^2} = 1 \tag{4.2}$$

$$\frac{(x_2 - h_2)^2}{{a_2}^2} + \frac{(y_2 - k_2)^2}{{b_2}^2} = 1 \tag{4.3}$$

If the equations of both ellipses are defined by equations 4.2 and 4.3 respectively where $(h_1,\ k_1)$ and $(h_2,\ k_2)$ are their respective centre coordinates, $h_1 = p$, $k_1 = ((D_{LOS1} + 2p)/2)$, $h_2 = ((D_{LOS2} + 2p)/2)$; and $k_2 = p$; in a similar manner to [111], the Bezout determinant is defined by the quadratic polynomial:

$$R(y) = u_4 y^4 + u_3 y^3 + u_2 y^2 + u_1 y + u_0 \tag{4.4}$$

$$\text{where } u_0 = \det\begin{pmatrix} v_2 & v_4 \\ v_4 & v_{10} \end{pmatrix}, u_1 = \det\begin{pmatrix} v_0 & (v_7 + v_9) \\ -v_2 & v_{10} \end{pmatrix} - 2\det\begin{pmatrix} v_3 & 1 \\ -v_4 & 1 \end{pmatrix},$$

$$u_2 = \det\begin{pmatrix} v_0 & (v_6 + v_8) \\ -v_2 & (v_7 + v_9) \end{pmatrix} - \det\begin{pmatrix} v_3 & -v_4 \\ 2v_1 & v_3 \end{pmatrix},$$

$$u_3 = \det\begin{pmatrix} v_0 & v_5 \\ -v_2 & (v_6 + v_8) \end{pmatrix} - 2\det\begin{pmatrix} v_1 & 0 \\ 0 & v_3 \end{pmatrix}, u_4 = \det\begin{pmatrix} v_0 & v_1 \\ v_1 & v_5 \end{pmatrix}$$

$$v_0 = 2\det\begin{pmatrix} {a_{00}}^{(0)} & {a_{01}}^{(0)} \\ {a_{00}}^{(1)} & {a_{01}}^{(1)} \end{pmatrix}, v_1 = \det\begin{pmatrix} {a_{00}}^{(0)} & {a_{11}}^{(0)} \\ {a_{00}}^{(1)} & {a_{11}}^{(1)} \end{pmatrix}, v_2 = \det\begin{pmatrix} {a_{00}}^{(0)} & {b_0}^{(0)} \\ {a_{00}}^{(1)} & {b_0}^{(1)} \end{pmatrix},$$

$$v_3 = \det\begin{pmatrix} {a_{00}}^{(0)} & {b_1}^{(0)} \\ {a_{00}}^{(1)} & {b_1}^{(1)} \end{pmatrix}, v_4 = \det\begin{pmatrix} {a_{00}}^{(0)} & c^{(0)} \\ {a_{00}}^{(1)} & c^{(1)} \end{pmatrix}, v_5 = 2\det\begin{pmatrix} {a_{01}}^{(0)} & {a_{11}}^{(0)} \\ {a_{01}}^{(1)} & {a_{11}}^{(1)} \end{pmatrix},$$

$$v_6 = 2\det\begin{pmatrix} {a_{01}}^{(0)} & {b_1}^{(0)} \\ {a_{01}}^{(1)} & {b_1}^{(1)} \end{pmatrix}, v_7 = 2\det\begin{pmatrix} {a_{01}}^{(0)} & c^{(0)} \\ {a_{01}}^{(1)} & c^{(1)} \end{pmatrix}, v_8 = \det\begin{pmatrix} {a_{11}}^{(0)} & {b_0}^{(0)} \\ {a_{11}}^{(1)} & {b_0}^{(1)} \end{pmatrix},$$

$$v_9 = \det\begin{pmatrix} {b_0}^{(0)} & {b_1}^{(0)} \\ {b_0}^{(1)} & {b_1}^{(1)} \end{pmatrix}, v_{10} = \det\begin{pmatrix} {b_0}^{(0)} & c^{(0)} \\ {b_0}^{(1)} & c^{(1)} \end{pmatrix}$$

Writing equations 4.2 and 4.3 initially in their quadratic forms and finally in matrix forms, yield equations 4.5 and 4.6 respectively:

$$\mathbf{Y_0}^{\mathbf{T}}\mathbf{A_0}\mathbf{Y_0} + \mathbf{B_0}^{\mathbf{T}}\mathbf{Y_0} + c_0 = 0 \tag{4.5}$$

$$\text{where } \mathbf{Y_0} = \begin{pmatrix} x \\ y \end{pmatrix}, \mathbf{A_0} = \begin{pmatrix} {a_{00}}^{(0)} = {b_1}^2 & {a_{01}}^{(0)} = 0 \\ {a_{01}}^{(0)} = 0 & {a_{11}}^{(0)} = {a_1}^2 \end{pmatrix},$$

$$\mathbf{B_0} = \begin{pmatrix} {b_0}^{(0)} = -2h_1{b_1}^2 \\ {b_1}^{(0)} = -2k_1{a_1}^2 \end{pmatrix},$$

$$c_0 = {h_1}^2{b_1}^2 + {a_1}^2{k_1}^2 - {a_1}^2{b_1}^2$$

$$\mathbf{Y_1}^{\mathbf{T}}\mathbf{A_1}\mathbf{Y_1} + \mathbf{B_1}^{\mathbf{T}}\mathbf{Y_1} + c_1 = 0 \tag{4.6}$$

$$\text{where } \mathbf{Y_1} = \begin{pmatrix} x \\ y \end{pmatrix}, \mathbf{A_1} = \begin{pmatrix} {a_{00}}^{(1)} = {b_2}^2 & {a_{01}}^{(1)} = 0 \\ {a_{01}}^{(1)} = 0 & {a_{11}}^{(1)} = {a_2}^2 \end{pmatrix},$$

$$\mathbf{B_1} = \begin{pmatrix} {b_0}^{(1)} = -2h_2{b_2}^2 \\ {b_1}^{(1)} = -2k_2{a_2}^2 \end{pmatrix},$$

$$c_1 = {h_2}^2{b_2}^2 + {a_2}^2{k_2}^2 - {a_2}^2{b_2}^2$$

As a consequence, the Bezout determinant parameters become defined as thus:

$$v_0 = 0, v_1 = \det \begin{pmatrix} {b_1}^2 & {a_1}^2 \\ {b_2}^2 & {a_2}^2 \end{pmatrix}, v_2 = -\det \begin{pmatrix} 2{b_1}^2{b_2}^2 & 0 \\ 0 & -(h_2 + h_1) \end{pmatrix},$$

$$v_3 = \det \begin{pmatrix} -{b_1}^2 & 2k_1{a_1}^2 \\ -{b_2}^2 & 2k_2{a_2}^2 \end{pmatrix}, v_4 = \det \begin{pmatrix} -{b_1}^2 & ({h_1}^2{b_1}^2 + {a_1}^2{k_1}^2 - {a_1}^2{b_1}^2) \\ {b_2}^2 & ({h_2}^2{b_2}^2 + {a_2}^2{k_2}^2 - {a_2}^2{b_2}^2) \end{pmatrix},$$

$$v_5 = 0, v_6 = 0, v_7 = 0, v_8 = \det \begin{pmatrix} -{a_1}^2 & 2h_1{b_1}^2 \\ {a_2}^2 & 2h_2{b_2}^2 \end{pmatrix},$$

$$v_9 = \det \begin{pmatrix} 2h_1{b_1}^2 & 2k_1{a_1}^2 \\ 2h_2{b_2}^2 & 2k_2{a_2}^2 \end{pmatrix},$$

$$v_{10} = \det \begin{pmatrix} -2h_1{b_1}^2 & ({h_1}^2{b_1}^2 + {a_1}^2{k_1}^2 - {a_1}^2{b_1}^2) \\ 2h_2{b_2}^2 & ({h_2}^2{b_2}^2 + {a_2}^2{k_2}^2 - {a_2}^2{b_2}^2) \end{pmatrix}$$

With these defined parameters as well as the defined values of a and b, solving equation 4.4 for y where $R(y) = 0$, determines all the y coordinates of the intersection points of E_1 and E_2. For each y value, the corresponding x value is determined by substituting y into either equations 4.5 or 4.6 and solving for x. In the case where y is substituted into equation 4.5, $y_1 = y$ and $x_1 = x$; and in a similar manner, when y is substituted into equation 4.6, $y_2 = y$ and $x_2 = x$.

4.4 Communications Channel Consideration

The UWB transmit signal $x(t)$ depicted in Figure 4.7 typically takes the form of the second derivative of the Gaussian impulse function. With ΔT defined as the nominal time duration of $x(t)$, equation 4.7 gives its mathematical representation [21, 112].

$$x(t) = \left(1 - 16\pi \left(\frac{t}{\Delta T}\right)^2\right) e^{-8\pi(t/\Delta T)^2} \tag{4.7}$$

The use of this impulse function derivative as a UWB transmit signal is made possible by carefully allocating ΔT specific values which ensure that the pulse width of the signal is approximately 0.39 ns [21, 23, 24]. This careful allocation results in a -10dB bandwidth of 7.5GHz with a maximum spectrum occurring at 5.78GHz.

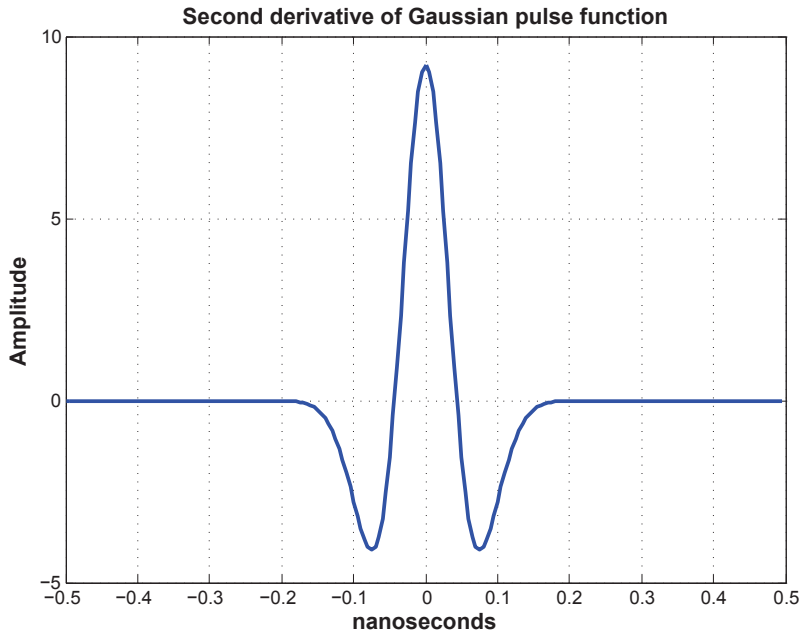

Figure 4.7: UWB Signal: Second derivative of Gaussian Impulse

This coincides with the maximum PSD allowed by the FCC for UWB communications [21, 113]. With the primary target application for the proposed TROA technique being indoor medical and bio-medical applications, modern literature informs us that theoretically, UWB communications and specifically UWB signals have the potential to enable these applications with an acceptable time delay resolution of 50 cm or better [84]. However, multipath-driven time delays expected in a practical indoor environment typically depend on the propagation scenario (i.e. LOS or NLOS); and type of building (i.e. residential or commercial). In [114], the authors have presented typical time delay values for a varied albeit familiar range of transceiver (i.e. T_x - R_x) separation distances.

4.4.1 The UWB Channel Model

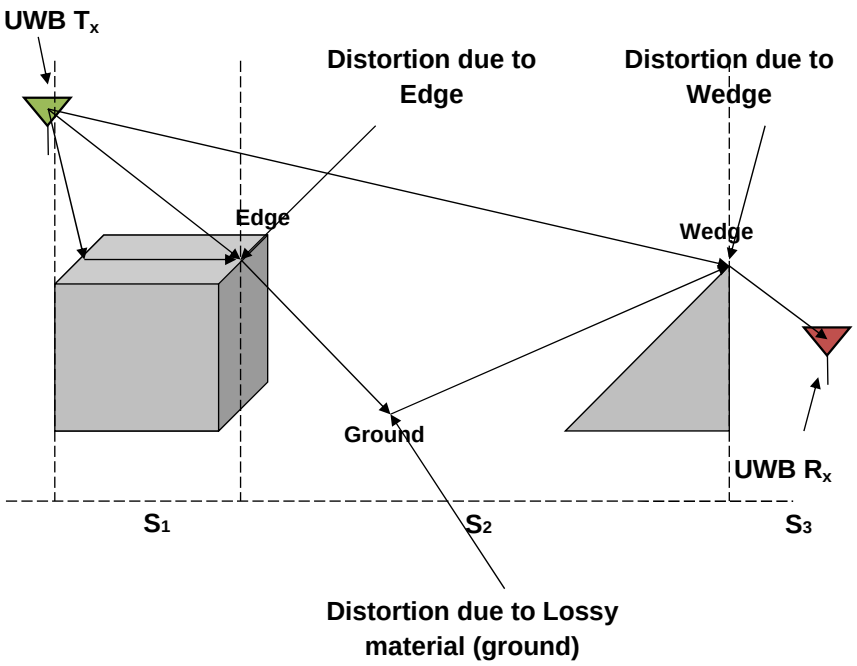

Figure 4.8: Physics-based pulse distortion model

Generally, there are two approaches taken in the modelling of the UWB communication channel namely the widely known and accepted empirical approach [113, 115, 116] and the physics-based approach [115, 116]. In contrast to the physics-based approach; and due to the inadvertent complexity in modelling pulse distortions, empirical approaches are not readily available in a generalised closed form; and this is where physics-based modelling comes into play [116]. At this junction, it is noteworthy to mention that in physics, signal distortions due to reflections are fundamentally dissimilar to signal distortions due to diffraction [116]. From a multilateration vantage point, the parameter of utmost importance is the first arriving MPC of the originally transmitted UWB signal [21, 64]. Nevertheless, the successful detection and subsequent estimation of this MPC at a receiver end is in most cases significantly hindered by the environmentally driven reflections and diffractions. This hindrance brings about a need to model the UWB communication channel in an attempt to cater for the destructive effects (i.e. pulse distortions) reflections and diffractions will have on the transmitted UWB signal. The physics-based approach models the indoor UWB communication channel as a collation of individually localised scattering centre ($\mathbf{S_{i=1,2,3....n}}$) models similar to that which Figure 4.8 depicts.

For the distortion model depicted in Figure 4.8 which typifies the conventional and well studied two-ray indoor communications model that is used in a lot of UWB applications, there are three scattering centres ($\mathbf{S_{i=1,2,3}}$); and each of them characterises the distortion of the UWB signal in its region by means of the impulse response of the UWB signal to the reflection or diffraction brought about by the surrounding inanimate object(s). The characteristic impulse response that corresponds to each of the scattering centres are well documented in [115, 116].

Additionally, at any given time, the arrival path of the UWB signal into scattering centre S_i is governed by the departure trajectory of the signal arriving from the preceding scattering centre (i.e. S_{i-1}).

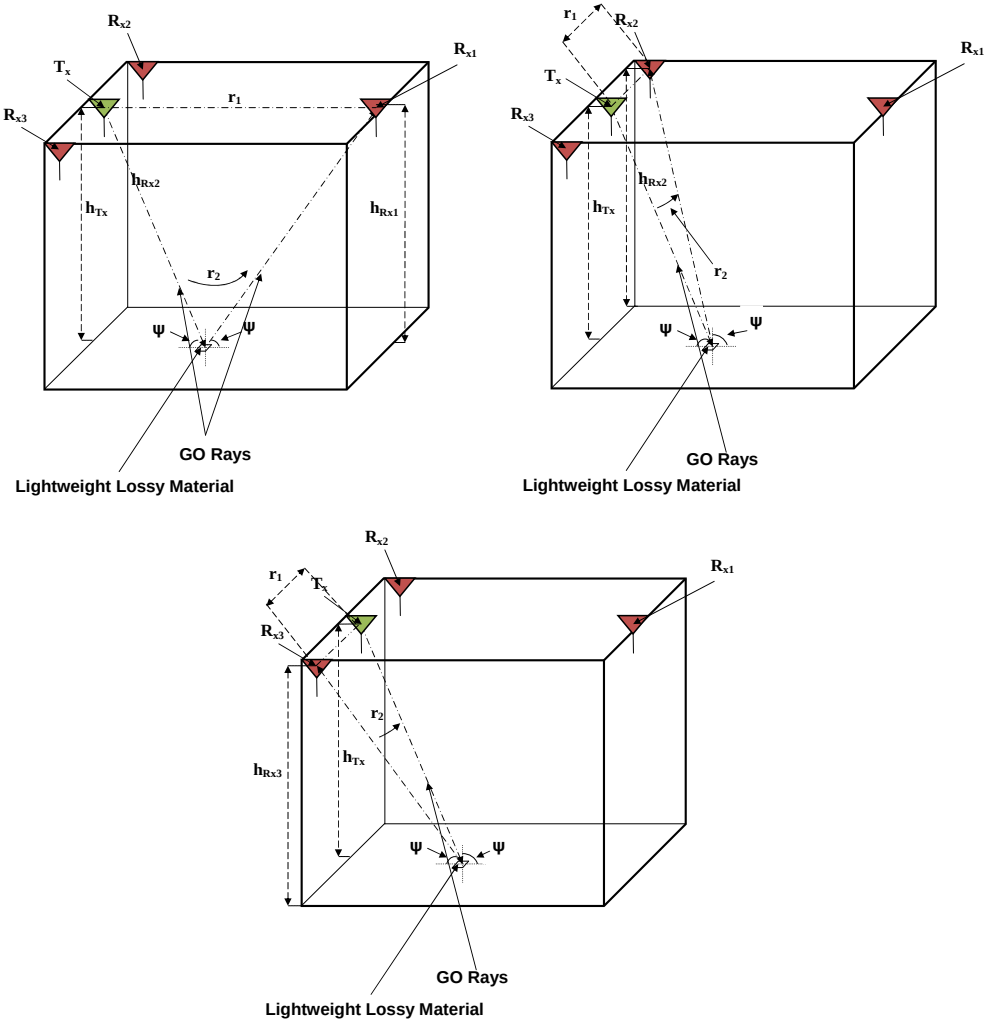

Figure 4.9: UWB channel model description for proposed TROA

Having mentioned that, for the research work presented in this chapter, the modelling of the UWB communications channel is entirely governed by the physics-based approach that is pertinent to S_2 in Figure 4.8, when it is considered as an

isolated scattering centre. As shown in Figure 4.9, for the channel model, the dependency of the arrival path of the UWB signal on the departure trajectory of the signal from the preceding scattering centre is replaced by a fixed omni-directional UWB transmitter (T_x). T_x and the respective receivers are placed at the corners of the ceiling just as Figure 4.9 depicts at specific coordinates which were defined in verbatim in the previous section. With reference to [116] and considering the vantage point that pairs T_x with R_{x1} (i.e. VP_3 from the previous section), for non-zero values of the incidence angle ψ of the transmitted UWB signal $x(t)$ where ϵ_r and σ refer to the relative dielectric constant of the lossy material and its conductivity respectively, the transfer function and its analogous impulse response $h(\tau)$ associated with $x(t)$ when it suffers some distortion pulse-wise in a scattering centre similar to S_2 is as a direct consequence of Geometric Optics (GO) Rays (i.e. reflection off the lossy material); and is defined as:

$$h(\tau) = \frac{1}{r_1}\ \delta(\tau) + \frac{1}{r_2}\ R_1(\tau)\ \otimes\ \delta(\tau - \tau_1) \tag{4.8}$$

where

$$R_1(t) = \pm\ K\delta(t) + R_{01}(t),$$

and

$$R_{01}(t) = \text{Reflection Coefficient of transmitted UWB signal}$$

$$= \left(\frac{4k}{1-k^2}\right)\left(\frac{e^{-at}}{t}\right)\sum_{n=1}^{\infty}(-1)^{n+1}nK^nI_n(at),$$

$$\tau_1 = \frac{(r_2 - r_1)}{c}, K = \frac{(1-k)}{(1+k)},$$

$$k = \begin{cases} \sqrt{\epsilon_r - \cos^2\psi}/(\epsilon_r \sin\psi) & \text{for vertical polarization} \\ \sin\psi/\sqrt{\epsilon_r - \cos^2\psi} & \text{for horizontal polarization} \end{cases}$$

$$\psi = \arctan\frac{(h_{T_x} + h_{R_x})}{d}, r_1 = \sqrt{(h_{T_x} - h_{R_x})^2 + d^2},$$

$$r_2 = \sqrt{(h_{T_x} + h_{R_x})^2 + d^2}, a = \frac{120\pi\sigma c}{2\epsilon_r}$$

Just as [115, 116] have pointed out extensively, based on the fact that $I_n(at)$ is the modified Bessel function, for values of $at \leq 1$, $R_{01}(t)$ can be manipulated and finally reduced to:

$$R_{01}(t) \approx K\ \frac{2k}{1-k^2}\ e^{-(1+K)at}$$

Without loss of generality, in our indoor environment and with reference to Figure 4.9, the values of h_{T_x}, $h_{R_{x1}}$ and $h_{R_{x2}}$ are the same; and hence ψ, r_1 and r_2 can all be respectively re-defined as:

$$\psi = \arctan\frac{2h}{d}, r_1 = d, r_2 = \sqrt{2h^2 + d^2}$$

where

$$h = h_{T_x} = h_{R_{x1}} = h_{R_{x2}} = h_{R_{x3}}$$

It suffices to say that the impulse response definition for the vantage point that pairs T_x with R_{x1} also follows through from the other two vantage points that pairs T_x with R_{x3} and R_{x2} respectively just as Figure 4.9 illustrates. Intuitively, the values for the UWB channel model parameters wholly depend on the lossy

material being used for the localisation task. However typical values of ϵ_r and σ are 2.07 and 0.005 respectively when the lossy material being considered is the material used to make a wooden door frame [96]. When the lossy material being considered is the material used to make a cement surface, the values of ϵ_r and σ are 6 and 0.0166 respectively [21]. The primary aim of explicitly defining the UWB channel model is to demonstrate the theoretical feasibility of our approach in potential real-world experiments. The indirect implications of the simplified UWB channel model on the validation of our technique, were considered. As it is demonstrated in Section 4.5, these implications are in the form of the defined standard deviation range of the normally distributed TOA measurement variation.

4.4.2 UWB Channel Model for Multiple UWB Signal Interactions

Figure 4.10 depicts the structure of a typical UWB channel model for multiple signal $x(t)$ interactions when the vantage point that pairs T_x with R_{x1} is considered. As with the previous modelling process, the modelling of the UWB multipath channel is based on the physics-based approach that corresponds to the isolated scattering centre S_2 in Figure 4.8. Depending on the specified indoor UWB application, multiple interactions between the transmitted UWB signal $x(t)$ and surrounding lossy materials which are either similar or dissimilar to the NOI, occurs [115, 116]. Hence it is sufficient to model the impulse response of the channel to both cases (i.e. Case A and Case B) independently. Case 'A' refers to a scenario whereby the surrounding lossy materials in the defined O2SS are

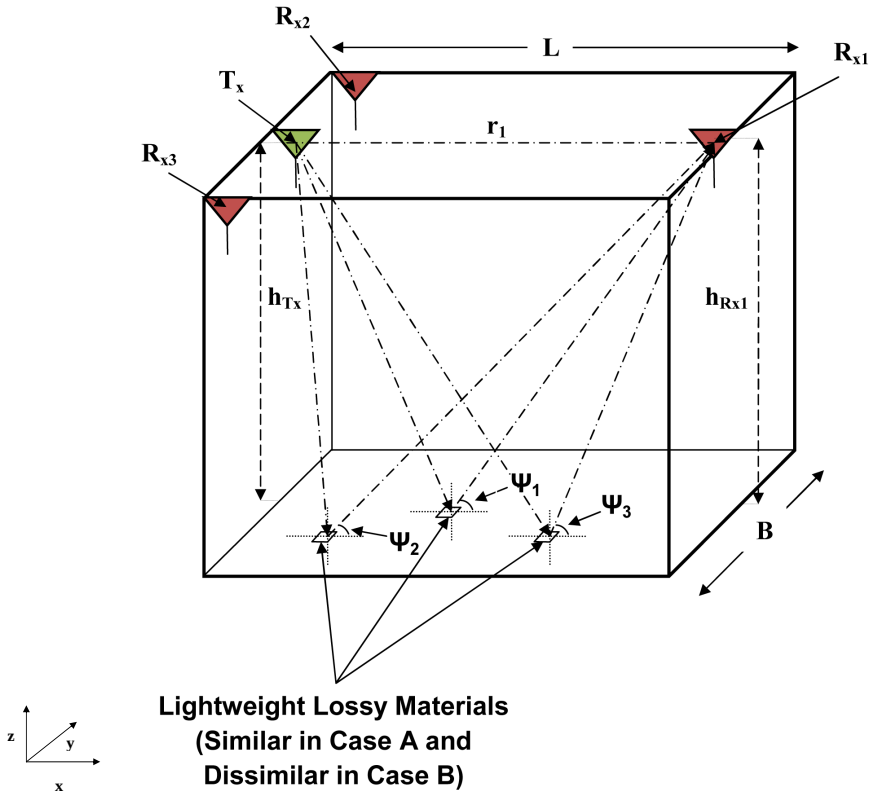

Figure 4.10: UWB Multipath Channel Model description

similar to the NOI in terms of their ϵ_r and σ parameter values; and case 'B' refers to a scenario whereby the surrounding lossy materials in the defined O2SS have dissimilar parameter values to the NOI. The impulse responses $h_1(\tau)$ and $h_2(\tau)$ of the multipath channel for both cases A and B can be derived respectively from the generalised multipath definition explicitly detailed in [115, 116].

4.4.3 UWB Multipath Channel Power Delay Profile

For a given impulse response $h(t)$ of a multipath channel, a measure of how dispersed the received signal is with respect to the originally transmitted UWB

signal $x(t)$, is called the 'power delay profile' [19, 117]. Essentially, the power delay profile indicates the degree of dispersion of the received signal; and is measured as the spatial average of $|h(t)|^2$ [19, 117]. With the physics based modelling process of $h(t)$ being partially dependent on the electrical properties of the lossy material and the NOI, the time of arrival of the multipath components also becomes dependent on the electrical properties of the lossy material. Hence the power delay profile for every defined propagation scenario is dissimilar.

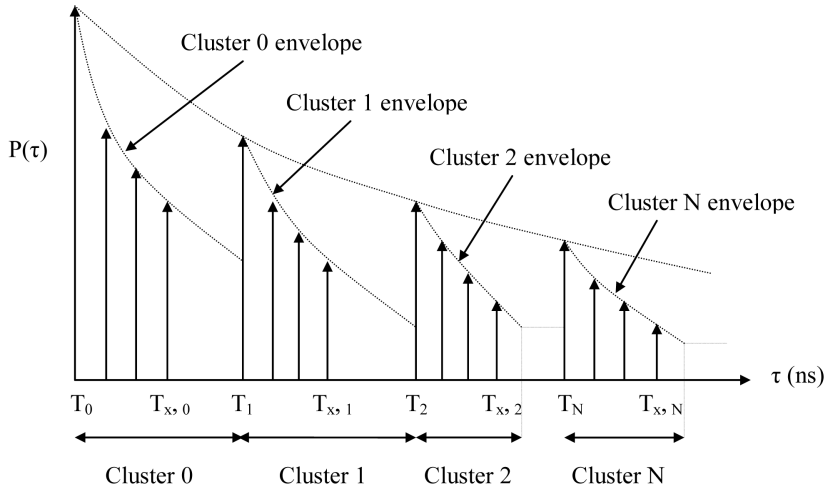

Figure 4.11: Illustration of the Power Delay Profile of the UWB multipath channel

However, just as Figure 4.11 depicts, the power delay profile for UWB channels typically assumes an exponential shape within each cluster and the mean energy of each cluster assumes an exponentially decaying outlook [19, 117]. T_i refers to the first MPC in cluster i while $T_{x,i}$ refers to the x^{th} MPC in cluster i. Numerical values for path arrival times and cluster power corresponding to the LOS and NLOS in residential, office, industrial and outdoor environment have been reported in [118].

4.5 Validation of Technique

4.5.1 TROA vs. TOA vs. TSOA (Effectiveness Test)

Innately, the effectiveness of any geometric multilateration technique relies heavily on the accuracy of the initially obtained TOA measurements. Notwithstanding, it suffices to conclude that a necessary comparison between two or more multilateration techniques in an attempt to determine their order of effectiveness, becomes one that has to be driven by an introduced and calculated variation in the TOA measurements. To this effect and considering LOS propagation conditions all through these series of simulations, the TOA measurement variation for all three methods (i.e. TROA, TOA and TSOA) is modelled as a normally distributed Gaussian random variable $N(0, \sigma^2)$; and for each method, 1000 random samples are generated for a defined standard deviation (σ) range of the TOA measurements. This range of σ is fixed to coincide with a localisation accuracy that spans from 3 cm to 30 cm (i.e. 0.1 ns to 1 ns) just as it was done in chapter 3. The NOI was subjected to a number of fixed coordinates in a 2D grid, and in

Category	Description
A	x is equal to y (i.e. $x = y$)
B	x is less than y
C	x is greater than y
D	x is even and y is odd OR x is odd and y is even
E	x and y are both odd
F	x and y are both even
G	x is a multiple of y

Table 4.1: Categorisation of Coordinates

an attempt to generalise the proposition that TROA outperforms TSOA and

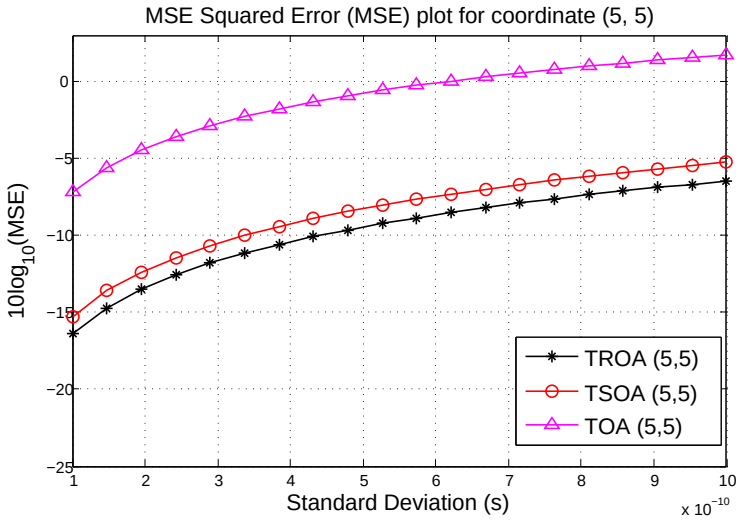

Figure 4.12: Mean Squared Error (MSE) comparison for Category A

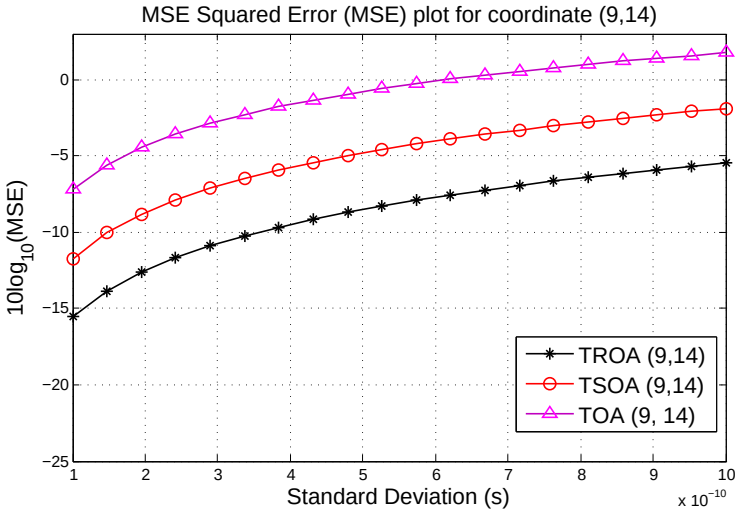

Figure 4.13: Mean Squared Error (MSE) comparison for Category B

TOA in all cases, these fixed coordinates were classified into 7 functional categories. Just as Table 4.1 depicts explicitly, the coordinates were categorised according to the typical numerical patterns in which an estimate of the NOIs position can be obtained. For each category, a pair of x and y coordinate that lies within the O2SS where $A \leq R_{\text{UWB}}$, was selected and the MSE analysis aimed

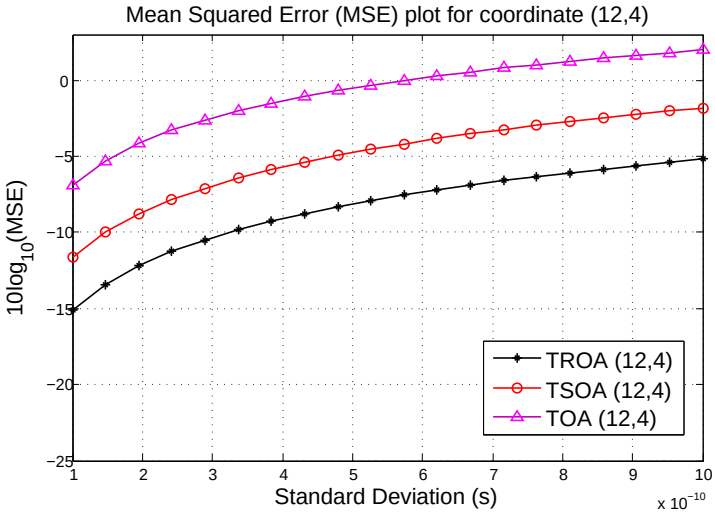

Figure 4.14: Mean Squared Error (MSE) comparison for Category C

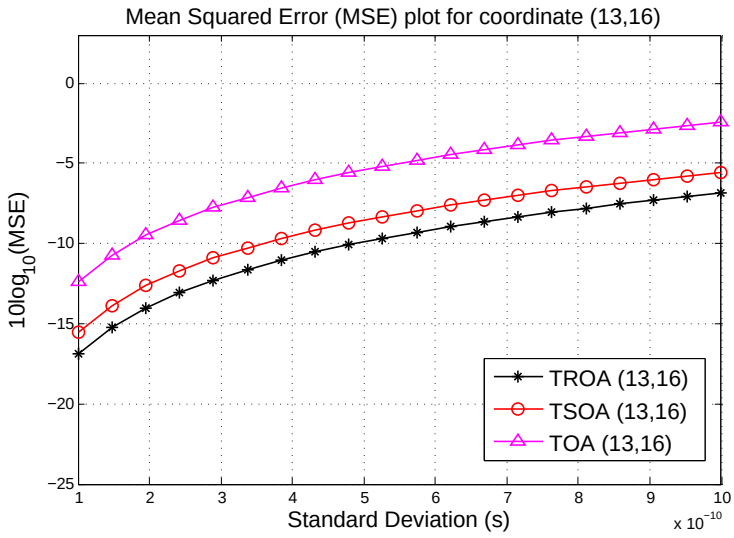

Figure 4.15: Mean Squared Error (MSE) comparison for Category D

at determining the effectiveness of TROA in comparison to TSOA and TOA were carried out. The initial TOA measurements that result in the determination of all defined coordinates in each of the categories using TROA, TOA and TSOA were respectively corrupted with the randomly generated gaussian noise samples over the defined σ range; and the estimate of NOI's location was subsequently

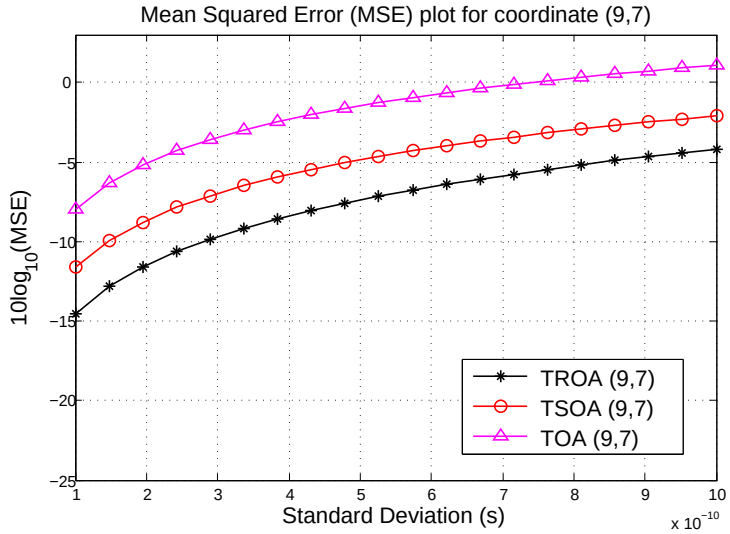

Figure 4.16: Mean Squared Error (MSE) comparison for Category E

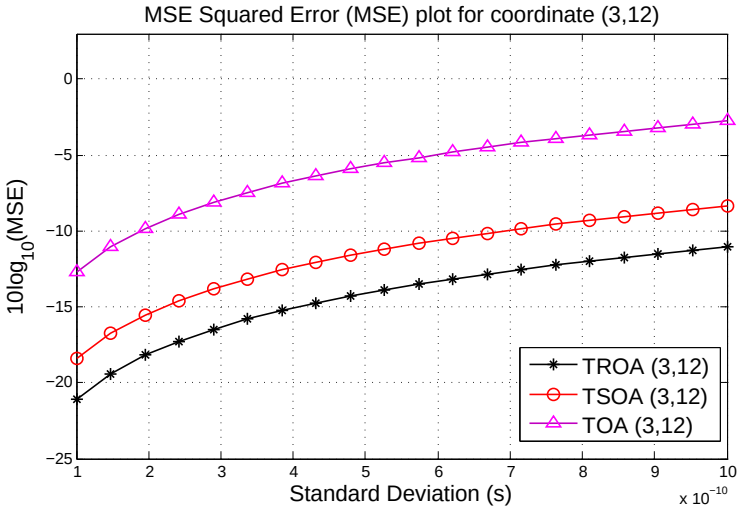

Figure 4.17: Mean Squared Error (MSE) comparison for Category F

redetermined. Figures 4.12 to 4.18 show the resultant σ vs. MSE plots for the specified σ range when the fixed coordinates are compared with the coordinates redetermined using the corrupted TOA measurements. These plots clearly show that a corruption in the TOA measurements just as it is bound to happen in practice either by means of interference, mild NLOS propagation scenarios, pulse

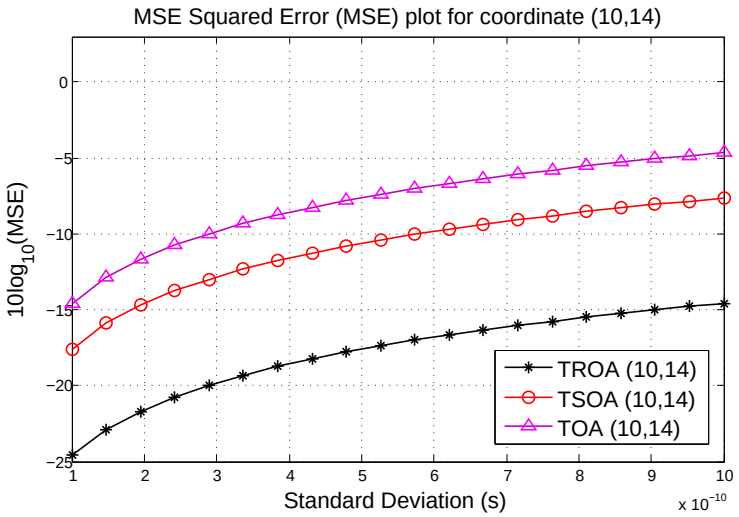

Figure 4.18: Mean Squared Error (MSE) comparison for Category G

distortion or unresolved multipath signals, has as expected a negative effect on the localisation effectiveness on all three methods. In an apparent disagreement with literature, these plots also show that TSOA has a better performance than TOA. However, this better performance can be attributed to the extra receiver requirement TSOA needs to perform the same positioning task as TOA (i.e. TSOA = 4 R_x and TOA = 3 R_x); and hence backing up literature's statement that TSOA does not necessarily provide any additional performance advantages over existing multilateration techniques [19]. Quite significantly, it is also clear to see from these MSE plots that TROA will always have a relatively better position estimation effectiveness in terms of MSE when compared to the other two methods over the defined σ range.

By inspecting Figures 4.12 to 4.18 a bit further, it can also be observed that although TSOA has a comparatively good position estimation performance when the Category A coordinate (5,5) is considered, TROA performs better than TSOA

in all categories. To verify that TROA will always perform better than TSOA for Category A coordinates, the previously described efficiency test (excluding the

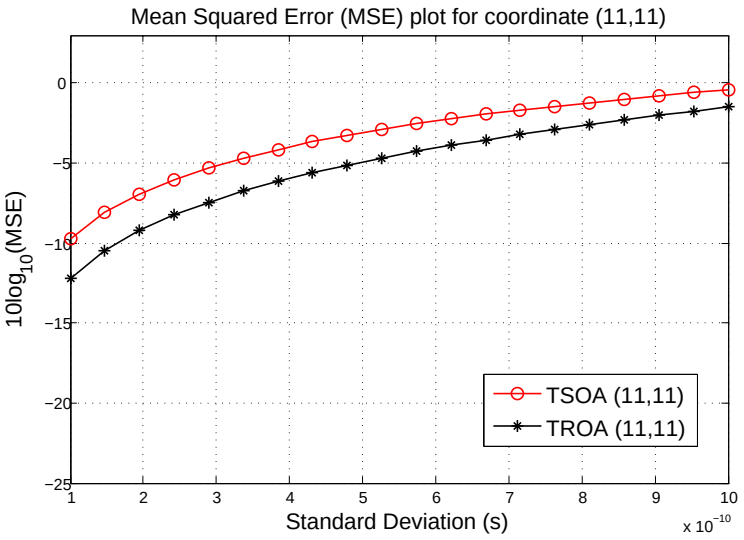

Figure 4.19: TROA vs. TSOA for (11, 11)

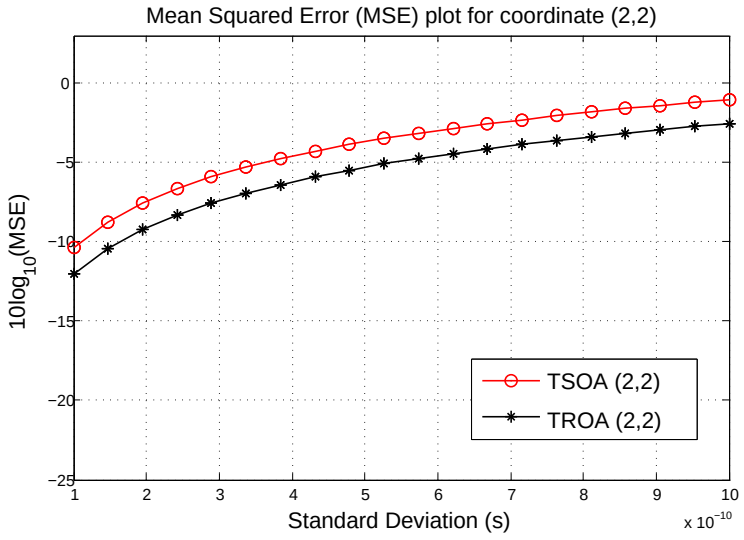

Figure 4.20: TROA vs. TSOA for (2, 2)

TOA positioning technique) was conducted once again on three more Category A coordinates namely $[x, y] = [2, 2; 11, 11; 14, 14]$. Just as Figures 4.19 to 4.21

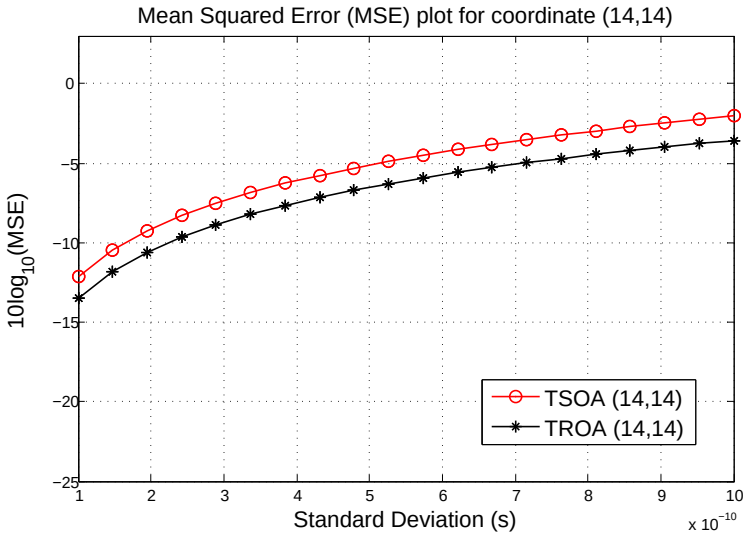

Figure 4.21: TROA vs. TSOA for (14, 14)

depicts, TROA will always perform better than TSOA even though its (TSOA) position estimation ability of Category A coordinates is of a considerably good level of efficiency.

4.5.2 Efficiency Test of TROA via CRLB

To study the efficiency of the proposed TROA approach, the MSE's were compared to a derived CRLB for the problem at hand (details of the CRLB derivation are given in Appendix B). Figures 4.22 and 4.23 illustrate the estimation performance of our approach for the x coordinate and y coordinate of the NOI, respectively on both the conventional and logarithm scales. The position estimation performance has been studied for 3 different position of the NOI within the indoor environment of interest; the considered positions are: $[x, y] = [5, 5; 12, 4; 9, 14]$. In these three cases, the TROA approach shows good performances where the MSEs are close to their respective CRLBs.

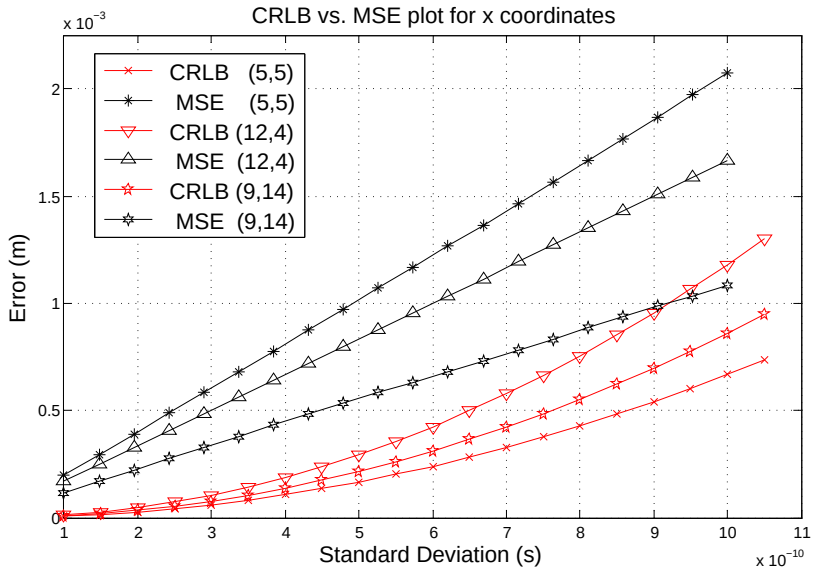

Figure 4.22: CRLB vs. MSE comparison for x coordinates of (5,5), (12,4) and (9,14)

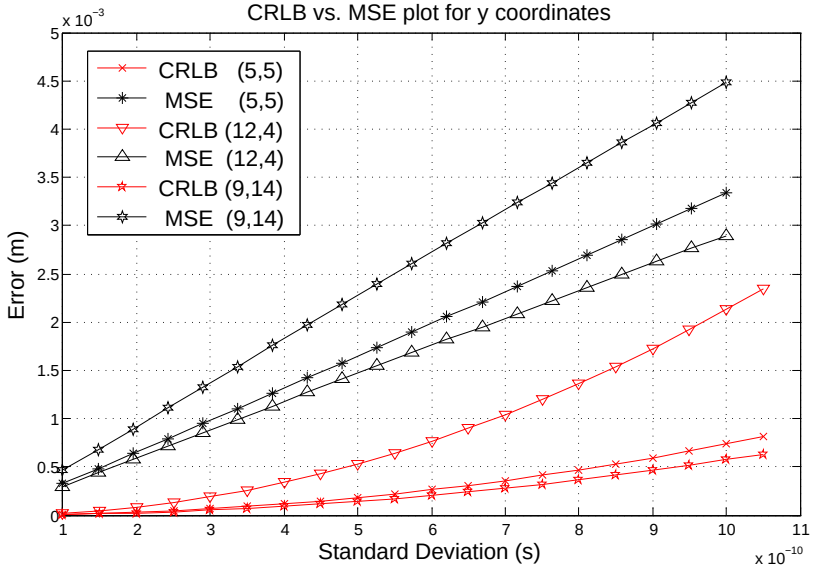

Figure 4.23: CRLB vs. MSE comparison for y coordinates of (5,5), (12,4) and (9,14)

4.6 Conclusion

4.6.1 Summary

In conclusion, a *novel* UWB-driven multilateration technique for position estimation in an indoor environment has been presented in this chapter. The presented technique exploits the inherent properties of UWB signal propagation; and its definition is in conjunction with the operational principles of the widely overlooked and under-studied TSOA position estimation technique. The accuracy of the proposed approach for a network of three receivers and one transmitter has been studied and presented. By means of a series of statistically driven MSE analyses, it has been shown that in comparison with TOA and TSOA, the proposed TROA technique possesses a much higher accuracy with regards to position estimation. The CRLBs have been computed using TROA measurement set; and it has also been shown that the proposed TROA technique shows good performances when the CRLB is directly compared with the MSE.

4.6.2 Contributions

The main research contributions presented in this chapter can be summarised as follows:

- Explicit definition and description of a *novel* time-based position estimation technique which is coined as Time Reflection of Arrival (TROA). TROA is wholly UWB-driven and unlike conventional position estimation techniques, it does not require the NOI to be either active or semi-passive.
- Explicit definition of the optimum 2-D TROA solution space in typical

indoor environment shapes (i.e. square and rectangle).

- Derivation of a new theoretical lower bound on the covariance of the TROA estimator based on the Cramér-Rao lower bound (CRLB) to determine the efficiency of TROA.

These research contributions have been documented and reported in a technical journal paper titled "A Novel UWB-based Multilateration Technique for Indoor Localisation". In February 2014, it was accepted for publication by the IET Communications Journal and has recently been included in the July 2014 edition [119].

Chapter 5

Case Study: Fall Detection Algorithm for Alzheimer's Disease (AD) Patients

5.1 Introduction & Problem Statement

In this chapter, an inherently novel and Ultra-Wideband (UWB) driven algorithm that performs the task of detecting unrecovered falls by an Alzheimer's Disease (AD) patient is presented. The proposed algorithm achieves this by cleverly using an element of the AD patient's location information in a 3-D solution space to determine their real-time postural orientation (i.e. fallen down, standing up, lying down) in a specified indoor environment. The utilised element is the 'z' coordinate of the patient's location information and it is obtained from a known point on the patients body. When this element is measured relative to the ground plane of coordinates (0, 0, 0), the height of the patient or the vertical distance

(V_d) between the patient and the floor is defined. Based on the specified AD patient's physical attributes, V_d is subsequently compared with a set of pre-defined heights that correspond to postural activities exclusively carried out by the patient. As it is shown in the following sections, this is done in order to facilitate the determination of the real-time postural orientation of the patient and ultimately ascertain if they have fallen down. Once a fall has been inferred and ascertained, the duration in which the patient's V_d value remains in the fall defining range is monitored for a fixed time to determine if they have recovered from the fall[1]. In the event that the V_d value either fails to increase within the allocated time or fluctuates sporadically within the allocated time, an alarm is triggered and a medical personnel is notified. For the entirety of this work, TSOA is employed as the underlying position estimation technique. TSOA is chosen because as implied in chapter 3, even though there is an additional receiver requirement for its implementation in comparison to both TOA and TDOA, it offers a better accuracy[2].

5.2 Background

Dementia to all intents and purposes is an unremitting disease that affects people that are of the ages of 65 and above (i.e. elderly people) [120–122]. One of the most common forms of dementia that is usually observed in this category of people is Alzheimer's Disease (AD) [120, 121]. With AD, the sufferer's reduced

[1] A V_d value that gradually increases with time is an indicator that the patient attempting to recover from the fall while a V_d value that remains constant over a period of time indicates no recovery attempt.

[2] It is noteworthy to mention that at the time this algorithm was formulated, TROA was yet to be conceptualised. Hence future work could entail a comparison between a fully defined 3-D TROA and TSOA to determine the better technique accuracy-wise.

brain capacity and functionality which is as a direct result of a combination of the adverse effect of this disease and the drugs being administered to combat it, makes them a lot more prone to a constant deterioration in their cognitive functions. Notably, this ultimately leads to a high occurrence of involuntary falling. In some cases, the involuntary fall is relatively mild and the patient is able to recover from it in a timely manner, while in other cases, the severity of the fall results in the inability of the patient to recover from it. In this work, we focus wholly on unrecovered falls and explicitly define an algorithm that detects such falls by using the patient's location information.

5.3 The Fall Detection Algorithm

The proposed algorithm embarks on the wireless fall detection process by constantly monitoring and measuring the vertical distance (V_d) between a fixed point on the body of a patient and the ground. For every measured value of V_d, a direct comparison is made with a pre-defined range of vertical distances (V_{pre}) which are collated in a preceding step by subjecting the patient to key postural orientations which are deemed as fall identifiers. Upon completion of this comparison, if it is determined that V_d corresponds to a measurement in the V_{pre} range that ascertains a fall, the algorithm is designed to trigger an alarm for the system to send a notification message to a designated Emergency Health Support Contact (EHSC). The EHSC, who could be the patient's primary care-giver or a nearby medical consultant, is sent this notification once a timer which is set to a defined value of '**alert**' seconds, has elapsed.

5.3.1 Measuring V_d

To measure the V_d between a fixed point on the body of the AD patient and the ground, an Ultra-Wideband (UWB) driven Time Sum of Arrival (TSOA) localisation scheme is used. With reference to the 3-D position estimation process detailed in Section 3.4.5.1 and Figure 5.1, the location of this fixed point is determined by initially splitting the indoor environment which typically takes the form of a 3-D solution space (x,y,z), into two independent 2-D solution spaces (x,y) and (y,z) respectively. Post-splitting of the solution space, the location defining coordinates are then determined using TSOA in the relevant 2-D solution space.

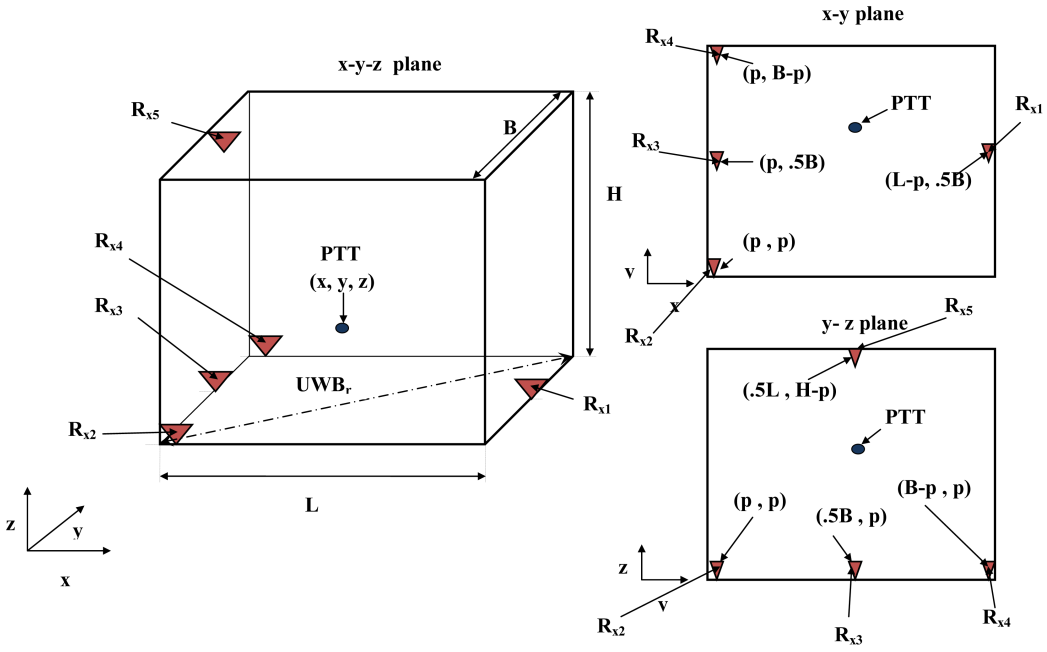

Figure 5.1: Aerial View of the defined DSS for TSOA localisation

The fixed point on the body of the AD patient is characterised by a passive tag (PTT) which assumes the form of a wrist band; and the patient is required to

wear it at all times on their wrist when they are in the desired solution space (DSS). The DSS refers to an indoor environment that is defined in accordance with the stringent UWB indoor transmission range limitations which currently is in the order of tens of meters [21, 23, 24]. Having mentioned that, with reference to Figure 5.1, the DSS is designed with calculated and deliberate values of Length (L), Breadth (B); and Height (H) which ultimately ensures that the magnitude of UWB_r never exceeds the desired transmission range of 30 m. Subsequently, the fall detection problem becomes one of determining the coordinates of the wrist band as this gives the coordinates of the patients wrist. Based on this and with reference to the DSS, V_d which was earlier defined as the vertical distance between a fixed point on the body of the patient and the ground, can be re-defined as the 'z' element when the 3-D location of the wrist band is determined using the UWB-driven TSOA localisation scheme. With reference to Figure 5.1, it is quite clear that the 'z' element of the 3-D location of the wrist band is only determined when the (y,z) solution space is solved in 2-D. Hence it suffices to conclude that for this fall detection application, solving the (x,y) solution space becomes redundant. Solving for V_d in $(y,\ z)$ solution space: Essentially, 2-D TSOA localisation is achieved by arranging a minimum of four reference nodes in a DSS, carefully pairing them; and thereafter making coordinate defining measurements based on signal propagation between these pairings.

Each pairing defines an ellipse that has a coordinate which defines the 2-D coordinate of the node of interest (NOI) [7, 19]. To determine the absolute value of this coordinate, multiple ellipses are defined and the intersection of them all yields this absolute value. In most cases, it is enough to consider only three reference node pairings (i.e. only three ellipses are defined) because the intersection of

their defined ellipses will always leads to one unique coordinate namely the 2-D location of the NOI. In this work, the determined 2-D coordinate of the NOI implies the 2-D location of the wrist band (i.e. PTT). As Figure 5.2 depicts, for each relevant pairing, the PTT based wrist band transmits an UWB signal $x(t)$ to the two reference nodes in the pairing. The arrival times of $x(t)$ at both reference nodes are identified; and the signal travel distances (D_{PTT-Rx_1} and D_{PTT-Rx_2}) are determined respectively by multiplying these arrival times with the speed of light (c). The sum of the resultant distances is called the 'range sum'; and it is used to define the ellipse. Equation 5.1 gives the general equation of ellipse E_1 where a_1 which is the semi major axis of the ellipse is defined as half of the range sum. In turn, b_1 which is the semi minor axis of E_1 is defined in accordance with the description depicted in Figure 5.2.

$$\mathbf{Y_0}^{\mathbf{T}}\mathbf{A_0}\mathbf{Y_0} + \mathbf{B_0}^{\mathbf{T}}\mathbf{Y_0} + \mathrm{c}_0 = 0 \tag{5.1}$$

$$\text{where } \mathbf{Y_0} = \begin{pmatrix} \mathrm{x} \\ \mathrm{y} \end{pmatrix}, \mathbf{A_0} = \begin{pmatrix} {\mathrm{a}_{00}}^{(0)} = {\mathrm{b}_1}^2 & {\mathrm{a}_{01}}^{(0)} = 0 \\ {\mathrm{a}_{01}}^{(0)} = 0 & {\mathrm{a}_{11}}^{(0)} = {\mathrm{a}_1}^2 \end{pmatrix},$$

$$\mathbf{B_0} = \begin{pmatrix} {\mathrm{b}_0}^{(0)} = -2\mathrm{h}_1{\mathrm{b}_1}^2 \\ {\mathrm{b}_1}^{(0)} = -2\mathrm{k}_1{\mathrm{a}_1}^2 \end{pmatrix},$$

$$\mathrm{c}_0 = {\mathrm{h}_1}^2{\mathrm{b}_1}^2 + {\mathrm{a}_1}^2{\mathrm{k}_1}^2 - {\mathrm{a}_1}^2{\mathrm{b}_1}^2$$

With three ellipses defined based on three relevant pairings, the 2-D coordinate of

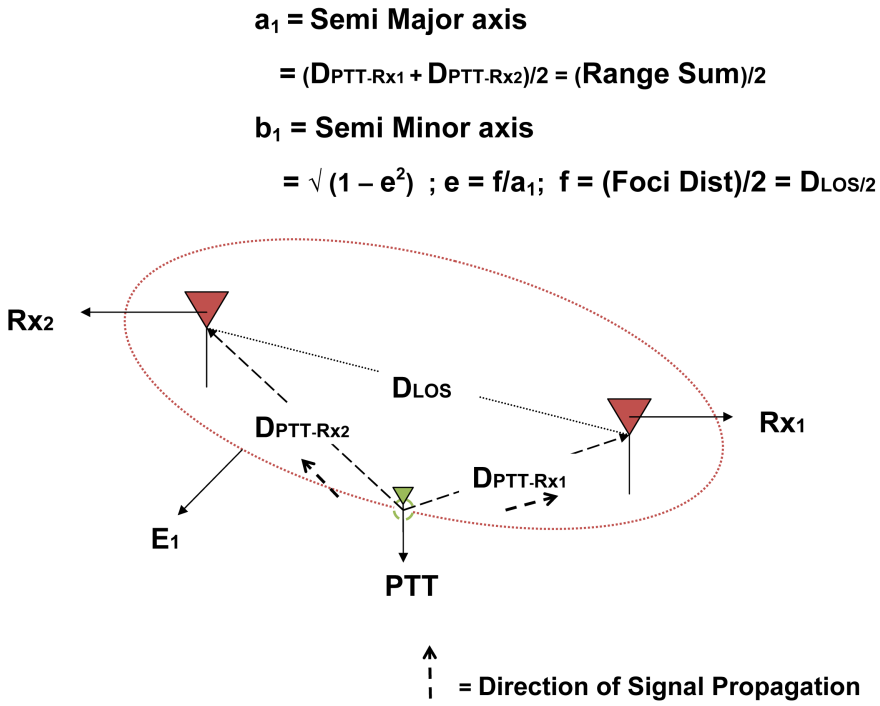

Figure 5.2: Time Sum of Arrival (TSOA) ellipse generation

the PTT becomes the unique intersection point of the ellipses. Consequently, the z element of the intersection coordinate becomes V_d. Algorithm 3 (in Appendix A) illustrates the coordinate determining process based on the three defined ellipses. 'rangesuma', 'rangesumb' and 'rangesumc' are the respective range sum measurements for the specified pairings. Meetpoint(E_1,E_2,E_3) defines the unique intersection point of the three ellipses; and ultimately the coordinate of V_d.

5.3.2 The V_d range

As Figure 5.3 depicts, the two key postural orientations deem as fall identifiers are 'standing' and 'sitting'. These postural orientations are deemed as fall identifiers because of the rapid deterioration in the cognitive functions of an AD patient, they

will always be at a greater risk of falling whenever they are in a non-lying postural orientation [123–127]. Furthermore, because 'standing' and 'sitting' encompasses all other non-lying postural orientations when postural activities (i.e. walking and running) are performed, these fall identifiers are instrumental in the time characteristic modelling process of non-lying postural orientations. For example, when a patient performs either the walking or running postural activity, with respect to the 'standing' postural orientation, these activities can be intuitively modelled as a standing orientation that spans for a time duration of $t = t_0 : t_0 + \alpha$ for walking; and $t = t_0 : t_0 + \beta$ for running[3]

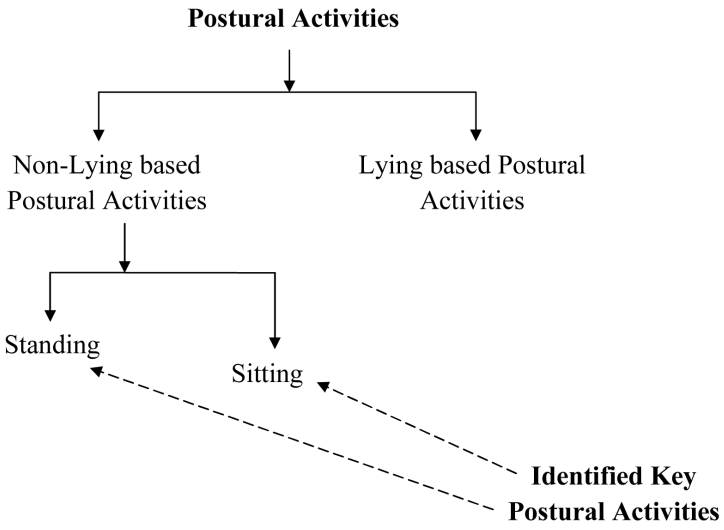

Figure 5.3: Taxonomy of postural activities

This intuitive modelling is possible because the postural orientation associated with either the running and walking postural activity when we consider V_d measurements, will always be likened to standing. For both cases of standing and

[3] α and β are arbitrary integer values that define the time it takes the postural activity to be completed. For example, with t_0 being the initial time (i.e. $t_0 = 0$), it takes the patient α seconds to walk and β seconds to run.

sitting by a patient, an upper boundary on their respective V_{pre} is defined as the distance between the ground and the wrist band when the arm which has the wrist band on it is extended all the way to the top. In turn, the lower boundary is defined as the distance between the ground and the wrist band when the arm which has the wrist band on it is extended all the way down. h_{21} and h_{22} are the upper and lower boundaries for the standing postural position respectively while h_{31} and h_{32} are the upper and lower boundaries for the sitting postural position respectively.

At this junction, two key terms namely a '**fall suspicion**' and a '**true fall**'are defined. A fall suspicion is defined as an event whereby an AD patient's real time V_d measurement becomes less than h_{32}. A $V_d < h_{32}$ measurement suggests that the patient is assuming an almost unnatural postural orientation which in itself doesn't ascertain a fall but becomes a worry if it remains the same for a long duration. Quantifying this long duration facilitates the translation of a fall suspicion into a true fall. A fall suspicion becomes a true fall when the V_d measurement remains less than h_{32} for a duration of a specified time of '**alert**' seconds. This timed measurement inadvertently mimics a scenario whereby the AD patients has fallen and does not recover within the given critical time constraint. According to [123, 128], Figure 5.4 illustrates all the typical fall scenarios; and characterises them according to the expected result an ideal fall detection system should give. For this work, we focus on the 8 defined unrecovered falls (i.e. falls without recovery). Each of the defined unrecovered falls end up with the AD patient either lying flat on the floor or being in a lateral position (i.e. lying sideways), and hence it is sufficient to translate the V_d during those 8 instances to measurements that are always less than h_{32}. Algorithm 4 depicts the main fall detection

algorithm; and its functionality is as thus. Essentially, all through the day, the algorithm constantly receives the V_d measurement from function TSOA(null) and compares it with pre-defined h_{32} value as previously explained. If it is detected that V_d is less than h_{32}, the timer '**alert**' seconds is triggered. Upon the elapsing of the timer, the algorithm check compares the measurement once again; and if V_d remains less than h_{32}, the EHSC is immediately notified.

Category	Name	Outcome	Vd translation for Patient
Backward fall	End Sitting	Positive	
	End Lying (Without Recovery)	Positive	Vd < h32
	End in Lateral Position (Without Recovery)	Positive	Vd < h32
	With Recovery	Negative	
Forward fall	On the Knees	Positive	
	With forward arm protection (Without Recovery)	Positive	Vd < h32
	End Lying flat (Without Recovery)	Positive	Vd < h32
	With rotation, ending in the lateral right position (Without Recovery)	Positive	Vd < h32
	With rotation, ending in the lateral left position (Without Recovery)	Positive	Vd < h32
	With recovery	Negative	
Lateral fall to the right	End Lying flat (Without Recovery)	Positive	Vd < h32
	With recovery	Negative	
Lateral fall to the left	End Lying flat (Without Recovery)	Positive	Vd < h32
	With recovery	Negative	
Syncope	Vertical slipping against a wall finishing in sitting position	Negative	
Neutral	To sit down on a chair then to stand up (consider chair height)	Negative	
	To lie down on the bed then to rise up.	Negative	
	To cough or sneeze	Negative	
	To walk a few meters	Negative	
	To bend down, catch something on the floor and then rise up.	Negative	

Figure 5.4: Fall detection evaluation scenarios

5.4 Simulation and Results

With the fall detection algorithms's successful execution depending primarily on the employed TSOA technique, a test of the effectiveness of TSOA in the defined

DSS becomes a requirement because it also inadvertently acts as an indicator of the fall detection algorithm's effectiveness.To test the effectiveness of TSOA, the widely used test parameter namely the MSE is invoked [99]. The MSE of a known estimator (i.e. TOA, TSOA, TDOA) in a DSS is defined as the scalar difference between the true value of the parameter under test and its implied value which is given by the estimator; and expressed in [99], it is represented mathematically

$$\mathrm{MSE}(\theta_{\mathrm{i}=y,z}) = \mathrm{E}[(\theta'_{\mathrm{i}=y,z} - \theta_{\mathrm{i}=y,z})^2] \tag{5.2}$$

by equation 5.2. where 'i' refers to the element in the solution space that is under test (i.e. y or z), $\theta_{i=y,z}$ refers to the true value of the element and $\theta'_{i=y,z}$ refers to the implied value of the element . The realistic TSOA measurement error variance is modelled as a random variable of normal distribution (i.e. $N(0, \sigma^2)$); and 1000 random samples is generated per σ. The σ range is defined in accordance with an indoor localisation accuracy that spans from 0.03 m and 0.3 m (i.e. 0.1 ns to 1 ns). Essentially, this defined range mimics the influence of signal noise (i.e. multipath propagation, interference) when the TSOA measurement is carried out in a relatively noise-free environment up until an extremely noisy environment. For this effectiveness test, we randomly select six (6) possible known locations of the PTT; and these locations are (12,0.9), (10,0.5), (12,0.4), (13,0.95), (8,0.7), (9,0.2). For each known location, $x(t)$ is propagated from the PTT to the relevant reference node pairing as described in Section 5.3.1; and their respective arrival times is determined. The determined arrival times are added to every defined σ value in the range and the rangesum is determined. This process is repeated for two more reference node pairings; and consequently, the implied value of the

PTT's coordinate is determined according to Algorithm 3. Figure 5.5 depicts the MSE values for the σ range when both the true values and the implied values of the PTT are considered. With the maximum MSE value obtained when all 6 locations are considered within the defined σ range being approximately 0.0007 metres, it is clear that the TSOA algorithm is very effective amidst the defined realistic TSOA measurement error variance; and hence the effectiveness of the overall fall detection algorithm is assured.

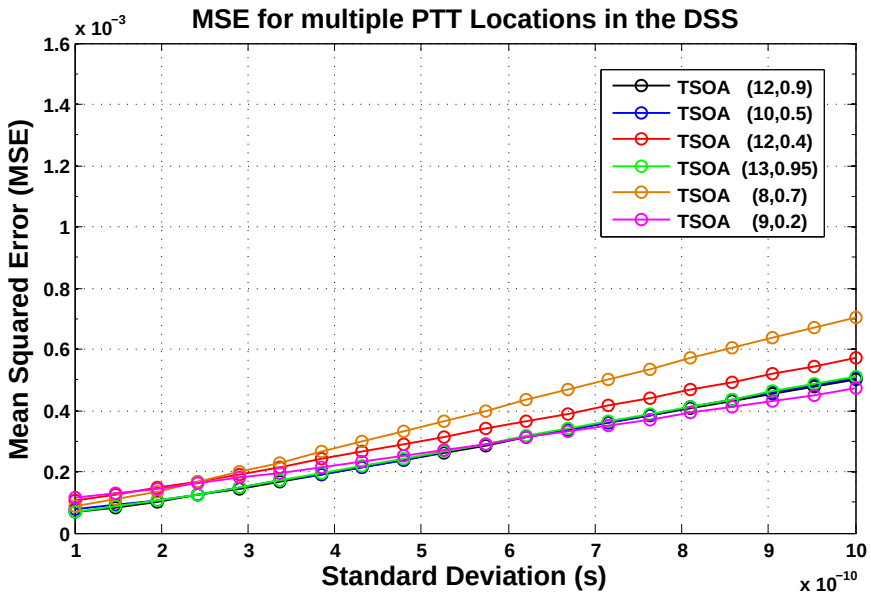

Figure 5.5: Mean Squared Error (MSE) for multiple PTT Locations

5.5 Conclusions

5.5.1 Summary

In conclusion, a novel fall detection algorithm that is aimed at detecting unrecovered falls suffered by AD patients has been presented and explicitly detailed. With the presented algorithm being predominantly driven by indoor position estimation, the typically unvoiced TSOA technique is employed as the driving force. By means of a series of MSE analyses, the effectiveness of TSOA in a range of noisy environments has been shown; and this inadvertently serves as a means of validation of the fall detection algorithm.

5.5.2 Contributions

The main research contributions presented in this chapter so far can be summarised as follows:

- A novel method of detecting falls by Alzheimer's Disease Patients using UWB-based position estimation techniques.

These research contributions have been documented and reported in a technical letter titled "A Novel UWB-driven Fall Detection algorithm for determining unrecovered falls of Alzheimer's Disease (AD) Patients". The letter has been sent to the IET Healthcare Technology Letters for possible publication and a decision relating to this is imminent.

Chapter 6

Conclusions and Future Research Directions

6.1 Conclusions

Undoubtedly, the utilisation of indoor position estimation techniques to successfully complete specific tasks is an appealing choice for modern multidisciplinary applications that have an element of object localisation in them. For most of these applications, being able to accurately estimate the position(s) of their respective OOI's does not necessarily complete the desired task. However, its successful completion is significantly reliant on an accurate estimate of the OOI. To this effect, research work into enhancing the accuracy levels of conventional position estimation techniques is constantly gathering momentum. For time-based position estimation systems, it has been widely proven in literature that along with UWB's other inherent properties, its comparatively large frequency spectrum and very high time-domain resolution makes it a prime candidate to be the technology enabler which guarantees accurate position estimates of the OOI. However, with the UWB technology being relatively new in the commercial scene, it is still in

the process of living up to its future promise. From a position estimation vantage point, for UWB to fully live up to its projected potential, the factors that affect the accuracy of time-based position estimation systems which are UWB driven, need to be addressed. In no particular order, the main factors are the multipath propagation, MAI and NLOS. For the entirety of the research work presented in this thesis, the multipath propagation issue has been singled out and addressed.

The existence of multipath propagation which is a direct consequence of the interaction of the transmitted UWB signal with different objects in the defined propagation environment results in the reception of multiple copies of the received signal at the receiving end. With multiple copies received, it becomes a cumbersome task to identify the relevant copies of the received signals that are required to complete the position estimation task. In most cases, the propagation scenario is assumed to be two-path[1] and this significantly reduces the number of received signals to two. This reduction is very beneficial to conventional position estimation techniques because the range or proximity measurements required to implement them become quite trivial to determine. In a practical environment however, the two-path scenario is not readily obtained due to the ever-presence of objects with different inherent properties. To this effect, in Chapter 3, a pre-localisation algorithm that ultimately aims to convert the practical propagation scenario from *multipath* to *two-path* has been proposed in this thesis. Through a series of sampling, template creation and matching, the proposed algorithm utilises the unique electrical properties of the transmitted UWB signal as well as its reflection coefficient to distinguish between the signals that have inter-

[1]Barring the OOI, the other objects in the environment are neglected in a two-path propagation scenario, hence the multiple copies of the received signal are omitted.

acted with the OOI from those that have interacted with other objects in the environment. The distinguished signals are then subsequently used to determine the range or proximity measurements required for position estimation using the specified technique. Following the propagation scenario conversion, the mode of deployment of the transmitter and receivers for position estimation using the UWB-driven EL positioning scheme was addressed. It has been shown that by properly considering the placement and deployment of the relevant transmitter and receivers as well as the UWB signal transmission range, the EL positioning scheme could be achieved notably more accurately using a reduced number of receivers.

In Chapter 4, a novel position estimation technique has been presented. In contrast to conventional techniques, the proposed technique which is coined as TROA estimates the position of the OOI without the requirement for it to be either active or semi-passive; or have either an active or semi-passive component that facilitates signal propagation. The reflection properties of the employed UWB signal ensures that the OOI remains wholly passive. As it has been shown, based on a series of range or proximity measurements obtained from the required number of transmitter-receiver combinations, the 2-D estimate of the OOI's position is determined as the intersection point of three ellipses. When compared to TOA and TSOA by means of a series of MSE analyses, it has been shown that TROA offers a better level of accuracy. It has also been shown by means of CRLB derivation and analysis that the proposed technique achieves a good performance when the MSE and CRLB values are considered.

In Chapter 5, a fall detection technique that is based on the operating principles of position estimation has been presented. As it has been described, the

reliance of the algorithm on an accurate estimate of the wristband being worn by the PIC results in the performance evaluator of the algorithm being that of the employed position estimation technique. To that effect, the performance of the employed TSOA has been determined by means of an MSE analysis.

6.2 Future Research Directions

To extend and enrich the research work presented in this thesis, the following research directions are suggested:

- TROA which has been presented in Chapter 4 has been shown to have a comparatively good position estimation performance when the location of a single NOI is required. One possible extension to this work would be to investigate the effect of transmitter/receiver placement in the O2SS on the accuracy of TROA. The ultimate aim of this would be to identify the transmitter/receiver placement that would lead to the highest level of position estimation accuracy.

- With the localisation and monitoring of multiple patients in facilities such as care homes and hospital wards being the target application area, another possible extension to this work would be to extend TROA's positioning capabilities from a single NOI to multiple NOI's. With each patient fitted with a wrist-band which have dissimilar electrical properties, intuitively, it would possible to distinguish and identify individual targets when the $\mathbf{S_2}$ scattering centre described in Chapter 4 is once again considered.

Appendix A

Algorithm 1 Proposed 2-D Elliptical Localisation (EL)

procedure PositionEstimate
    (x_{noi}, y_{noi}) = (0, 0) ▷ **Parameter Initialization**
    rangesuma = 0; rangesumb = 0
    trigger ← datestr(now, 'hh:mm:ss')

    while trigger ≠ '24:00:00' **do**
        rangesuma ← prelocalise(T_x-R_{x1})
        plot(E_1, rangesuma)
        rangesumb ← prelocalise(T_x-R_{x3})
        plot(E_2, rangesumb)

        y(1) = meet1(E_1, E_2) ▷ **1st Intersection Point**
        z(1) = meet1(E_1, E_2)
        y(2) = meet2(E_1, E_2) ▷ **2nd Intersection Point**
        z(2) = meet2(E_1, E_2)
        if x(1) > 0 && y(1) > 0 **then**
            x_{noi} ← x(1); y_{noi} ← y(1)
        else if x(2) > 0 && y(2) > 0 **then**
            x_{noi} ← x(2); y_{noi} ← y(2)
        end if

        return (x_{noi}, y_{noi}) ▷ **NOI's Coordinate**
    end while
end procedure

Algorithm 2 Determine NOI's Coordinate using TSOA Multilateration

```
1: procedure TsoaMultilateration
2:     (x_noi, y_noi) = (0, 0)                          ▷ Parameter Initialization
3:     trigger ← datestr(now, 'hh:mm:ss')
4:
5:     while trigger ≠ '24:00:00' do
6:         x(1) = meet1(E_1, E_2)                       ▷ 1st Intersection Point
7:         y(1) = meet1(E_1, E_2)
8:         x(2) = meet2(E_1, E_2)                       ▷ 2nd Intersection Point
9:         y(2) = meet2(E_1, E_2)
10:        x(3) = meet3(E_1, E_3)                       ▷ 1st Intersection Point
11:        y(3) = meet3(E_1, E_3)
12:        x(4) = meet4(E_1, E_3)                       ▷ 2nd Intersection Point
13:        y(4) = meet4(E_1, E_3)
14:
15:        if x(1) == x(3) && y(1) == y(3) then
16:            x_noi ← x(1) ← x(3); y_noi ← y(1) ← y(3)
17:        else if x(1) == x(4) && y(1) == y(4) then
18:            x_noi ← x(1) ← x(4); y_noi ← y(1) ← y(4)
19:        else if x(2) == x(3) && y(2) == y(3) then
20:            x_noi ← x(2) ← x(3); y_noi ← y(2) ← y(3)
21:        else if x(2) == x(4) && y(2) == y(4) then
22:            x_noi ← x(2) ← x(4); y_noi ← y(2) ← y(4)
23:        end if
24:
25:        return (x_noi, y_noi)                        ▷ NOI's Coordinate
26:    end while
27: end procedure
```

Algorithm 3 PPT's Vertical Distance Algorithm

```
1: procedure TSOA(null)[z]
2:     (y_noi, z_noi) = (0, 0)                          ▷ Parameter Initialization
3:     rangsuma = 0; rangesumb = 0; rangesumc = 0
4:     trigger ← datestr(now, 'hh:mm:ss')
5:
6:     while trigger ≠ '24:00:00' do
7:         rangesuma ← rangesum(PTT,R_x2,R_x3)
8:         plot(E_1, rangesuma)                         ▷ Ellipse E_1 Definition
9:         rangesumb ← rangesum(PTT,R_x3,R_x4)
10:        plot(E_2, rangesumb)                         ▷ Ellipse E_2 Definition
11:        rangesumc ← rangesum(PTT,R_x3,R_x5)
12:        plot(E_3, rangesumc)                         ▷ Ellipse E_3 Definition
13:
14:        (y_noi, z_noi) = meetpoint(E_1, E_2, E_3)
15:        return (y_noi, z_noi)                        ▷ PPT's Coordinate
16:    end while
17:
18:    V_d ← z_noi
19:    return V_d                                       ▷ PTT's Vertical Distance
20: end procedure
```

Algorithm 4 Fall Detection Algorithm

```
1: procedure FD(null)
2:     while trigger ≠ '24:00:00' do
3:         Day ← datestr(now, 'dddd')
4:         Date ← datestr(now, 'dd-mmm-yyyy')
5:         Time ← datestr(now, 'hh:mm:ss')
6:         h32 ← 'xx'
7:         znoi ← TSOA(null)
8:         alert ← 'xx:xx:xx'
9:         StartTime ← Time
10:
11:        if znoi < h32 then
12:            while (StartTime - Time) ≠ alert  do
13:                Time
14:            end while
15:            if znoi < h32 then
16:                ALERT RAISED AT EHSC!!
17:                break
18:            else
19:            end if
20:        end if
21:        trigger ← datestr(now, 'hh:mm:ss')
22:    end while
23: end procedure
24:
25: main
26:     znoi= 0.00                          ▷ Parameter Initialization
27:     trigger ← datestr(now, 'hh:mm:ss')
28:     FD(null)
29: end main
```

Appendix B

Derivation of CRLB for TROA

A set of random data z with parameter of interest x are considered and it is assumed that the probability density $p(z;x)$ satisfies the regularity condition:

$$E\{\frac{\partial \ln p(z;x)}{\partial x}\} = 0 \tag{1}$$

Where the ensemble mean is taken with respect to $p(z;x)$. The variance of any unbiased estimator must satisfy the following inequality, for every parameter x to be estimated [99]:

$$var(x) \geq \frac{1}{E\{\frac{\partial \ln p(z;x)}{\partial x}\}^2} \tag{2}$$

The denominator in the above expression is called Fisher Information $\mathbf{J}(\mathbf{x})$ for the data x resulting in the following expression:

$$\mathbf{J}(\mathbf{x}) = -E\{\frac{\partial^2 \ln p(z;x)}{\partial x^2}\} \tag{3}$$

It follows that when the CRLB is achieved, the variance equals the inverse of

the Fisher information. Intuitively, the more information we have, the lower the CRLB is. $\mathbf{J}(\mathbf{x})$ has the property of a mesure of information, hence it is non-negative and additive in the case of independent observations. The CRLBs provide a lower bound on the covariance that is asymptotically achievable by any unbiased estimation algorithm. To study the efficiency of the proposed TROA approach, the MSEs of the parameter estimation is compared to their corresponding Cramér-Rao lower bounds (CRLBs). Letting the target location $x \in \mathbb{R}^2$ be the parameter of interest and $\hat{x}$ be an estimate of it obtained from the measurement vector $\mathbf{z}$. The error covariance $\mathbb{E}[(\hat{x} - x)(\hat{x} - x)^T]$ is bounded below by:

$$\mathbb{E}[(\hat{x} - x)(\hat{x} - x)^T] \geq \mathbf{J}^{-1} \tag{4}$$

$$\mathbf{J} = \mathbb{E}[\nabla_x \ln p(\mathbf{z}|x)(\nabla_x \ln p(\mathbf{z}|x))^T] \tag{5}$$

where $\mathbb{E}[.]$ determines the expectation value.

Additionally the unknown time of emission t_0 is to be estimated. Therefore, for position estimation, the parameter of interest is the extended position state of the emitter:

$$x^{(+)} = (t_0, x^T)^T \in \mathbb{R}^3 \tag{6}$$

Given the measurement vector $\mathbf{z}_t$, the CRLB for TROA position estimation for one time step is computed from the inverse of the Fisher information for TROA,

a 3×3 matrix:

$$\mathbf{J}_t = \frac{\partial \mathbf{h}_t^T}{\partial x^(+)} \mathbf{R}_t^{-1} \frac{\partial \mathbf{h}_t}{\partial x^(+)} \tag{7}$$

The Jacobian of the measurement function is:

$$\frac{\partial \mathbf{h}_t}{\partial x^{(+)}} = \begin{pmatrix} \frac{\partial h_1}{\partial t_0} & \frac{\partial h_1}{\partial x} & \frac{\partial h_1}{\partial y} \\ \frac{\partial h_2}{\partial t_0} & \frac{\partial h_2}{\partial x} & \frac{\partial h_2}{\partial y} \\ \frac{\partial h_3}{\partial t_0} & \frac{\partial h_3}{\partial x} & \frac{\partial h_3}{\partial y} \end{pmatrix} = \begin{pmatrix} c & \frac{x-x_1}{r_1} & \frac{y-y_1}{r_1} \\ c & \frac{x-x_2}{r_2} & \frac{y-y_2}{r_2} \\ c & \frac{x-x_3}{r_3} & \frac{y-y_3}{r_3} \end{pmatrix} \tag{8}$$

The computation of the FIM follows as:

$$\begin{aligned} \mathbf{J}_t &= \begin{pmatrix} c & c & c \\ \frac{x-x_1}{r_1} & \frac{x-x_2}{r_2} & \frac{x-x_3}{r_3} \\ \frac{y-y_1}{r_1} & \frac{y-y_2}{r_2} & \frac{y-y_3}{r_3} \end{pmatrix} \times \begin{pmatrix} \frac{1}{\sigma_1^2} & 0 & 0 \\ 0 & \frac{1}{\sigma_2^2} & 0 \\ 0 & 0 & \frac{1}{\sigma_3^2} \end{pmatrix} \\ &\quad \times \begin{pmatrix} c & \frac{x-x_1}{r_1} & \frac{y-y_1}{r_1} \\ c & \frac{x-x_2}{r_2} & \frac{y-y_2}{r_2} \\ c & \frac{x-x_3}{r_3} & \frac{y-y_3}{r_3} \end{pmatrix} \\ &= \sum_{i=1}^{3} \begin{pmatrix} \frac{c^2}{\sigma_i^2} & \frac{c}{\sigma_i^2}\frac{x-x_i}{r_i} & \frac{c}{\sigma_i^2}\frac{y-y_i}{r_i} \\ \frac{c}{\sigma_i^2}\frac{x-x_i}{r_i} & \frac{1}{\sigma_i^2}\frac{(x-x_i)^2}{r_i^2} & \frac{1}{\sigma_i^2}\frac{(x-x_i)(y-y_i)}{r_i^2} \\ \frac{c}{\sigma_i^2}\frac{y-y_i}{r_i} & \frac{1}{\sigma_i^2}\frac{(x-x_i)(y-y_i)}{r_i^2} & \frac{1}{\sigma_i^2}\frac{(y-y_i)^2}{r_i^2} \end{pmatrix} \end{aligned} \tag{9}$$

The Fisher information can be expressed by:

$$\mathbf{J}_t = \begin{pmatrix} J_{11} & J_{12} & J_{13} \\ J_{21} & J_{22} & J_{23} \\ J_{31} & J_{32} & J_{33} \end{pmatrix} = \begin{pmatrix} J_t & J_{t,pos} \\ J_{pos,t} & \mathbf{J}_{pos} \end{pmatrix} \tag{10}$$

where $\mathbf{J}_{pos}$ is the Fisher information of the position space, J_t The FIM of the time space and the others are the cross terms. The CRLB of the position space can be computed using the matrix inversion lemma [99]. The time of emission is treated as nuisance parameter. It can be shown that $\mathbf{J}_{pos} = \mathbf{J}_{\Delta t_i}, i = 1, \ldots, 3$.

References

[1] A. W. Darkins and M. A. Cary, *Telemedicine and Telehealth: Principles, Policies, Performance and Pitfalls*. Springer Publishing Company, INC, Publications, 2000. 1, 17

[2] A. C. Norris, *Essentials of Telemedicine and Telecare*. John Wiley and Sons, INC, Publications, 2002. 1, 17

[3] S. Brownsell, *Assistive Technology and Telecare: Forging Solutions for Independent Living* . Policy Press, 2003.

[4] M. J. Fisk, *Social Alarms to Telecare: Older People's Services in Transition.* Policy Press, 2003.

[5] N. Oudshoorn, *Telecare Technologies and the Transformation of Healthcare (Health, Technology and Society)* . Palgrave Schol, Print UK, 2011. 1

[6] M. Maheu, P. Whitten, and A. Allen, *E-Health, Telehealth, and Telemedicine: A Guide to Startup and Success* . Jossey-Bass, 2011. 1, 17

[7] D. Munoz, F. Bouchereau, C. Vargas, and R. Enriquez-Caldera, *Position Location Techniques and Applications*. Academic Press, Elsevier Inc Pub-

lications, 2003. 2, 3, 4, 5, 25, 40, 41, 42, 43, 44, 45, 46, 47, 48, 49, 50, 51, 61, 62, 82, 86, 97, 98, 100, 101, 102, 135

[8] D. Mohapatra and S. B. Suma, "Survey of location based wireless services," in *Proceedings IEEE International Conference on Personal Wireless Communications, ICPWC*, pp. 358– 362, Jan. 2005. 2

[9] T. H. I. Yamada, T. Ohtsuki and L. Zheng, "An indoor position estimation method by maximum likelihood algorithm using RSS," in *Proceedings Annual Conference ,SICE*, pp. 2927–2930, Sept. 2007. 2, 44

[10] N. Uchitomi, A. Inada, M. Fujimoto, T. Wada, K. Mutsuura, and H. Okada, "Accurate indoor position estimation by Swift-Communication Range Recognition (S-CRR) method in passive RFID systems," in *Proceedings International Conference on Indoor Positioning and Indoor Navigation (IPIN)*, pp. 1–7, Sept. 2010.

[11] D. Hauschildt and N. Kirchhof, "Improving indoor position estimation by combining active TDOA ultrasound and passive thermal infrared localization," in *Proceedings 8th Workshop on Positioning Navigation and Communication (WPNC)*, pp. 94–99, Apr. 2011.

[12] R. Hongliang, M. Meng, and X. Lisheng, "Indoor Patient Position Estimation Using Particle Filtering and Wireless Body Area Networks," in *Proceedings 29th Annual International Conference of the IEEE Engineering in Medicine and Biology Society, EMBS*, pp. 2277–2280, Aug. 2007. 44

[13] M. K. M. Aso and T. Hattori, "A new location estimation method based

on maximum likelihood function in cellular systems," in *Proceedings 54th IEEE Conference on Vehicular Technology,VTC*, pp. 106– 110, 2001. 44

[14] J. K.-Y. N. K. Man-Kin Chu and K. R.P.H.Leung, "A New Approach for Locating Mobile Stations under the Statistical Directional Propagation Model," in *20th International Conference on Advanced Information Networking and Applications, AINA*, pp. 932–940, Apr. 2006.

[15] P. M. T. Roos and H. Tirri, "A Statistical Modeling Approach to Location Estimation," in *IEEE Trans. Mobile Comput.*, pp. 59–69, Mar. 2002. 2, 44

[16] I. Yu, K.; Sharp and Y. Jay Guo, *Ground-Based Wireless Positioning*. Wiley - IEEE, 2009. 2, 41, 43

[17] J. Figuerias and S. Frattasi, *Mobile Positioning and Tracking: From Conventional to Cooperative Techniques*. Wiley, 2010. 25, 40, 42, 43, 44, 46

[18] L. Yunhao and Y. Zheng, *Location, Localization, and Localizability: Location-awareness Technology for Wireless Networks*. Springer Publications, 2011. 3, 4, 5, 41, 44, 51, 59, 98, 101, 102

[19] Z. Sahinoglu, S. Gezici, and I. Guvenc, *Ultra-Wideband Positioning Systems: Theoretical Limits, Ranging Algorithms and Protocols*. Cambridge University Press, 2008. ix, 2, 4, 6, 9, 10, 11, 15, 17, 25, 34, 40, 41, 42, 43, 44, 45, 46, 47, 49, 50, 51, 52, 53, 54, 55, 56, 61, 63, 67, 82, 97, 98, 100, 102, 103, 120, 125, 135

[20] T. M. Toolan and D. W. Tufts, "Detection and estimation in non-stationary

environments," in *Proceedings IEEE Asilomar Conference on Signals, Systems & Computers*, pp. 797–801, Nov. 2003. 3

[21] M. Ghavami, L. Michael, and R. Kohno, *Ultra Wideband Signals and Systems in Communication Engineering*. John Wiley and sons publication, 2004. 5, 6, 7, 8, 10, 13, 15, 19, 25, 26, 28, 31, 32, 33, 34, 35, 36, 37, 38, 40, 50, 51, 54, 55, 59, 64, 65, 66, 71, 75, 78, 83, 102, 103, 107, 112, 113, 114, 118, 135

[22] IEEE 802.11x, "IEEE 802 Standards." http://www.ieee802.org/11/. 5

[23] J. H. Reed, *An Introduction to Ultra Wideband Communication Systems*. Prentice Hall PTR, 2005. 5, 6, 7, 8, 10, 11, 13, 15, 19, 25, 26, 27, 28, 31, 32, 33, 34, 35, 38, 39, 41, 51, 59, 65, 66, 71, 78, 102, 107, 112, 135

[24] I. Opperman, M. Hamalainen, and J. Iinatti, *UWB theory and applications*. John Wiley and Sons, 2004. 5, 6, 7, 8, 10, 11, 12, 13, 14, 15, 19, 25, 26, 28, 29, 31, 32, 33, 34, 35, 36, 38, 39, 40, 41, 42, 43, 44, 45, 46, 47, 48, 49, 50, 51, 52, 59, 61, 63, 65, 66, 67, 71, 75, 78, 82, 100, 102, 103, 107, 112, 135

[25] Federal Communications Commission, "Part 15- Radio Frequency Devices." http://www.ecfr.gov/cgi-bin/text-idx?rgn=div5;node=47:1.0.1.1.16, 2006. 8, 9

[26] L. Yang and G. Giannakis., "Ultra-wideband communications: an idea whose time has come," in *IEEE Signal Processing Magazine, vol.21, no.6,*, pp. 26– 54, 2004. 8, 13, 15, 28, 33, 37, 39

[27] Time Domain Corporation, "Comments to Time Domain Corporation,

Docket 98-154. In the Matter of Revision of Part 15 of the FCC's Rules Regarding Ultra wide-band Transmission Systems," 1998. 13, 53, 54

[28] H. Lucken, *Communication and Localization in UWB Sensor Networks: A Synergetic Approach (Google eBook)*. Logos Verlag Berlin GmbH, 2013. 13

[29] G. B. Giannakis, Z. Liu, X. Ma, and S. Zhou, *Space-Time Coding for Broadband Wireless Communications*. John Wiley and Sons, INC, Publications, 2006. 14

[30] S. Gezici, Z. Tian, G. Giannakis, H. Kobayashi, A. Molisch, H. Poor, and Z. Sahinoglu, "Localization via ultra-wideband radios: a look at positioning aspects for future sensor networks," in *IEEE Signal Processing Magazine,vol. 22, no. 4*, pp. 70–84, 2005. 15, 16

[31] S. M. Kay, *'Fundamentals of Statistical Signal Processing: Estimation Theory'*. Prentice Hall Signal Processing Series, 1993. 15

[32] O. Onalaja and M. Ghavami, "Telecare: A sensor network approach," in *Proc. SWICOM/APSR*, 2012. 17, 18

[33] K. Doughty, G. Williams, P. J. King, and R. Woods, "DIANA-a telecare system for supporting dementia sufferers in the community," in *Proceedings of the 20th Annual International Conference of the IEEE Engineering in Medicine and Biology Society*, pp. 1980–1983, 1998. 90

[34] F. Magrabi, N. H. Lovell, and B. G. Celler, "Methodology for designing telecare systems: a case study in cystic fibrosis monitoring," in *IEEE*

EMBS International Conference on Information Technology Applications in Biomedicine, pp. 60–64, 2000.

[35] G. Williams, K. Doughty, K. Cameron, and D. A. Bradley, "A Smart fall and activity monitor for telecare applications," in *Proceedings of the 20th Annual International Conference of the IEEE Engineering in Medicine and Biology Soceity*, pp. 1151–1154, 1998.

[36] A. Gund, I. Ekman, K. Lindcrantz, B. A. Sjoqvist, E. L. Staaf, and N. Thorneskold, "Design evaluation of a home-based telecare system for Chronic Heart Failure patients," in *30th Annual International Conference of the IEEE Engineering in Medicine and Biology Society*, pp. 5851–5854, 2008. 17, 90

[37] Y. Zhou, C. L. Law, Y. L. Guan, and F. Chin, "Indoor elliptical localization based on asynchronous uwb range measurement," in *IEEE Trans. Instrum. Meas. vol. 60, no. 1*, Jan. 2011. 19, 59, 61, 62, 63, 66, 67, 77, 78

[38] A. D. Angelis, S. Dwivedi, and P. Handel, "Characterization of a flexible uwb sensor for indoor localization," in *IEEE Trans. Instrum. Meas. vol. 62, no. 5*, pp. 905–913, May. 2013.

[39] A. Cazzorla, G. D. Angelis, A. Moschitta, M. Dionigi, F. Alimenti, and P. Carbone, "A 5.6-GHz UWB Position Measurement System," in *IEEE Trans. Instrum. Meas. vol. 62, no. 3*, pp. 675–683, Mar. 2013. 19

[40] B. Allen, M. Ghavami, A. Armogida, and H. Aghvami, "The holy grail of wire replacement?," in *IEE Communications Engineer Magazine, vol.1, no.5,*, pp. 14– 17, Oct. - Nov. 2003. 25

[41] M. Win and R. Scholtz, "Ultra-wide bandwidth time-hopping spread-spectrum impulse radio for wireless multiple-access communications," in *IEEE Trans.Commun. vol. 48, no. 4*, pp. 679– 689, 2000. 25, 59, 64

[42] X. Shen, W. Zhuang, H. Jiang, and J. Ca, "Medium access control in ultra-wideband wireless networks," in *IEEE Trans. Vehic. Technol.*, pp. 1663–1677, 2005. 26

[43] M. D. Benedetto, T. Kaiser, A. F. Molisch, I. Opperman, C. Politano, and D. Porcino, "UWB Communication Systems: A Comprehensive Overview," in *Hindawi Publishing Corporation*, 2006. 28, 29, 39

[44] B. Hu and N. Beaulieu, "Accurate evaluation of multiple-access performance in TH-PPM and TH-BPSK UWB systems," in *IEEE Trans. Commun., vol.52, no.10*, pp. 1758– 1766, 2004. 28, 30

[45] J. G. Proakis, *Digital Communications*. Addison Wesley, 4th Edition, 2000. 32, 33

[46] A. Naanaa and S. Belghith, "Performance enhancement of a time hoppingpulse position modulation ultra-wideband system using guided local search," in *IET Journal of Commun.*, pp. 2212–2220, 2011. 33

[47] Z. J. Q. Zhu and C. Zou, "On the performance of different modulation schemes for UWB systems in a multipath channel," in *Proceedings of the IET International Conference on Wireless, Mobile and Multimedia Networks*, pp. 1–4, Nov. 2006. 33

[48] A. A. Zaman and M. Islam, "Modulation schemes and pulse shaping in ultra

wideband," in *Proceedings of the IEEE Southeast Conference*, pp. 142–146, Apr. 2008. 34

[49] R. Hidayat and Y. Miyanga, "IR-UWB pulse position modulation and pulse shape modulation through S-V channel model," in *Proceedings of the 2nd International Conference on Communication Software and Networks (ICCSN 10)*, pp. 214–217, Feb. 2010. 34

[50] J. R. Foerster, "The effects of multipath interference on the performance of UWB systems in an indoor wireless channel," in *Proc. Spring Vehic. Technol.*, 2001. 36

[51] H. Hashemi, "Impulse response modelling of indoor radio propagation channels," in *IEEE Journal on Selected Areas in Communications*, pp. 967–978, 1993. 36, 37, 38

[52] K. Pahlavan and A. Levesque, *Wireless Information Networks*. John Wiley & Sons, Inc., 1995. 37

[53] A. A. Saleh and R. A. Valenzuela, "A statistical model for indoor multipath propagation," in *IEEE Journal of Selcted Areas in Communications*, pp. 128–137, 1987. 37

[54] A. F. Molisch, D. Cassioli, C.-C. Chong, S. Emami, A. Fort, B. Kannan, J. Karedal, J. Kunisch, H. G. Schantz, K. Siwiak, , and M. Z. Win, "A comprehensive standardized model for ultrawideband propagation channels," in *IEEE Trans. Antennas Propagat. vol. 52, no.11*, pp. 3151–3166, 2006. 37

[55] M. Win and R. Scholtz, "On the robustness of ultra-wide bandwidth signals

in dense multipath environments," in *IEEE Commun. Letters vol. 2*, pp. 10–12, 1998. 38

[56] K. Colling and P. Ciorciari, "Ieee military communications conference, milcom," in *Ultra wideband communications for sensor networks*, pp. 2384–2390, 2005. 39

[57] K. Muthukrishnan, M. E. M. Lijding, and P. J. M. Havinga, "Towards smart surroundings: Enabling techniques and technologies for localization," in *Proc. Int. Workshop on Location and Context-Awareness*, p. 350362, May 2005. 40, 42

[58] J. Hightower and G. Borriello, "Location systems for ubiquitous computing," in *IEEE Computer*, pp. 57–66, 2001.

[59] I. Guvenc, "Enhancements to RSS based indoor tracking systems using Kalman filters," in *M.S. Thesis, University of New Mexico*, 2002.

[60] A. Bensky, *Wireless Positioning Technologies and Applications (GNSS Technology and Applications) Series: GNSS Technology and Applications.* Artech House Publishers, 2008. 40, 51

[61] A. Sayed, A. Tarighat, and N. Khajehnouri, "Network-based wireless location: challenges faced in developing techniques for accurate wireless location information," in *IEEE Signal Processing Magazine, vol. 22, no. 4*, pp. 24–40, July 2005. 42

[62] D. Niculescu and B. Nath, "Dv based positioning in ad-hoc networks," in *Telecomms. Syst., vol. 2, no. 2*, 2004. 42

[63] J. J. Caffery, *Wireless Location in CDMA Cellular Radio Systems*. Boston: Kluwer Academic Publishers, 2000. 46, 47

[64] L. P. Eisenhart, *'Coordinate Geometry (Reprint)'*. Dover Publications, 2005. 47, 98, 99, 114

[65] P. Stoica and A. Nehorai, "Music, maximum likelihood, and cramer-rao bound," in *IEEE Transactions on Acoustics, Speech, and Signal Processing, vol. 37, no. 5*, pp. 720–741, 1989. 48

[66] Y. Bresler and A. Macovski, "Exact maximum likelihood parameter estimation of superimposed exponential signals in noise," in *IEEE Transactions on Acoustics, Speech, and Signal Processing, vol. ASSP-34*, pp. 1081–1089, 1986.

[67] I. Ziskind and M. Wax, "Maximum likelihood estimation via the alternating projection maximization algorithm," in *IEEE Transactions on Acoustics, Speech, and Signal Processing, vol. 36*, pp. 1553–1560, 1988.

[68] P. Stoica and K. Sharman, "Maximum likelihood methods for direction-of-arrival estimation," in *IEEE Transactions on Acoustics, Speech, and Signal Processing, vol. 38, no. 7*, pp. 1132–1143, 1990. 48

[69] R. Schmidt, "Multiple emitter location and signal parameter estimation," in *IEEE Transactions on Antennas and Propagation*, pp. 276–280, 1986. 48

[70] G. Bienvenu and L. Kopp, "Adaptivity to background noise spatial coherence for high resolution passive methods," in *Proc. IEEE Int. Conf. Acoust., Speech, Signal Processing*, pp. 307–310, 1980. 48

[71] R. Roy and T. Kailath, "Esprit- estimation of signal parameters via rotational invariance techniques," in *IEEE Transactions on Acoustics, Speech, and Signal Processing, vol. 37, no. 7*, pp. 984–994, 1989. 48

[72] F. O. Akgul and K. Pahlavan, "Aoa assisted nlos error mitigation for toa-based indoor positioning systems," in *IEEE Military Communications Conference, MILCOM*, pp. 1–5, 2007. 49

[73] V. Y. Zhang and A.-S. Wong, "Combined aoa and toa nlos localization with nonlinear programming in severe multipath environments," in *IEEE Wireless Communications and Networking Conference*, pp. 1–6, 2009.

[74] S. Zhu, F. Sun, and X. Chen, "Joint uwb toa and aoa estimation under 1-bit quantization resolution," in *IEEE Communications in China (ICCC)*, pp. 321–326, 2013.

[75] L. Taponecco, A. A. D'Amico, and U. Mengali, "Joint toa and aoa estimation for uwb localization applications," in *IEEE Transactions on Wireless Communications vol. 10, no. 7*, pp. 2207–2217, 2011. 49

[76] A. F. Molisch, K. Balakrishnan, and C. C. Chong, "IEEE 802.15.4a channel model - final report. Sep., 2004." http://www.ieee802.org/15/pub/TG4a.html. 50

[77] H. V. Poor, *Classical, Semi-classical and Quantum Noise: Multiple-Access Interference, Chapter 12, pp. 145-155* . Springer, US, 2012. 50

[78] J. Riba and A. Urruela, "A non-line-of-sight mitigation technique based on

ml-detection," in *Proc. IEEE Int. Conf. Acoust., Speech, and Sig. Processing (ICASSP), vol. 2*, pp. 153–156, 2004. 51

[79] D. B. Jourdan and N. Roy, "A non-line-of-sight mitigation technique based on ml-detection," in *Proc. IEEE Position, Location, and Navigation Symp. (PLANS)*, pp. 128–139, 2006.

[80] V. Dizdarevic and K. Witrisal, "On impact of topology and cost function on lse position determination in wireless networks," in *Proc. Workshop on Positioning, Navigation, and Commun. (WPNC)*, pp. 129–138, 2006.

[81] S. Venkatesh and R. M. Buehrer, "A linear programming approach to nlos error mitigation in sensor networks," in *Proc. IEEE Int. Symp. Information Processing in Sensor Networks (IPSN)*, pp. 301–308, 2006.

[82] P. C. Chen, "A non-line-of-sight error mitigation algorithm in location estimation," in *IEEE Int. Conf. Wireless Commun. Networking (WCNC), vol. 1*, pp. 316–320, 1999. 51

[83] K. Siwiak and J. Gabig, "IEEE 802.15.4IGa informal call for application response, contribution 11, Doc.: IEEE 802.15-04/266r0, July 2003." http://www.ieee802.org/15/pub/TG4a.htm. 52

[84] S. D. Amico, M. Matteis, O. Rousseaux, K. Philips, B. Gyselinck, D. Neirynck, and A. Baschirotto, *'Ultra Wide Band in Medical Applications' in 'Advances in Biomedical Sensing, Measurements, Instrumentation and Systems, Lecture Notes in Electrical Engineering'*. Springer Berlin Heidelberg, vol. 55, 2010. 53, 113

[85] IMEC, "Ultra Low Power Impulse Radio UWB Transceiver for Localisation and Streaming." http://www2.imec.be/content/user/File/NEW/Research/WirelessCommunication/Digitalbaseband/FEB2014IMPULSERADIOULTRA_WIDEBAND.pdf. 53

[86] Thales Research, "Thales UWB Through-Wall Radar Technology." http://ukgrads.thalesgroup.com/Files/TRTUWBradar.pdf. 53

[87] Time Domain, "TrackIT Systems: PulsON 350 RFID tracking system." http://www.thetrackit.com/library/TIS_P350_ONESHEET.pdf. ix, 54

[88] Multispectral Solutions, "PAL650 Precision Asset Location System." https://www.wpi.edu/Images/CMS/PPL/Multispectral.pdf. ix, 55

[89] Zebra Enterprise Solutions, "Zebra DART UWB positioning system." http://www.zebra.com/id/zebra/na/en/index/products/location/ultra_wideband.htm. ix, 54, 56, 57

[90] Zebra Enterprise Solutions, "Pal650 UWB positioning technology." http://www.zebra.com. 54

[91] R. J. Fontana, E. Richley, and J. Barney, "Commercialisation of an ultra wideband precision asset location system," in *Proceedings International Conference on Ultra Wideband Systems and Technologies (UWBST)*, pp. 369–373, Nov. 2003. 55

[92] Ubisense, "Ubisense real-time positioning system." http://www.ubisense.net. ix, 55, 56

[93] X. Huibin and W. Ying, "A linear algorithm based on tdoa technique for uwb localization," in *Electric Information and Control Engineering (ICEICE), 2011 International Conference on*, pp. 1013–1015, 2011. 59

[94] R. Agieb, I. Adly, and R. Ragai, "Two nodes uwb low power asset localization in wsn," in *Computer Applications Technology (ICCAT), 2013 International Conference on*, pp. 1–4, 2013.

[95] G. Mary and V. Prithiviraj, "Uwb localization techniques for precision automobile parking system," in *Electromagnetic Interference Compatibility, 2008. INCEMIC 2008. 10th International Conference on*, pp. 621–626, 2008. 59

[96] Z. Nai-tong and M. Jing, "Reflection characteristics analysis of ir-uwb signal," in *4th International Conference on Wireless Communications, Networking and Mobile Computing, 2008. WiCOM '08*, pp. 1–4, 2008. 64, 65, 68, 69, 70, 118

[97] K. D. Misra, *Permittivity Measurement, the Measurement, Instrumentation and Sensors Handbook*. CRC Press, IEEE Press, 1999. 64

[98] P. R. Barnes and F. M. Tesche, "On the direct calculation of a transient plane wave reflected from a finitely conducting half space," in *IEEE Trans. Electromagn. Compat., vol. 33*, pp. 90–96, 1991. 64

[99] S. Kay, *'Fundamentals of Statistical Signal Processing: Estimation Theory'*. Prentice Hall Signal Processing Series, 1993. 86, 141, 152, 155

[100] M. Kamel, S. Fawzy, A. El-Bialy, and A. Kandil, "Secure remote patient

monitoring system," in *1st Middle East Conference on Biomedical Engineering (MECBME)*, pp. 339–342, 2011. 90

[101] I. Sanchez-Tato, J. C. Senciales, J. Salinas, L. Fanucci, G. Pardini, F. Costalli, S. Dalmiani, J. M. Higuera, Z. Vukovic, and Z. Cicigoj, "Health @ Home: A telecare system for patients with chronic heart failure," in *5th International Conference on Broadband and Biomedical Communications (IB2Com)*, pp. 1–5, 2010. 90

[102] R. S. Kirby, J. D. McConnell, J. M. Fitzpatrick, C. Reohrborn, M. G. Wyllie, and P. Boyle, *Therapeautic Treatment for Benign Prostatic Hyperplasia*. Informa Healthcare, 2005. 91

[103] J. Blaivas and J. Weiss, *Benign Prostatic Hyperplasia and Lower Urinary Tract Symptoms, An Issue of Urologic Clinics*. Elsevier Health Sciences - Saunders, 2009. 91

[104] V. R. Jakkula, D. J. Cook, and G. Jain, "Prediction Models for a Smart Home Based Health Care System," in *21st International Conference on Advanced Information Networking and Applications Workshops*, pp. 761–765, 2007. 91

[105] V. C. Joseph, S.-H. Ahn, J. Kim, K.-H. Lee, and D.-H. Kirn, "Intelligent healthcare systems: re-defining personal healthcare solutions," in *7th International Conference on Advanced Communication Technology*, pp. 424–427, 2005. 91

[106] ICUWB, "Conference Proceedings." http://ieeexplore.ieee.org/

search/searchresult.jsp?newsearch=true&queryText=ICUWB+2011+Conference. 95

[107] WOSSPA, "Conference Proceedings." http://ieeexplore.ieee.org/search/searchresult.jsp?newsearch=true&queryText=WoSSPA+2013+Conference. 95

[108] FGCT, "Conference Proceedings." http://ieeeexplore.info/search/searchresult.jsp?newsearch=true&queryText=FGCT+2013. 95

[109] L. Kuen-Tsiar and C. Wei-Kai, "Mobile positioning based on TOA/TSOA/TDOA measurements with NLOS error reduction," in *Proceedings 8th Workshop on Positioning Navigation and Communication (WPNC)*, pp. 545– 548, Dec. 2005. 102

[110] O. Onalaja and M. Ghavami, "Uwb based pre-localisation algorithm for aiding target location in a multipath environment," in *IEEE International Conference on Ultra-Wideband (ICUWB)*, pp. 140–144, 2011. 103

[111] D. Eberly, *Intersection of ellipses* . [Online] http://www.geometrictools.com/Documentation/IntersectionOfEllipses.pdf, 2000. 108, 109

[112] O. Onalaja, M. Adjrad, and M. Ghavami, "Uwb-based elliptical target localization in an indoor environment," in *8th International Workshop on Systems, Signal Processing and their Applications (WoSSPA)*, pp. 103–107, 2013. 112

[113] A. Popa, "An optimization of gaussian uwb pulses," in *Proc. Int. Conf. on Development and Application Systems*, 2010. 113, 114

[114] S. Ghassemzadeh, L. Greenstein, T. Sveinsson, A. Kavcic, and V. Tarokh, "Uwb delay profile models for residential and commercial indoor environments," in *IEEE Trans. Veh. Technol.,vol. 54, no. 4*, pp. 1235–1244, 2005. 113

[115] R. Qiu, "A generalized time domain multipath channel and its application in ultra-wide-band (uwb) wireless optimal receiver design: system performance analysis," in *Proc. IEEE Wireless Commun. and Networking Conference, vol.2*, pp. 901–907, 2004. 114, 117, 118, 119

[116] R. Qiu, "A generalized time domain multipath channel and its application in ultra-wideband (uwb) wireless optimal receiver design-part ii: physics-based system analysis," in *IEEE Trans. Wireless Commun., vol.3, no. 6*, pp. 2312–2324, 2004. 114, 116, 117, 118, 119

[117] G. Llano, J. Cuellar, and A. Navarro, *Frequency UWB Channel, Ultra WidebandCommunications: Novel Trends - Antennas and Propagation* . Intech, 2011. 120

[118] B. Jadhavar and T. Sontakke, "Simulation and analysis of uwb indoor channel through s-v model for user location detection," in *Int. J. Comput. Electr. Eng., vol.3, no. 5*, 2011. 120

[119] IET, "Communications Journal." http://digital-library.theiet.org/content/journals/iet-com. 130

[120] J. Warner and N. Graham, *'Understanding Alzheimer's Disease and other Dementias'*. Family Doctor Publications Ltd, 2009. 132

[121] C. Cantley, *'A handbook of Dementia Care'*. Open University Press, 2001. 132

[122] O. James, *'Contented Dementia'*. Ebury Press, 2010. 132

[123] X. Yu, "Approaches and principles of fall detection for elderly and patient," in *10th International Conference on e-health Networking, Applications and Services*, pp. 42–47, 2008. 138, 139

[124] O. Mohamed, H.-J. Cho, and Y. Iraqii, "Fall detection systems for elderly care: A survey," in *6th International Conference on New Technologies, Mobility and Security (NTMS)*, pp. 1–4, 2014.

[125] S. Kozina, H. Gjoreski, M. Gams, and M. Lustrek, *'Evaluating AAL Systems Through Competitive Benchmarking: Efficient Activity Recognition and Fall Detection Using Accelerometers'*. Springer Berlin Heidelberg, 2013.

[126] F. Felisberto, N. Moreira, I. Marcelino, F. Fdez-Riverola, and A. Pereira, *'Advances in Intelligent and Soft Computing: Elder Care's Fall Detection System '*. Springer Berlin Heidelberg, 2011.

[127] S. Abbate, M. Avvenuti, P. Corsini, J. Light, and A. Vecchio, *'Monitoring of Human Movements for Fall Detection and Activities Recognition in Elderly Care Using Wireless Sensor Network: a Survey, Wireless Sensor Networks: Application - Centric Design'*. Online:

http://www.intechopen.com/books/wireless-sensor-networks-application-centric-design/monitoring-of-human-movements-for-fall-detection-and-activities-recognition-in-elderly-care-using-wi, 2010. 138

[128] D. Chen, W. Feng, Y. Zhang, X. Li, and T. Wang, "A wearable wireless fall detection system with accelerators," in *IEEE International Conference on Robotics and Biomimetics (ROBIO)*, pp. 2259–2263, 2011. 139